博士論文

Critical Heat Flux Enhancement in Downward-facing Pool Boiling with Honeycomb and Irradiation Effect

（ハニカムと照射による下向きプール沸騰における限界熱流束の改善）

宮　海光

Critical Heat Flux Enhancement in Downward-facing Pool Boiling with Honeycomb and Irradiation Effect

A Thesis
By
Haiguang GONG

Submitted to
The University of Tokyo
in partial fulfillment of the requirements for the degree of

Doctor of Philosophy

September 2017

Department: Nuclear Engineering & Management

Committee Chair:
Dr. Koji OKAMOTO, Professor, Head of Department (Nuclear Professional School)

Committee Members:
Dr. Akira YAMAGUCHI, Professor, Department of Nuclear Engineering and Management
Dr. Nejdet ERKAN, Project Associate Professor, Department of Nuclear Engineering and Management
Dr. Masahiro KONDO, Lecturer, Department of Nuclear Engineering and Management
Dr. Shoji MORI, Associate Professor, Yokohama National University

TABLE OF CONTENTS

Page

ABSTRACT

In nuclear power plants (NPPs), one of safety strategy responding to severe accident is to activate ex-vessel cooling system. With regard to the strategy, critical heat flux (CHF) in lower head of reactor vessel is a key standard to assess such kind of cooling ability. Thus far, especially after Fukushima accident safety analysis has been proven in present NPPs. However, for the new type of NPPs present evaluating criterion is not available. This is because the new ones are usually coming with a higher thermal power, which needs a higher cooling ability correspondingly. Thus the requirements for CHF enhancement has been back to the center by lots of researchers.

Recently, many researcher used different methods for CHF enhancement study, such as nano-particle, micro-fin, porous layer and so on. Regarding with these methods, it was found CHF can be enhanced. However, there is a need for further study. Thus, in this study, honeycomb and irradiation methods are selected for CHF enhancement study. Meanwhile, the bare surface was carried on as controlled experiment for future comparison. In this study, many factors are taken into consideration. These are inclination, honeycomb pore size, honeycomb structure, dose amount, dose source and some combination of several factors. Through experiment, CHF results can be obtained.

Based on honeycomb and irradiation experiment, the findings are list as follows:

- In bare surface case, CHF increases as inclination, which means the higher inclination it is the larger CHF value it shows;
- In honeycomb surface cases, a) solid honeycomb surface can enhance CHF compared with bare surface case. Moreover, porous honeycomb surface cam further enhance CHF performance; b) present pore size has no effect on CHF value; c) CHF also increases as inclination going up; d) CHF value increases as hole-area ratio;
- In irradiation cases, a) irradiation reduces contact angle, increasing surface hydrophilicity. Also, at same dose amount extent of angle decreasing is similar which means source type has no effect; b) in 5° bare surface case, CHF can be largely enhanced by high dose irradiation. Besides, source type has similar effect

on CHF performance; c) in 10° and 20° bare surface case, CHF cannot be enhanced; d) in all honeycomb surface case, irradiation cannot affect CHF performance;

Based on experiment findings, the discussion is given in the following.

- Inclination can affect BDF, one factor that can determine the speed of bubble removal from heating surface. More specifically, at high inclination, bubble removal speed is rapid so that BDF is larger. Under this circumstance, surface replenishment condition becomes better, which can provide surface with more coolant in unit time. In both bare and honeycomb surface, BDF becomes larger with increasing inclination.
- Separate phase circulation and bubble behavior restricted by honeycomb structure are the reason for CHF enhancement by application of honeycomb. Besides, additional water refluxing path can also enhance CHF performance.
- Pressure balance model can be used in downward-facing pool boiling. Through the comparison between formulation and experiment, it is known that CHF value is a balance of water refluxing and bubble removal mass flow rate, which means the lower value can determine the final CHF performance. In this study, according to formulation water refluxing mass flow rate decreases as hole-area ratio while bubble removal mass flow rate increases as hole-area ratio. So CHF can reaches the maximum when both mass flow rate are equal. Besides, this crossing point of both water refluxing and bubble removal mass flow rate curve is at the hole-area ratio 0.41.
- Irradiation can increase nucleation site area. If the nucleation site area is big, the level of water replenishment toward heating surface is larger, causing an improved heat transfer condition. That is the reason for CHF enhancement.
- From both surface modification method, it is found in downward-facing, bubble removal is dominant to determine CHF. This is reason why CHF is similar with same hole-ratio even though diameter is different and the reason why irradiation cannot enhance CHF in honeycomb surface case.

From the discussion based on experiment results, some conclusions can be made and these can provide some reference for future IVR design.

1) Pressure balance can be applicable in downward-facing boiling and CHF is a function of hole-ratio. With given parameter of honeycomb plate, the higher CHF region can be predicted;

2) Irradiation can increase nucleation site area, which is one reason for CHF enhancement. For future design, one of enhancing CHF method is try to increase nucleation site area;

3) How to remove bubble is key issue in downward-facing pool boiling. To enhance CHF, first try to increase bubble removal ability.

Keywords: critical heat flux enhancement; pool boiling; heat transfer; honeycomb; irradiation; inclination;

LIST OF FIGURES

LIST OF TABLES

NOMENCLATURE

Symbols

ºC	Degrees Celsius
θ	Surface inclination angle [º]
σ	Surface tension [N/m]
π	Ratio of a circle's circumference
α	Coefficient
γ	Hole-area ratio
δ_h	Thickness of honeycomb plate [m]
μ_l	Viscosity of water [Pa s]
ρ_f	Liquid density [kg/m^3]
ρ_l	Saturated liquid density [kg/m^3]
ρ_v	Saturated vapor density [kg/m^3]
$\Delta(\Delta T)$	Standard deviation of Temperature
Δh	Standard deviation of heat transfer coefficient
Δp	Pressure drop inside test section [Pa]
$\Delta p_{c,\max}$	Capillary pressure [Pa]
Δp_{du}	Pressure head due to bubble growth force [Pa]
Δp_l	Pressure drop caused by liquid flow in porous medium [Pa]

$\Delta p_{l,h}$	Frictional pressure drop caused by water flow through holes [Pa]
$\Delta p_{l,p}$	Frictional pressure drop caused by water flow through porous surface [Pa]
Δp_v	Pressure drop caused by vapor flow through channels [Pa]
Δq	Standard deviation of heat flux
ΔT	Superheat between water temperature and wall
Δt	Pitch or center distance between two holes [mm]
A_{CU}	Area of copper surface [m^2]
A_h	Area of hole-area [m^2]
A_p	Area of porous surface [m^2]
C_{CHF}	Coefficient at CHF point
C_s	Shear lift coefficient
d	Diameter of honeycomb plate [mm]
d_v	Width of vapor escape channel [mm]
G	Mass flux of bubble removal [kg/m^2 s]
$G_{a,br}$	Available mass flux of bubble removal [kg/m^2 s]
g	Gravitational acceleration [m/s^2]
h	Heat Transfer coefficient [W/m^2-K]
h_{fg}	Latent heat of vaporization [J/kg]
h_l	Water level [m]

K	Permeability [m^2]
k	Thermal conductivity [W/m-K]
L	Thickness of test piece [m]
m	Mass flow rate of bubble removal [kg/s]
$m_{a,br}$	Available bubble removal mass flow rate [kg/s]
$m_{a,wr}$	Available water refluxing mass flow rate [kg/s]
$m_{m,br}$	Maximum bubble removal mass flow rate [kg/s]
$m_{m,wr}$	Maximum water refluxing mass flow rate [kg/s]
n	Quantities of holes in honeycomb plate
n_{TC}	Number of temperature measurement points
Pa	Pascal
p	Pressure [Pa]
p_d	Dynamic pressure [Pa]
p_h	Hydraulic head [Pa]
q	Heat flux [MW/m^2]
q_w	Water flow speed [m/s]
q_{CHF}	Critical heat flux [W/m^2]
r_b	Radius of bubble [m]
r_{eff}	Effective radius [m]
Ti(yi)	Temperature at different locations [K]
X_i	Interval distance from boiling surface [mm]

Acronyms

NPPs	Nuclear Power Plants
IAEA	International Atomic Energy Agency
SAMG	Severe Accident Management guidelines
RPV	Reactor Pressure Vessel
ERVC	External Reactor Vessel Cooling
IVR	In-Vessel Retention
FSAR	Final Safety Analysis Report
SEM	Scanning Electron Microscope
RISA	Radiation Induced Surface Activation
PEEK	Polyether ether ketone
JAEA	Japan Atomic Energy Agency
BDF	Bubble Departure Frequency

1. INTRODUCTION

1.1 Background

Nuclear Power is the utilization of nuclear reaction to generate heat. Thus far, the most frequently used method is nuclear fission. Based on this, nuclear power plants (NPPs) are introduced for electric power generation. Basically, the NPPs are one of leading low carbon power generation methods compared with other ways to produce electricity [1]. For better development, International Atomic Energy Agency (IAEA) gives a safety standard. It is that NPPs should provide a high level of safety for protecting people and the environment from harmful effects of ionizing radiation [2]. However, there are many accidents happening in the history and these are against the safety standard. For example, some accident may cause significant damage to reactor fuel and resulting from more or less complete core meltdown, which is called as severe accidents [3]. In order to mitigate such consequence, severe accident management guidelines (SAMG) have been developed. SAMG's prime object is to protect remaining fission product boundaries and to limit actual or possible release [4].

Suppose there appears a severe accident and possible scenario process will be: due to unforeseen incidents, the fuel rods will melt and fall down to the lower head of reactor pressure vessel (RPV), forming into corium. At the beginning the corium can be cooled down with the rest water existing in RPV. After remaining water is boiled off, corium will start to heat up the lower head. The heat source is decay heat from the corium. Due to heating up, temperature of lower head will increase. If there is no management to control rising up, temperature will reach the melting point of lower head. Once reaching melting point, RPV failure will occur by thermal stresses and/or creep [5]. When RPV failure appears, corium will be released into the containment, further increasing the risk of radiation threat. Thus, for realizing IAEA safety standard and SAMG some measures must be taken into consideration.

According to defense-in-depth, RPV is regarded as one barrier to prevent and mitigate the release radiation or hazardous materials. Thus, if the integrity of lower head is ensured, the radioactive can be kept inside RPV. Here the effective system to achieve this target is called external reactor vessel cooling (ERVC). Figure. 1-1 [6] shows the schematic map of ERVC. During accident, ERVC is activated. Water will go inside through the inlet. Then it flows across outside wall of lower head, cooling down it. Under this situation, it is supposed that no radioactive wastes will be released. Thus, this is called in-vessel retention (IVR).

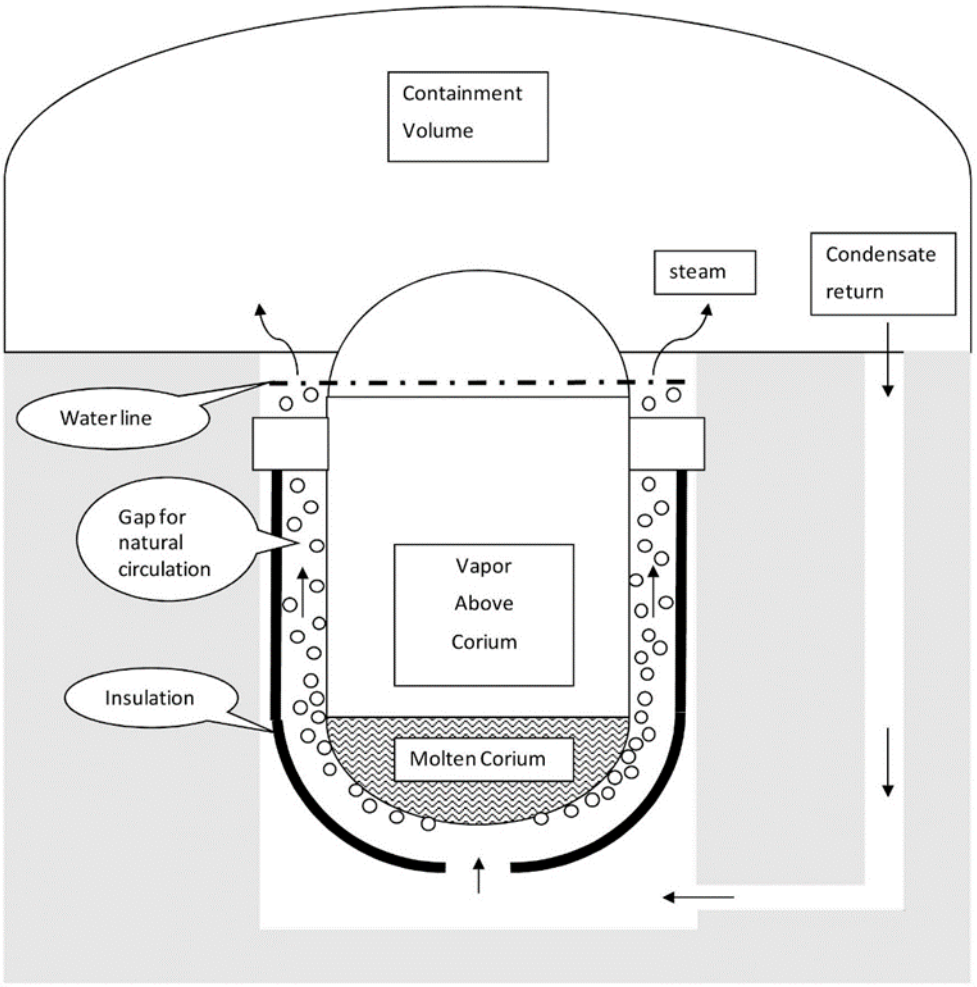

Figure 1-1: Schematic map of external reactor vessel cooling system [6].

1.2 Critical Heat Flux & Possible Issues for Future NPPs

1.2.1 Introduction of critical heat flux

Regarding with the assessment of cooling system, the cooling ability is one key issue. Usually, critical heat flux (CHF) is utilized for evaluating the effectiveness of cooling system. Here brief introduction of CHF is given. As it is shown in Figure. 1-2 [7], boiling curve means heat flux as a function of superheating. Suppose there is one heat flux at point A, so superheating is a little higher than 10 K and boiling condition is nucleate boiling. Then heat flux is increased to point B. At this time, superheating is near 100 K. After that, heat flux is slightly enhanced to, for example, point C. Even though it is little higher than point B, the superheating has already reached to thousand magnitude. Besides, boiling condition turns into film boiling. Thus, the point B is called CHF point. CHF point is one turning point because nucleate boiling becomes to film boiling and low superheating turns to be a much higher superheating level. From this circumstance, it is known that in cooling system heat flux must be controlled under CHF point.

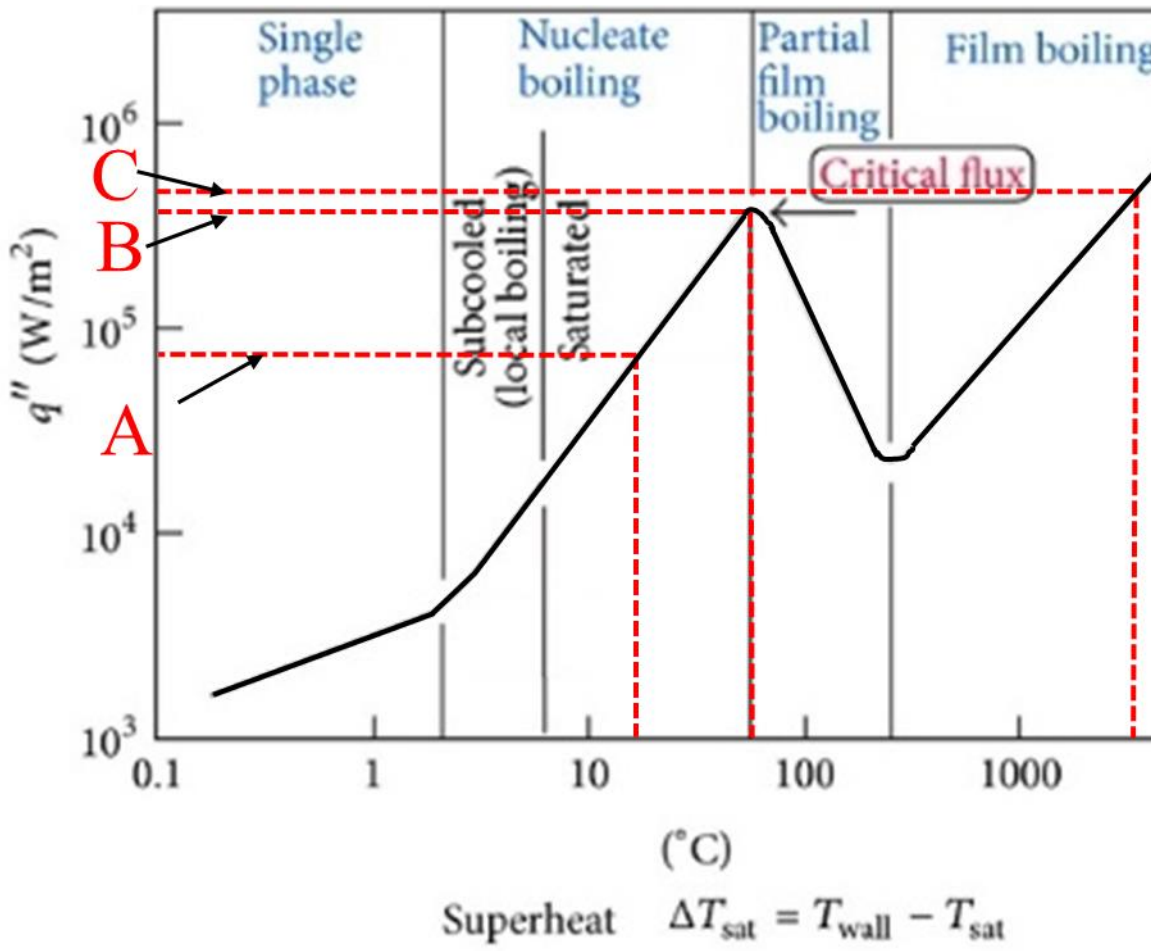

Figure 1-2: Heat flux as a function of superheating [7].

1.2.2 Possible issue for future NPPs

For present nuclear power plants, cooling ability is ensured because before plants operation, Final safety analysis report (FSAR) should be given. However, the 3rd generation NPPs will be used for electricity generation in the future. Among these new type generation, most of them have a higher power than present types (see Table 1-1 & Table 1-2) [8-10]. Because the megawatt electrical power is largely enhanced, it means corresponding thermal power improves. So the higher power needs higher cooling ability in the future design. Based on these tables and nuclear safety, there is a strong requirement for high CHF margin or CHF enhancement.

Table 1-1: Megawatt electrical of advanced power reactor under construction [8-10].

Reactor (reactor type)	Size, MWe
AP1000 (PWR)	1250
EPR (PWR)	1750
Hualong One (PWR)	1150

Table 1-2: Megawatt electrical of advanced power reactor under deployment [8-10].

Reactor (reactor type)	Size, MWe
ESBWR (BWR)	1600
APWR (PWR)	1530
Atmea1 (PWR)	1150

1.2 Literature Review

Before, many researchers focus on CHF enhancement study. According to previous study, CHF enhancement is due to the following reasons: extended surface area, nucleation site density, wettability, capillary wicking and wavelength decrease [11]. Some used micro fin structure to study the boiling phenomenon [12-14]. The CHF was enhanced compared with the bare surface, and it increased with the number of fins (Figure. 1-3). Studies had also investigated different orientations of the heating surface. Also CHF enhancement in nanoparticle solution had been found [15-16] (Figure. 1-4). In their study, Scanning Electron Microscopy (SEM) subsequent to boiling experiment revealed that lots of nanoparticles were deposited on test surface (Figure. 1-5). These kinds of coatings, forming an uneven surface, results in a large CHF increase in the end. Some researchers [17-18] focused on different angles from 0° (upward-facing) to 180° (downward-facing). The results showed that, as the angle increases, the CHF value decreases. Besides, the gap effect is another important factor that affects CHF. The CHF decreases with the gap distance [19-20].

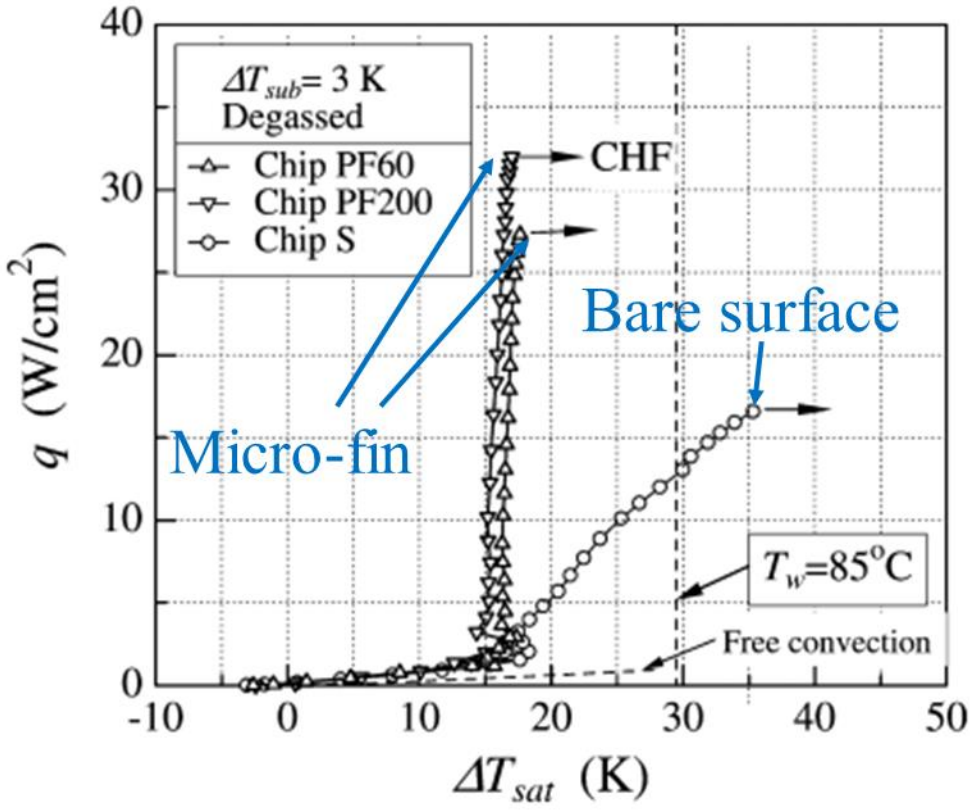

Figure 1-3: CHF comparison between bare surface and micro-fin surface [12].

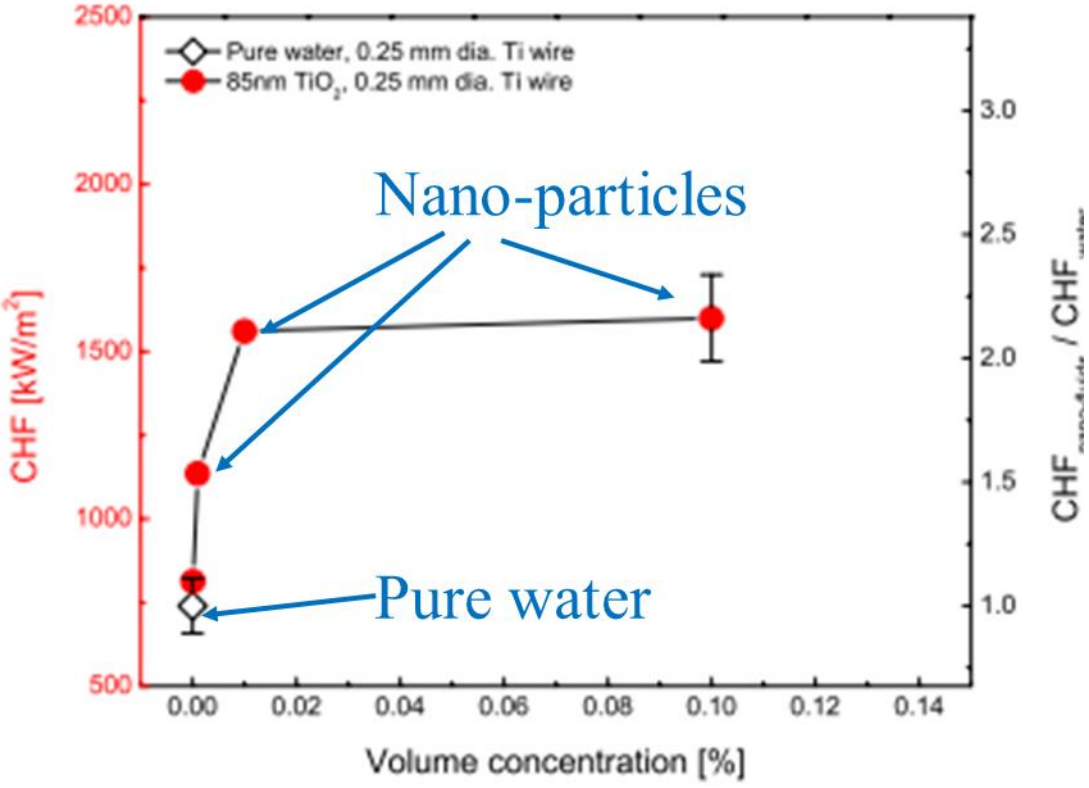

Figure 1-4: CHF comparison of Ti wire using pure water or nano-particles [15].

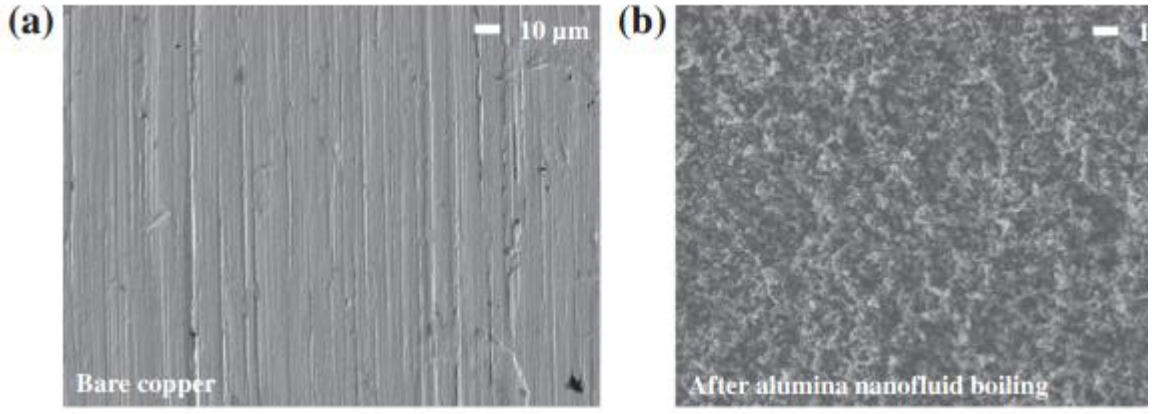

Figure 1-5: SEM images of (a) bare heater surface, (b) after alumina nano-fluid boiling CHF [16].

Some researchers used modulated porous-layer which is tightly attached to heating surface to study CHF enhancement [21-22]. They found the modulation can reduce the liquid-vapor counter-flow resistance adjacent to the surface. And two possible reasons,

hydrodynamic limit and viscous-drag limit are supposed as mechanism to determine CHF. Based on porous-layer structure theory, Mori [23-24] introduced a novel porous layer theory in their study. This porous layer is called honeycomb, which is made of ceramic particles. In his upward-facing pool boiling experiment, 2.5 times CHF enhancement has been found (Figure. 1-6).

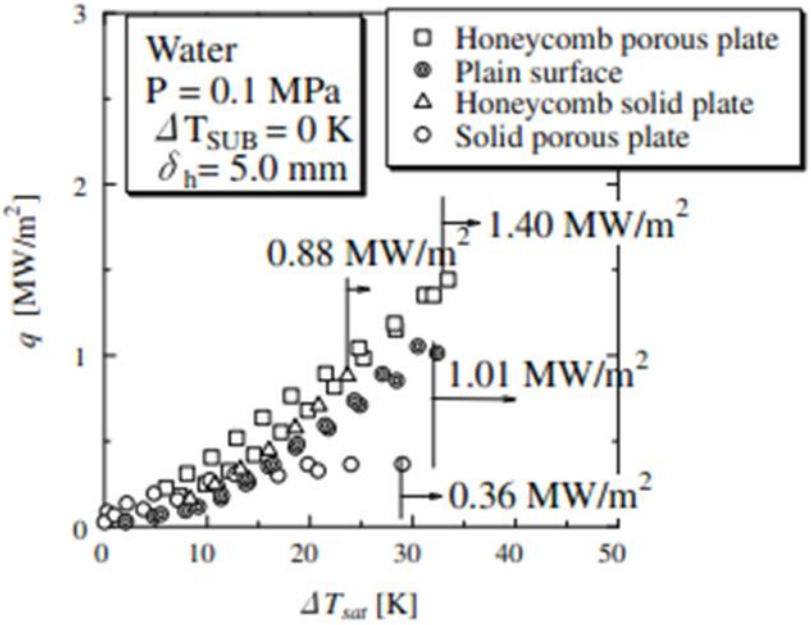

Figure 1-6: CHF value with different heating surface [23].

Radiation effect on CHF performance is also studies in this field. Imai and Koga [25] suggested that improvements in heat transfer require continuous water supplies in contact with the heating surface. Takamasa et al. [26] investigated the wettability of metal-oxide surfaces and found that it can be significantly improved by irradiating the surface with gamma rays. This improvement is due to cathodic and anodic reactions in the irradiation of metal-oxide surfaces. Okamoto et al. [27] used irradiated SUS304 for their experiments, which provided a CHF enhancement of ~20%. Besides boiling experiment, the quenching experiment with/without radiation effect was carried on. The results showed that quenching velocity after irradiation is increased with 20-30% [28] (Figure. 1-7). The reason for enhancement is that the radiation can activate cathodic and anodic reactions of the oxidized metal [29, Figure. 1-8]. Thus, this phenomenon was called as radiation induced surface activation (RISA).

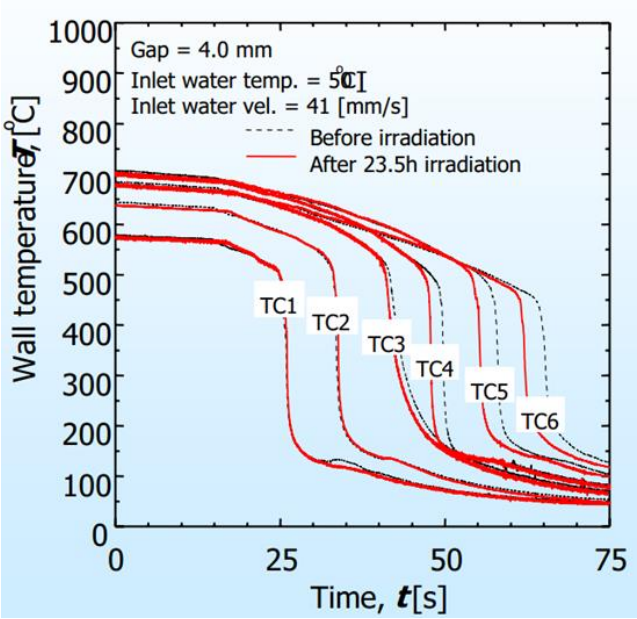

Figure 1-7: Comparison of quenching velocity before/after irradiation [28].

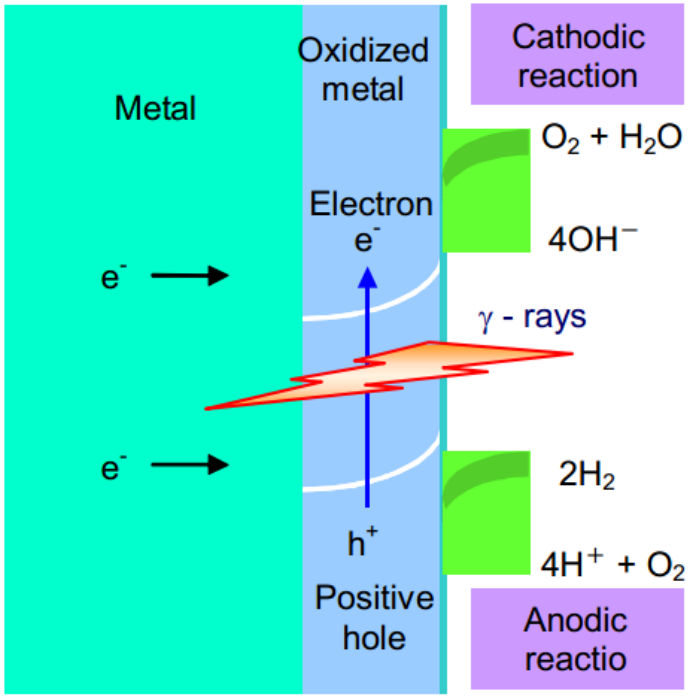

Figure 1-8: Assumed mechanism behind radiation induced surface activation [29].

In a word, even though there are many specific methods for CHF enhancement, the reason for CHF increase is due to surface modification. More specifically, nano-particles forms one porous layer deposition on heating surface and other methods, including honeycomb, micro-fin and so on, is directly to change surface figuration. However, present study is not enough, there is need for further study. Details will be explained in the next chapter.

2. OBJECTIVES

2.1 Final Goal

As it is explained in the previous chapter, safety is very important in NPPs. And many agencies state the meaning of safety. Here safety standard of IAEA is given. It is to protect people and the environment from ionizing radiation. Because accident may not be avoidable in the future operation in NPPs, some severe accident would happen. After that accident, the fuel rods will melt down and fall into lower head of RPV. As one barrier for prevent the radioactive from releasing, the integrity of lower head should be kept. Thus, the final goal of this study is to keep the integrity of lower head even under severe accident.

2.2 Intermediate Goal

There are many ways to ensure the integrity of low head. For example, replacing RPV with some material that can sustain with a higher temperature. However, this study focuses on cooling down RPV using external cooling system. Thus, this study has relation with boiling. The intermediate goal is to enhance CHF limitation of lower head.

2.3 Current Goal

Before the explanation of present goal, the summary of previous study will be given. Through the literature, it is found that CHF experiment using honeycomb and irradiation are relatively new field, which means there is a need for future study. The reasons are list in the following:

- Some researchers used ceramic honeycomb for CHF enhancement study. However, there exist some problem in the future application because of strength of ceramic materials. What's more, the previous study mainly paid attention to upward-facing study, ignoring downward-facing condition. However, downward-facing performance is necessary because facing direction of boiling during activation of ERVC is downward-facing. Thus, CHF performance using surface modification method on downward-facing is expected.
- Some researchers found that radiation had some effect on oxidized metal, not pure metal. Thus, study radiation effect on pure metal to see CHF enhancement is one target.
- In previous study, some studies tried to use combination method for experiment. For example, Mori et al [30] use the combination of nano-particle and honeycomb for CHF increase research. So, this study also tries to use the combination of honeycomb and radiation effect.

So in view of final goal and literature, an experimental study will be carried on. The current goal is to evaluate the effect of surface modification method by downward-facing pool boiling experiment. And this study summarize the current work. In the future additional work will be done to reach the final goal.

2.4 Key Words

Based on current goal, these key words are irradiation, honeycomb, CHF enhancement, inclined downward-facing and pool boiling. These words can be regarded as experimental condition and the details will be discussed in the next chapter.

3. EXPERIMENTAL FACILITY

Some contents of this chapter have already been published. [31]

3.1 Apparatus

Figure. 3-1 shows the schematic picture of experimental facility. The experimental equipment used in this study consists two important experimental parts. They were experimental equipment and data acquisition equipment respectively. The experimental equipment mainly contained a water tank and its support (Figure 3-2, this support can be inclined with some certain inclination angle, the details are in Appendix), a test section, a condenser (Figure 3-3), a preheater (Figure 3-4), and a thermocouple (Figure 3-5) measuring the pool water temperature to make sure temperature meet the requirements. Before testing, the pool water was heated to saturated conditions under atmospheric pressure. During experiment, the preheater was used to maintain a constant water temperature. Distilled water was used as coolant in the water tank. The data acquisition equipment included a high-speed camera (Figure 3-6) positioned under the water tank to capture the boiling phenomenon and a data logger (Figure 3-7) used for parameter measurement. During experiment, to clearly capture boiling phenomenon, one halogen lamp (Figure 3-8) was introduced.

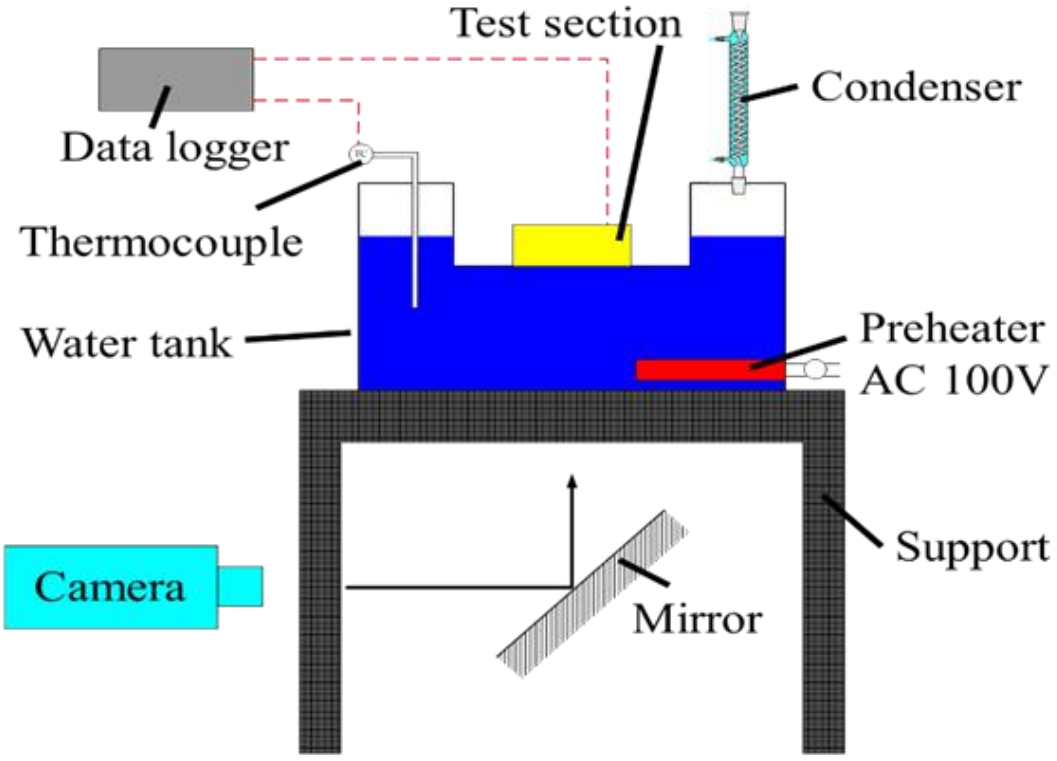

Figure 3-1: Schematic map of facility set-up.

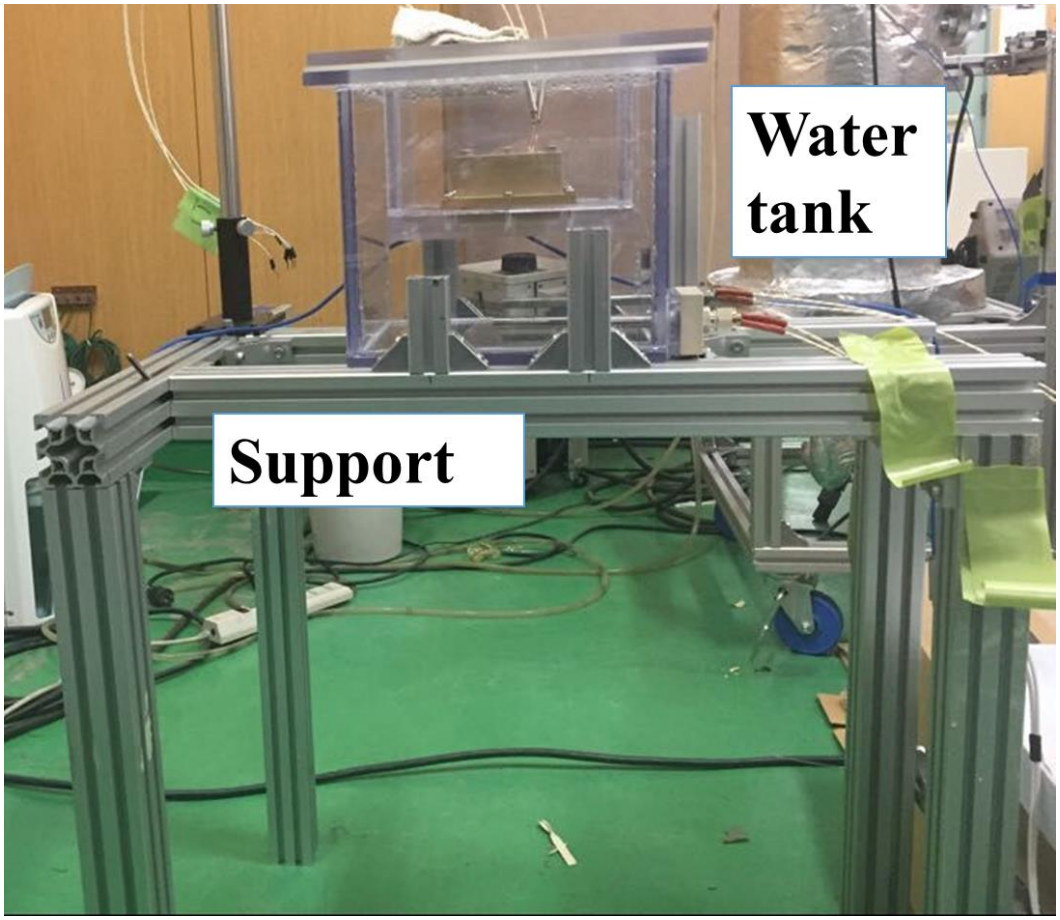

Figure 3-2: Physical picture of water tank and its support.

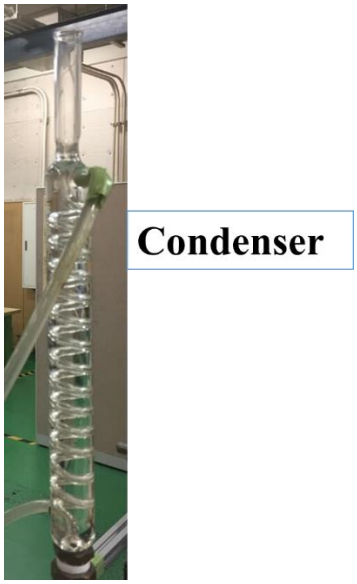

Figure 3-3: Physical picture of condenser.

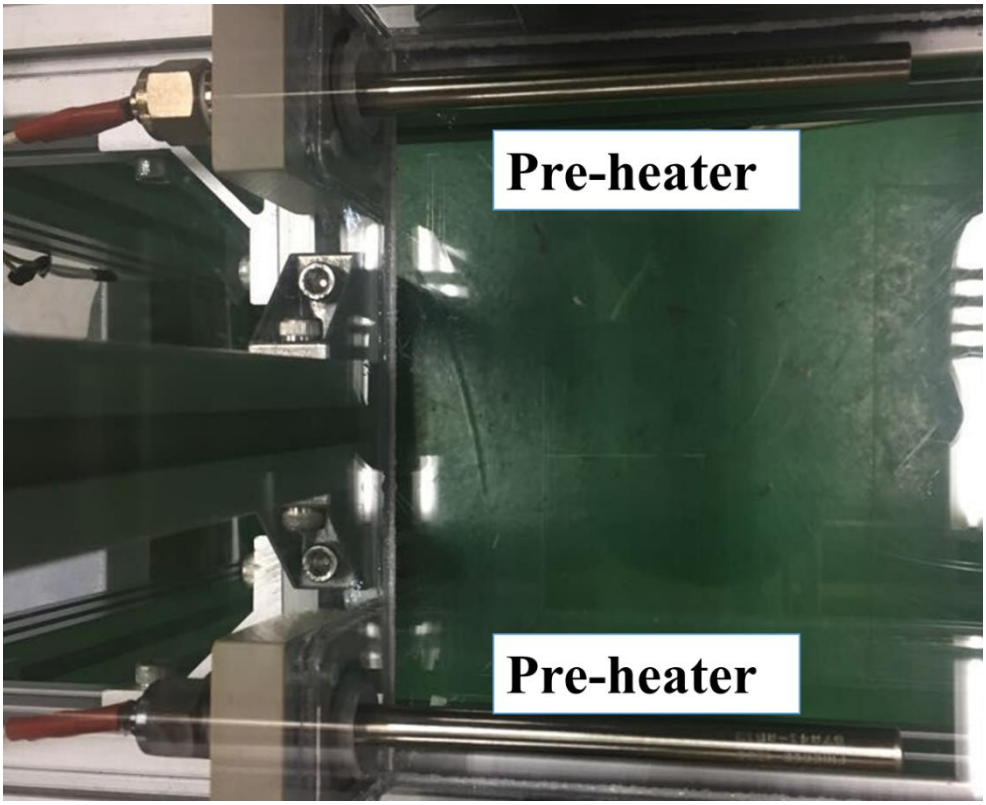

Figure 3-4: Physical picture of preheater.

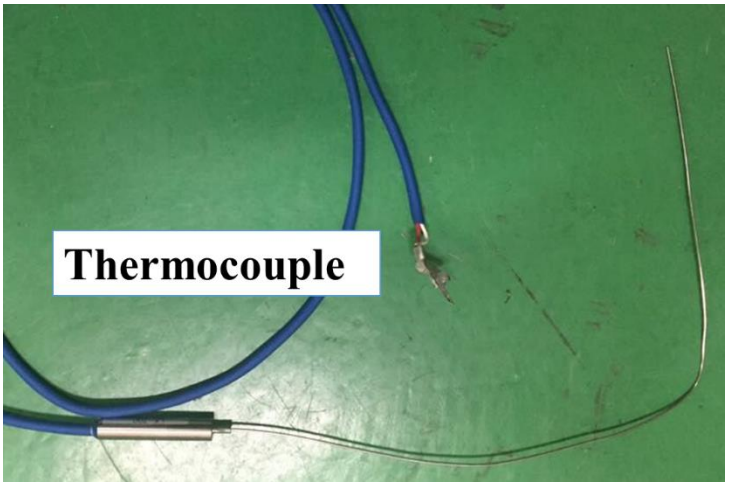

Figure 3-5: Physical picture of thermos-couple.

Figure 3-6: Physical picture of high-speed camera.

Figure 3-7: Physical picture of data logger.

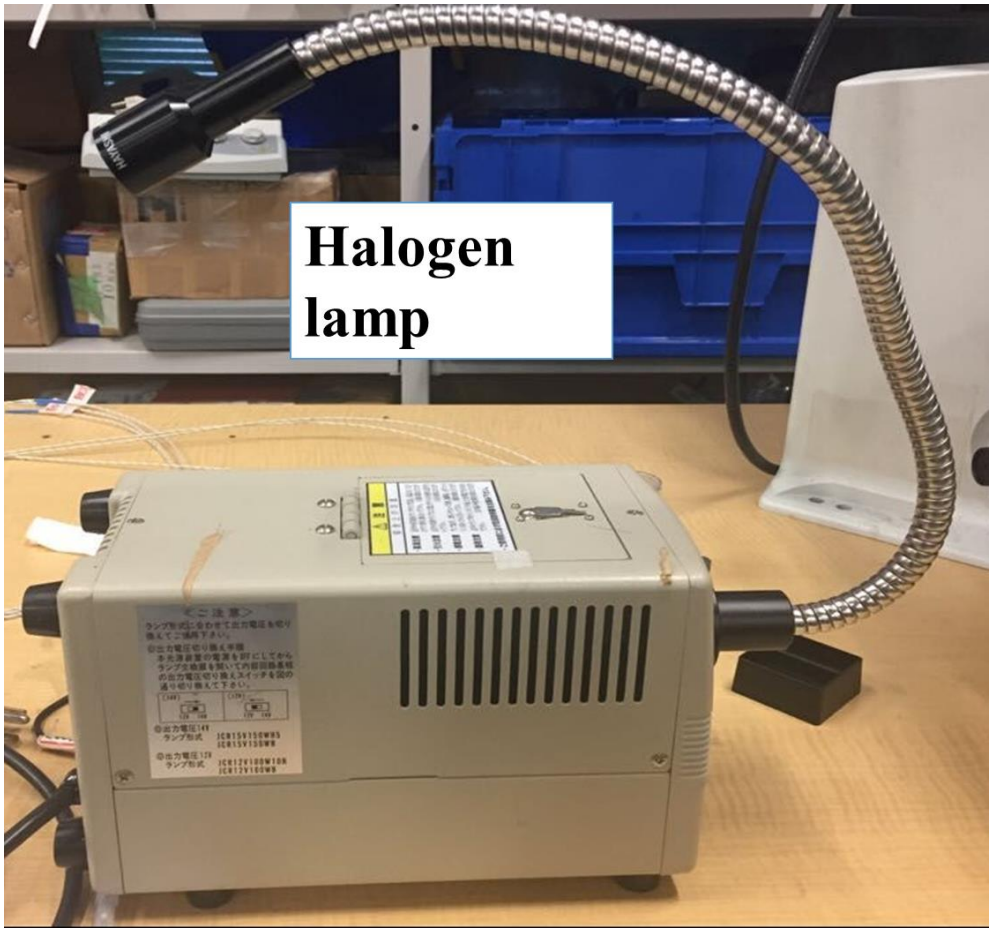

Figure 3-8: Physical picture of powerful lamp.

Figure 3-9 shows the schematic of the test section for the bare and honeycomb surfaces. The test sections comprised copper (heating zone) and polyether ether ketone (PEEK, thermal isolation zone). Here, copper was chosen as heating zone is the reason that the copper material has a high level of thermal conductivity, which generates a relatively low superheating during boiling when thermal power input is same [32]. In a word, copper was selected for safety consideration. The copper boiling surface was 30 mm × 30 mm. Cartridge heaters (Figure 3-10), with a 225-W power rating per heater, provided heat from the top of the test sections. Three apertures toward the bottom of the test sections, spaced at 3-mm intervals, housed the thermocouples. The three K-type thermocouples, with a 0.75% uncertainty, were used to measure the temperature at the center of the test sections. The test section for the honeycomb surface [Figure 3-9(b)] included a 1-mm gap between the copper and PEEK materials that allowed installation of the 1-mm thick honeycomb plate.

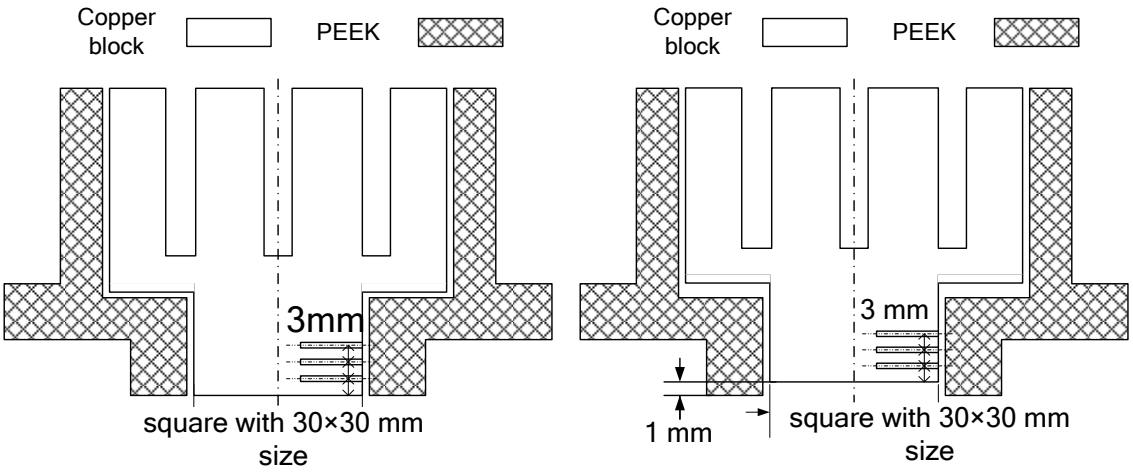

(a) test section for bare case study (b) test section for honeycomb study

Figure 3-9: Schematic figure of test section.

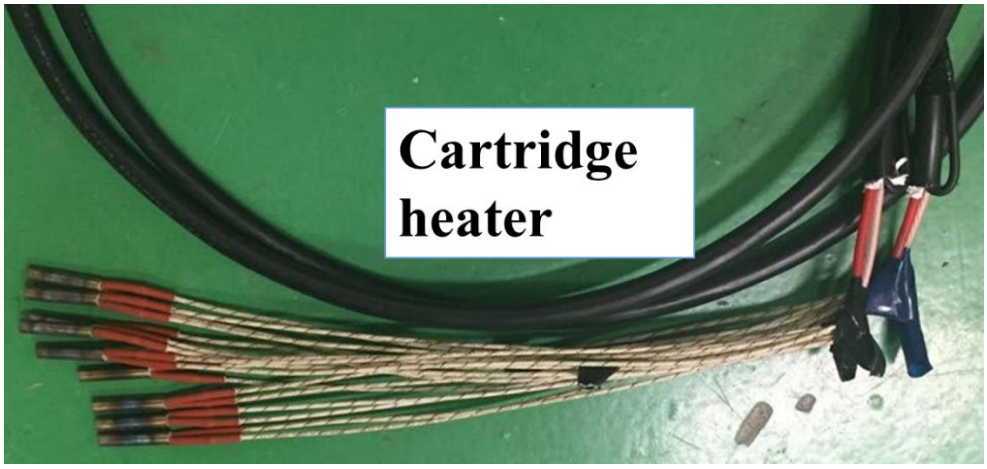

Figure 3-10: Physical picture of cartridge heaters.

Figure 3-11 depicts the test sections for the bare and honeycomb surfaces considered in this study. The boiling area of both surfaces was the same. The honeycomb surface was fabricated from sintered stainless steel. To better understand the pore size effects, honeycomb surfaces with different porosities (0-, 5-, 20-, and 100-μm pore sizes) were considered. Figure 3-12 depicts the test sections for the various honeycomb surfaces considered in this study. Besides, honeycomb structure is another key issue that will be taken into consideration. More specifically, honeycomb structure means hole diameter (defined as *d*, unit mm) and pitch or center distance between two adjacent holes (defined

as Δt, unit mm) (Figure 3-13). In this study, several different combinations of pitch and diameter are list in Table 3-1 and the physical picture of them are shown in Figure 3-14.

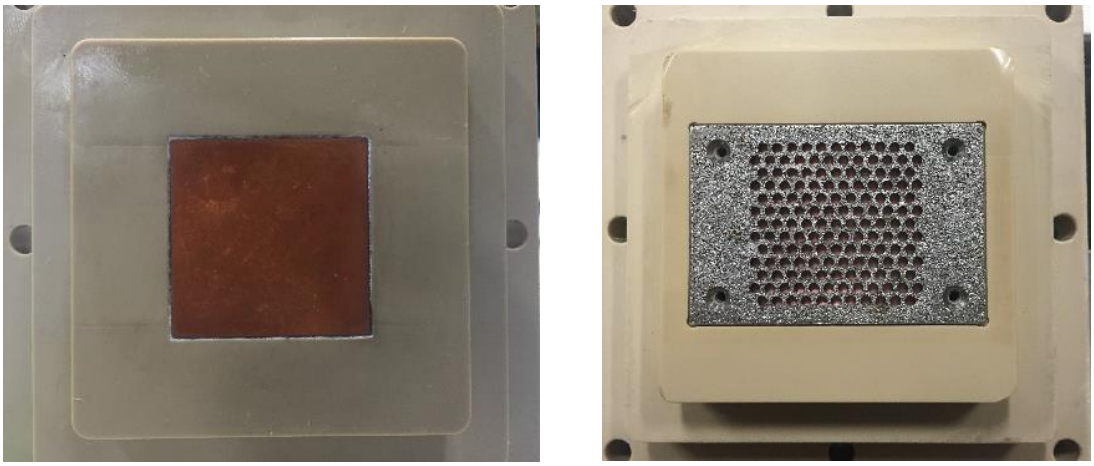

(a) Bare surface (b) Honeycomb structure

Figure 3-11: Different surfaces of test sections.

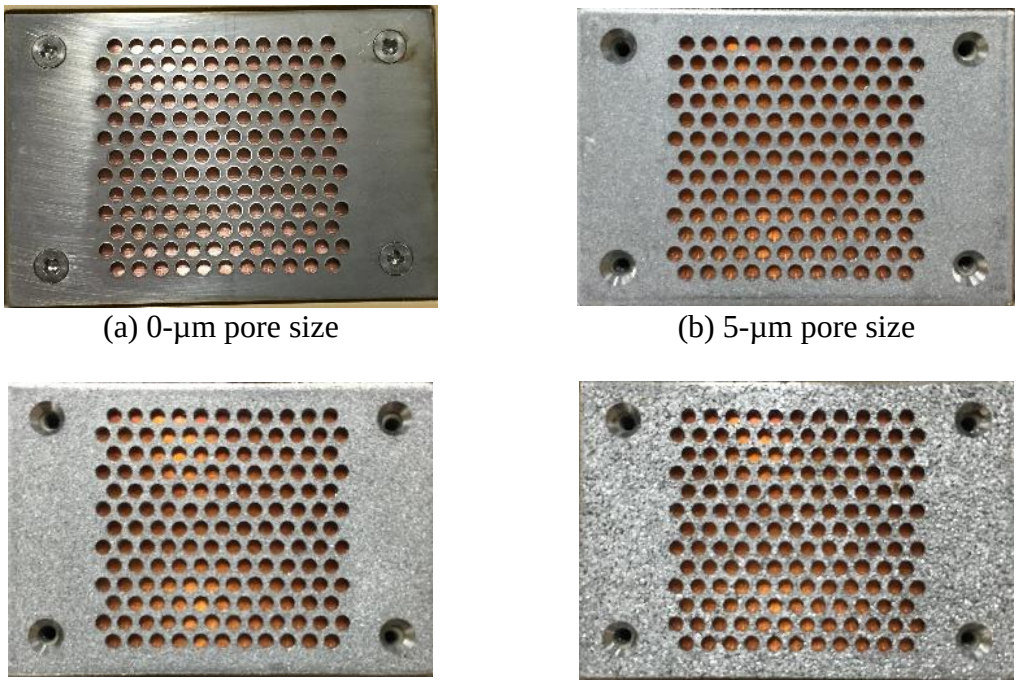

(a) 0-μm pore size (b) 5-μm pore size

(c) 20-μm pore size (d) 100-μm pore size

Figure 3-12: Honeycomb test sections with different porosities.

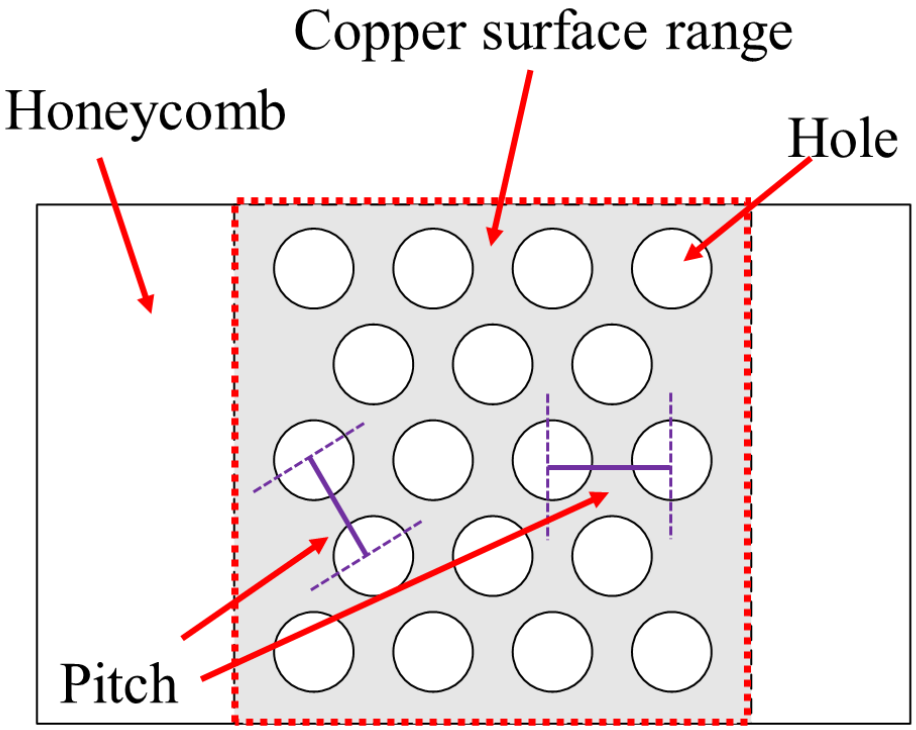

Figure 3-13: Introduction of honeycomb structure.

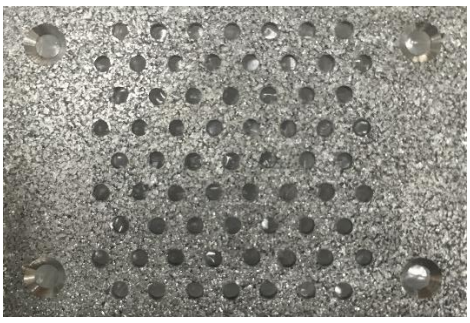

(a) Pitch/diameter, 4.0/1.7

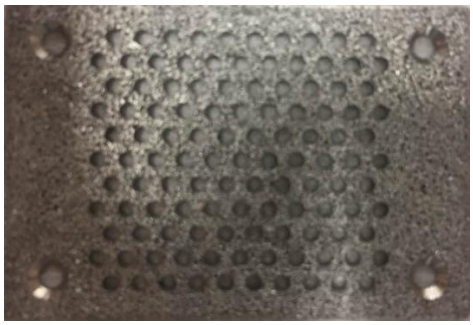

(b) Pitch/diameter, 3.0/1.7

(c) Pitch/diameter, 4.2/2.4

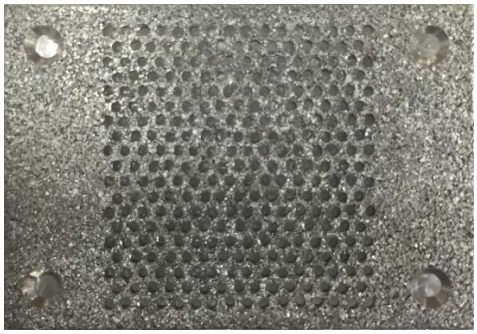

(d) Pitch/diameter, 1.8/1.0

Figure 3-14: Physical picture of honeycomb structure.

(e) Pitch/diameter, 2.5/1.7

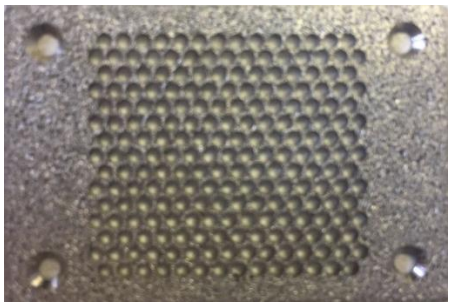

(e) Pitch/diameter, 2.1/1.7

Figure 3-14 (cont): Physical picture of honeycomb structure.

3.2 Irradiation Conditions

In this study, irradiation case is one kind of case that should be considered. The irradiation experiment were performed at the Japan Atomic Energy Agency (JAEA) facility. The copper block was irradiated before the experiments. To understand whether irradiation source has some effect on CHF performance, two different types of sources were chose. That are gamma-ray irradiation and electron-beam irradiation source, respectively. Figure 3-15 shows the setting position of the test sections. In the gamma-ray chamber, the dose rate was 15 kGy/h, and the test sections were placed close to the irradiation source. Based on the irradiation schedule of JAEA, the actual dose ranged from 930–1020 kGy. On the other hand, in the electron-beam chamber, the accelerator was set to 2-MV voltage and 1-mA current input. The test section was positioned 200 mm away from the beam exit. The exact dose rate is approximate 100 kGy/min. The thermocouples and PEEK were shielded from direct irradiation using protective covers. Because the gamma rays and electron beam were emitted in different directions (horizontal and vertical, respectively), the set-up was a little different. Based on dose rate given by JAEA, dose amount is only determined by irradiation time interval.

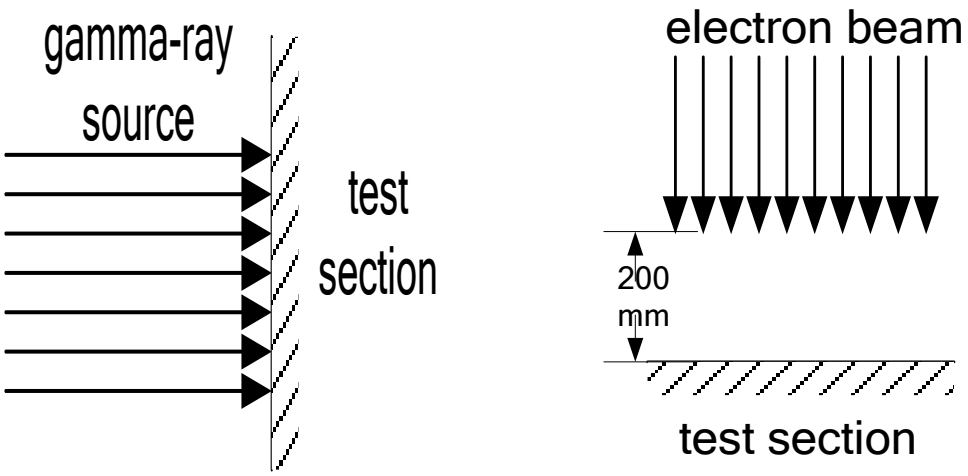

(a) Gamma-ray irradiation room (b) Electron-beam irradiation room

Figure 3-15: Facility set-up in different irradiation rooms.

3.3 Experimental Conditions

In this section, experimental conditions will be explained. According to key words suggested in last chapter, many factors, such as inclination, irradiation source, irradiation dose, honeycomb plate with different pore size, different types of honeycomb structure and so on were introduced. However, there were some common experimental conditions in all these cases. Thus, in the following explanation, the common static experimental conditions will be given and then the independent condition based on factors will be explained later.

3.3.1 Static experimental condition

Static experimental conditions means these were constant during whole experiment of all cases. Here it mainly contained conditions of pressure, water temperature, boiling area and light intensity of powerful lamp. Details are list in the following Table 3-1.

Table 3-1: Static experimental conditions in all cases.

Experimental parameters	Conditions
Water temperature	100ºC
Boiling area	30 × 30 mm in square
Pressure	Atmospheric, 101325Pa

3.3.2 Other experimental conditions (variable conditions)

In this study, the following conditions were taken into consideration according to current goal explained in Chapter 2. These were test section, inclination, porosity of honeycomb, honeycomb structure, irradiation dose and irradiation source. Some experiments were done with only one variable. Others were done with combination of several variables. For clear understanding, all cases were categorized based on experiment aim.

3.3.2.1 Bare surface cases

These cased were treated as controlled one, which will be compared with the results by using some surface modification methods. Besides, in bare surface cases the factor inclination were taken into consideration. As such, details of experimental conditions are list in Table 3-2.

Table 3-2: Test cases with bare surface.

Test cases	Inclination [º]
1	5
2	10
3	20

3.3.2.2 Honeycomb surfaces

Honeycomb surface is one kind of surface modification, which was used in this study to test whether CHF could be enhanced. Considering that honeycomb surface contains many variables and for better understanding honeycomb effect on CHF performance, the following parameters were carried on. Meanwhile, a mount of parameters would make experiment redundant. Thus, one basic honeycomb case would be chosen for comparison

in all honeycomb study. Here, the basic honeycomb case was that pore size 100-μm, diameter of hole 1.7 mm, pitch 2.5mm and inclination 5º.

- Pore size effect study

Honeycomb surface with different porosity (0-, 5-, 20-, and 100-μm pore sizes) were considered for two aims. One is to verify whether honeycomb surface had effect on CHF enhancement. The other one is to see if there is some variation when porosity is different. Table 3-3 lists honeycomb surface cases with different porosity.

Table 3-3: Honeycomb surface cases with different porosity.

Test cases	Pore size [μm]	Structure ($\Delta t/d$)	Inclination [º]
4	0	2.5/1.7	5
5	5	2.5/1.7	5
6	20	2.5/1.7	5
7	100	2.5/1.7	5

- Inclination effect study

In bare surface case, CHF variation along inclination was one target. For better comparison, inclination effect would also be done. Table 3-4 lists honeycomb surface cases with different inclination.

Table 3-4: Honeycomb surface cases with different inclination.

Test cases	Pore size [μm]	Structure ($\Delta t/d$)	Inclination [º]
7	100	2.5/1.7	5
8	100	2.5/1.7	10
9	100	2.5/1.7	20

- Honeycomb structure study

As it was shown in previous study, structure is one issue that could affect CHF performance [33-35]. As such, it is believed that honeycomb structure (it means pitch and diameter) may has similar effect on CHF variation. Table 3-5 lists honeycomb surface cases with different structure.

Table 3-5: Honeycomb surface cases with different structure.

Test cases	Pore size [μm]	Structure ($\Delta t/d$)	Inclination [°]
7	100	2.5/1.7	5
10	100	4.0/1.7	5
11	100	4.2/2.4	5
12	100	3.0/1.7	5
13	100	1.8/1.0	5
14	100	2.1/1.7	5

3.3.2.3 Irradiation study

In this study, both gamma-ray and electron-beam irradiation source were selected and irradiation experiments on both bare surface and honeycomb surface were carried on. To better understand irradiation effect on CHF performance, the following cases were categorized based on surface type of test section.

- Bare surface

Here, we supposed to observe CHF variation according to dose amount factor and inclination factor. The details are list in Table 3-6.

Table 3-6: Irradiation study on bare surface with different dose amount and inclination factor.

Test cases	Dose source	Dose amount [kGy]	Inclination [°]
15	Gamma-ray	1000	5
16	Electron-beam	300	5
17	Electron-beam	1000	5
18	Electron-beam	3000	5
19	Electron-beam	1000	10
20	Electron-beam	1000	20

- Honeycomb surface

The aim for doing honeycomb surface experiment by irradiation is similar with bare surface by irradiation. One difference is that, in these cases both two surface modification methods were combined in one experiment. The aim was to clearly understand whether combination has positive effect on CHF enhancement. Experiment cases are list in Table 3-7.

Table 3-7: Irradiation study on honeycomb surface with different dose amount and inclination factor.

Test cases	Dose source	Dose amount [kGy]	Inclination [°]
21	Gamma-ray	1000	5
22	Electron-beam	1000	5
23	Electron-beam	1000	10
24	Electron-beam	3000	10
25	Electron-beam	1000	20

3.4 Experimental Procedures

This section is one brief introduction of experimental procedures. It mainly contains about two parts, preparation before experiment and manipulation during experiment.

- Preparation before experiment

During preparation, such things should be done. a) Polish test section surface; b) Heat up water to saturated condition; c) Install facility (camera position set, condenser and so on) and connect signal cable (to record temperature); d) Degasing. Among them the important part is to polish test section surface, and details will be given in Appendix.

- Manipulation during experiment

There are two different manipulations during experiment. One is for steady state. The other one is for unsteady state (or called as CHF state). When experiment started, set thermal power of cartridge heater to one certain value and then waited until temperature got steady. Basically, when temperature had small fluctuation in 2 minutes it was r that boiling reached steady stage. Then recorded boiling phenomenon and further increased thermal power. However, temperature may become unsteady and increased suddenly (Figure 3-16) at some thermal power input. At this time, it meant CHF is appearing. The operation response to it is to quickly shut down thermal power and record boiling phenomenon.

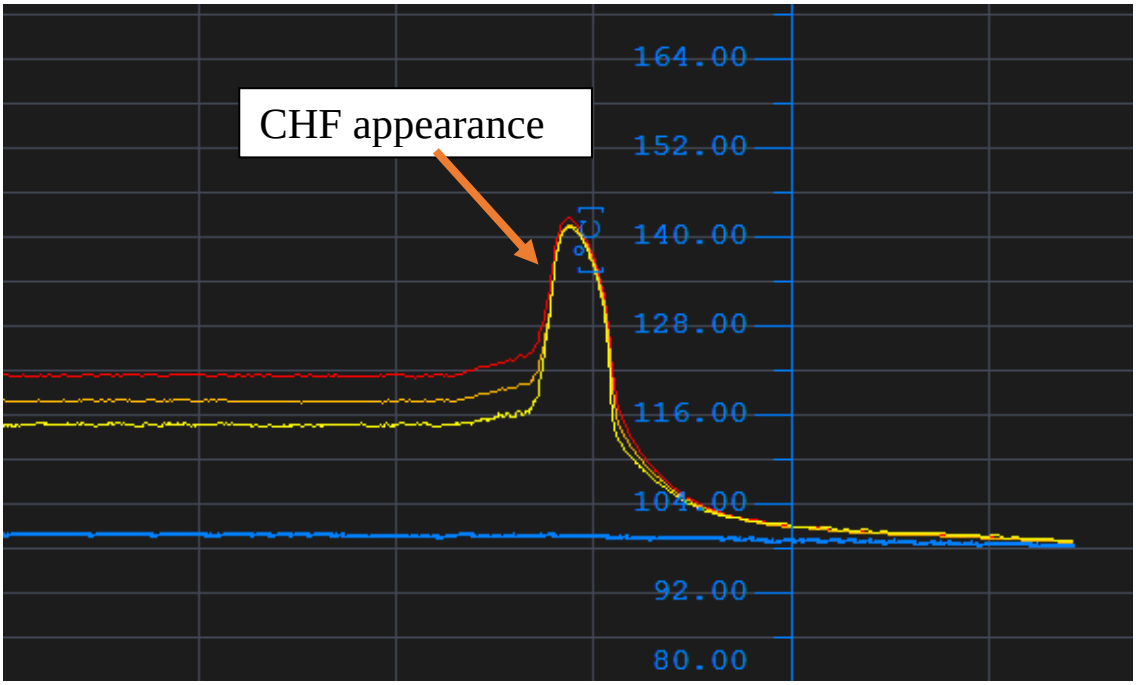

Figure 3-16: Definition of CHF appearance during data acquisition.

3.5 Heat Flux Calculation and Error Analysis

For each of the test cases considered in this study, we calculated the heat flux (q), superheat (ΔT), and heat transfer coefficient (h). For the temperature and interval distance, the least squares method was used to obtain an optimum linear curve, where the slope (dT/dx) was subsequently multiplied by the thermal conductivity (k) to calculate the heat flux (q) as follows:

$$q = k\, dT/dx \tag{2-1}$$

The heat transfer coefficient (h) was calculated as follows, where the y-intercept from the least squares curve determined the superheat (ΔT):

$$h = q/dT \tag{2-2}$$

Each of these parameters were assumed independent, so their respective standard deviations (Δq, $\Delta(\Delta T)$, and Δh) were determined as follows [36]:

$$\Delta q = \sqrt{\frac{s^2 n_{TC}}{\Delta}} \quad (2\text{-}3)$$

$$\Delta(\Delta T) = \sqrt{\frac{s^2 \sum T_i^2}{\Delta}} \quad (2\text{-}4)$$

$$\Delta h = \sqrt{(\frac{\partial h}{\partial(\Delta T)}\Delta(\Delta T))^2 + (\frac{\partial h}{\partial q}\Delta q)^2} \quad (2\text{-}5)$$

where the variable (s) and (Δ) were calculated as follows:

$$s = \sqrt{\frac{1}{n_{TC}-2}\sum[y_i - (bx_i + a)]^2} \quad (2\text{-}6)$$

$$\Delta = n_{TC}\sum x_i^2 - (\sum x_i)^2 \quad (2\text{-}7)$$

and *Ti*(*yi*) was the temperature at different locations, *xi* was the interval distance from the boiling surface, and n_{TC} was the number of temperature measurement points (three thermocouple positions).

Using Eq. (2-3), Table 3-8 lists the estimated uncertainty of the CHF values measured during experimentation as a function of surface type and inclination angle. The maximum uncertainty values observed during experimentation considered in this study are listed.

Table 3-8: Estimated uncertainty of the CHF values measured during the downward-facing pool boiling experiments.

Irradiation source	Type of test section	Uncertainty
Non-irradiation	Bare surface	4.9%
Non-irradiation	Honeycomb plate	2.7%
Gamma ray	Bare surface	14.6%
Gamma ray	Honeycomb plate	13.6%
Electron beam	Bare surface	16.5%
Electron beam	Honeycomb plate	14.2%

4. Bare Surface Discussion

In this chapter, bare surface experiment discussion is carried on. The aim of doing bare surface cases is as follows: a) First, experiment data in this study should be reliable because the data would be used for future comparison; b) Then, these cases were treated as controlled experiment, which would be used for comparison with experiment results by using surface modification (honeycomb surface and irradiation method for example); c) Inclination effect is supposed to be test in this study.

Based on this, work flow will be: 1) Do bare surface experiments and calculate CHF results; 2) Analyze boiling phenomenon to clearly understand boiling cycle; 3) Introduce one parameter to explain the reason for CHF appearance and find ways to enhance CHF value; 4) After experiments and analysis, a brief summary will be given.

Some contents of this chapter have already been published. [31]

4.1 Experiment Results

4.1.1 Experimental Facility and Conditions

Figure 4-1 shows the corresponding experimental facility. As it is shown, bare surface is chosen as test section. At the bottom of support, one block is utilized to tilt facility to realize the aim of bare surface inclination. Here the changed inclination will be 5º, 10º and 20º, respectively. Boiling pressure is under atmospheric condition, water temperature is 100ºC and the boiling area is 30 × 30 mm in square.

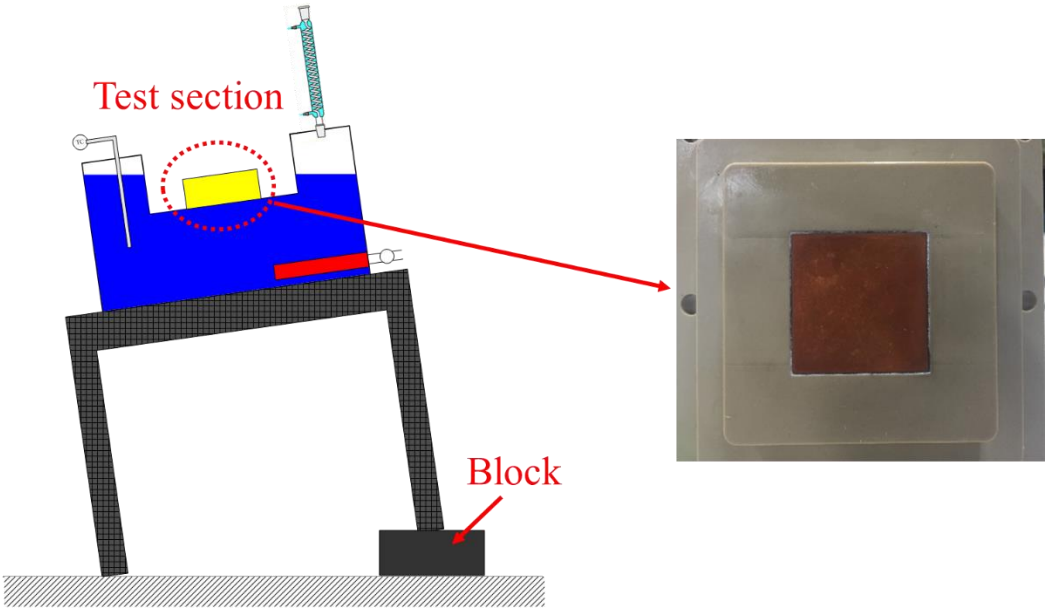

Figure 4-1: Experimental facility in bare surface cases.

4.1.2 CHF Results and Comparison

Table 4-1 lists the CHF values measured during the downward-facing pool boiling experiments for the bare surface test cases as a function of inclination. Each test case was evaluated twice to enhance data reliability. The results reflect the mean CHF value from the two tests. For a modest inclination of 5°, the CHF was 0.25 MW/m^2. As the inclination increased, the CHF increased. The CHF value for a 20° inclination was twice the CHF value for the 5°. The CHF values for 10° and 20° inclinations were not significantly different. Figure 4-2 shows the heat flux as a function of superheating (i.e., boiling curves) for each of the two tests involving the three bare surface test cases. As it is shown in this figure, when heat flux is same, the superheating of each case is similar.

Table 4-1: Measured CHF in downward-facing pool boiling experiments for the bare surface test cases.

Test case	Surface type	Inclination [°]	CHF [MW/m^2]	Enhancement
1	Bare	5	0.25	0%
2	Bare	10	0.47	88%
3	Bare	20	0.50	100%

Note: Enhancement means the increased percentage compared with test case 1.

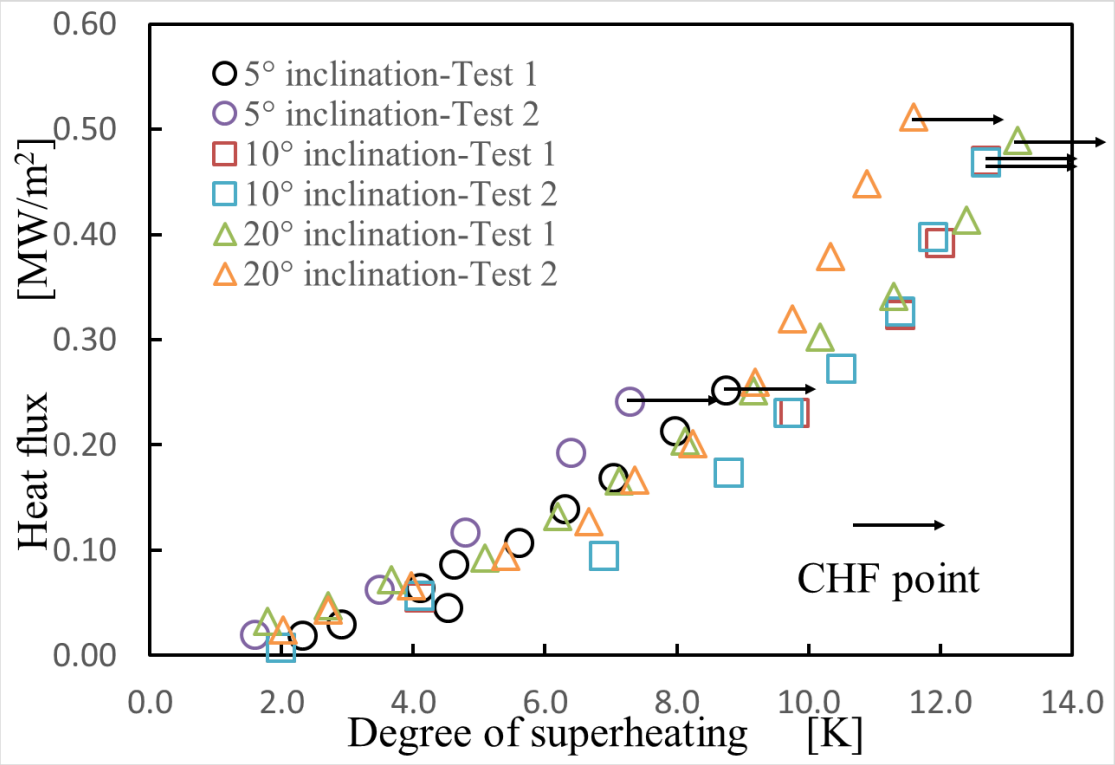

Figure 4-2: Heat flux as a function of superheating (i.e., boiling curves) for bare surface test cases with different inclinations.

Because the bare surface data will be used for future comparison, the first thing need to be done is to prove the reliability. El-Genk and Guo [37-38] had researched boiling of inclined and downward-facing surface in a saturated pool. In their study, a circular copper surface with 50.8 mm in diameter was used as one heating surface and 0º (downward-facing), 5º, 10º, 15º, 30º, 45º and 90º (vertical) were investigated. After several experiment, they gave one empirical equation (3-1) [39-40] and suggested that CHF value is a function of inclination angle.

$$q_{CHF}(\theta) = C_{CHF}(\theta)\sqrt{\rho_v}h_{fg}[\sigma g(\rho_l - \rho_v)]^{0.25} \quad (3\text{-}1)$$

$$C_{CHF}(\theta) = 0.034 + 0.0037\theta^{0.656} \quad (3\text{-}2)$$

Where, q_{CHF} means critical heat flux [W/m^2]; θ, surface inclination angle [º]; C_{CHF}, coefficient at CHF point; ρ_v, saturated vapor density [kg/m^3]; h_{fg}, latent heat of vaporization [J/kg]; σ, surface tension [N/m]; ρ_l, saturated liquid density [kg/m^3].

Figure 4-3 shows the comparison of data in this study and data from Genk. As it is shown, the blue curve means empirical equation proposed by Genk, the green square means experimental data from Genk and results in this study are shown in purple dot. From comparison, CHF results in this study fit the curve well, which means this data can be used for future comparison.

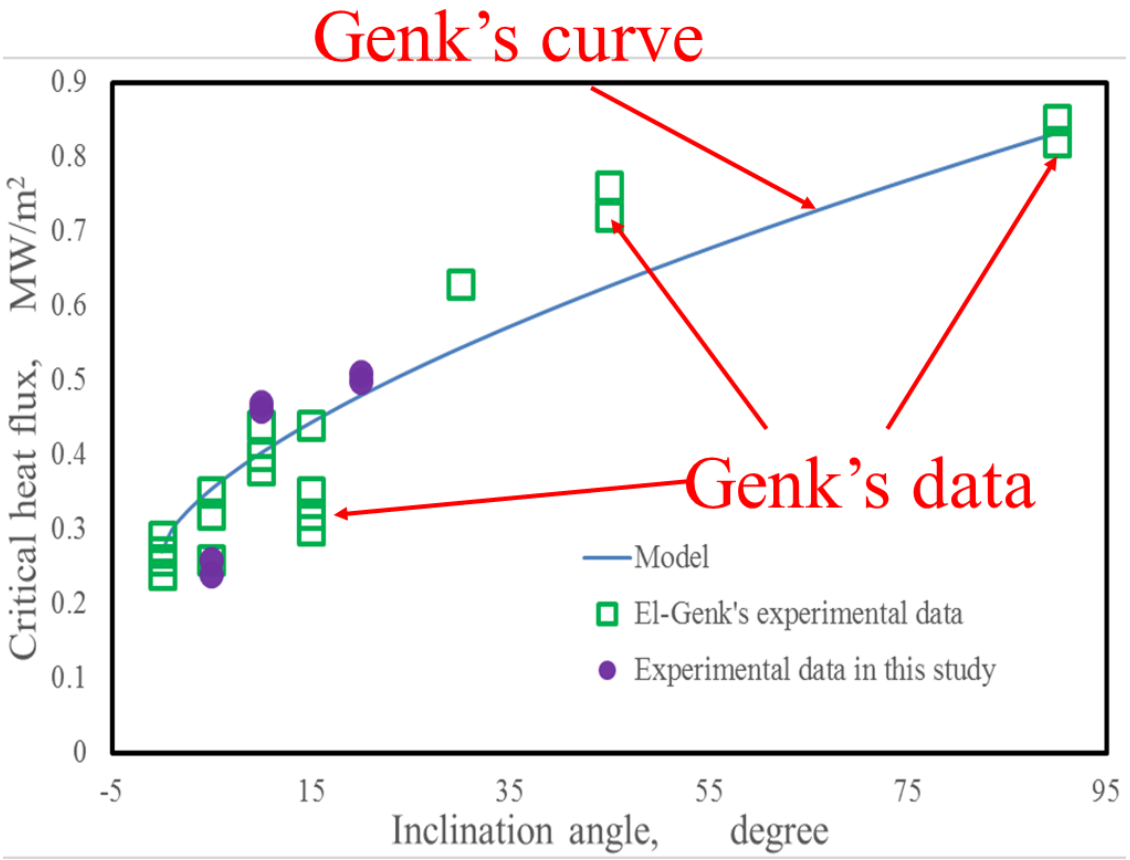

Figure 4-3: CHF comparison between data in this study and results from Genk.

4.2 Boiling Phenomenon

From comparison, it is found CHF is function of inclination and experiment data is reliable. Thus, next step is try to clearly understand the CHF enhancement by inclination. Before going further, the boiling phenomenon should be understood first.

To begin with, snapshots of one case with different heat flux will be given. From video observation, boiling phenomenon is similar in case 1-3 so that only snapshots in 5º (case 1) will be list in Figure 4-4. As it is shown, when heat flux is low some separate bubbles (like [Figure 4-4 (a-b)]) are generating on copper heating surface and then moves upward due to inclination. Then when thermal power input is increased, many bubbles will generate on heating surface. Because of the large quantities, some close bubbles will combine into a big bubble (like [Figure 4-4 (c-d)]). In Figure 4-4 (e-f), the heat flux is largely increased so that bubble generation becomes heavily. At the bottom of copper heating surface, the separate bubbles has already formed into a large vapor film, covering some local area. It only provides heating surface with a limited space for water refluxing and bubble generation. From these snapshots, it is obviously that copper surface occupied by vapor film (or bubble) becomes large as the heat flux increases.

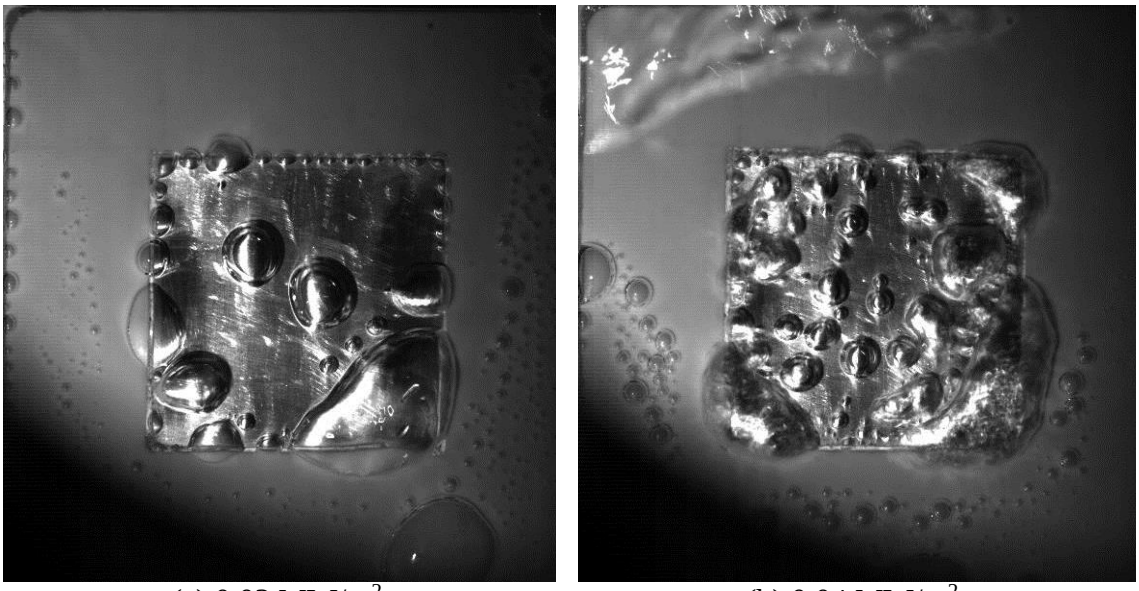

(a) 0.03 MW/m^2 (b) 0.04 MW/m^2

Figure 4-4: Snapshots of boiling phenomenon under different heat flux in case 1

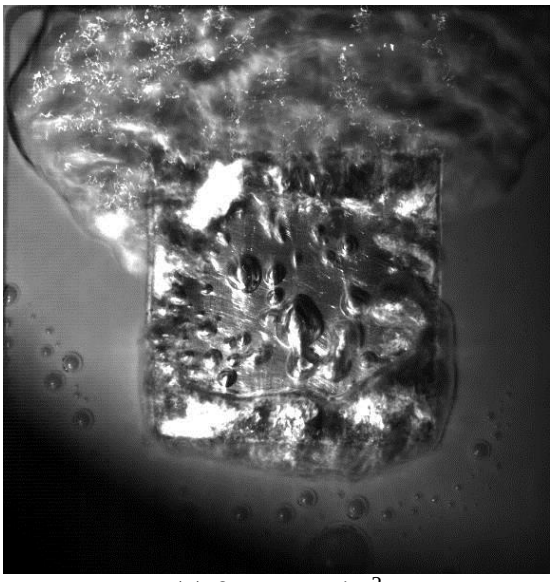

(c) 0.12 MW/m^2

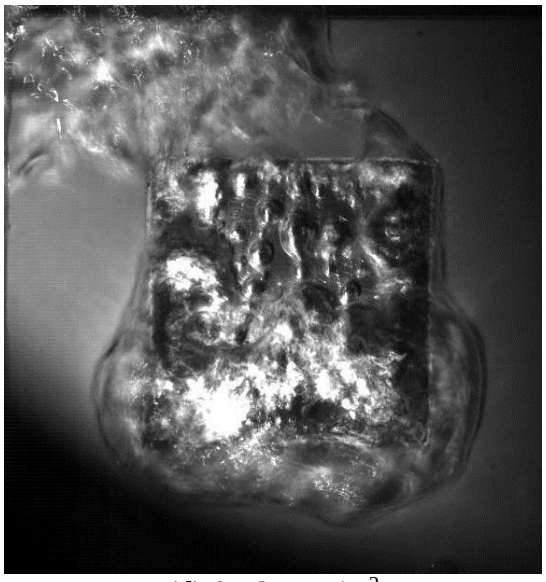

(d) 0.16 MW/m^2

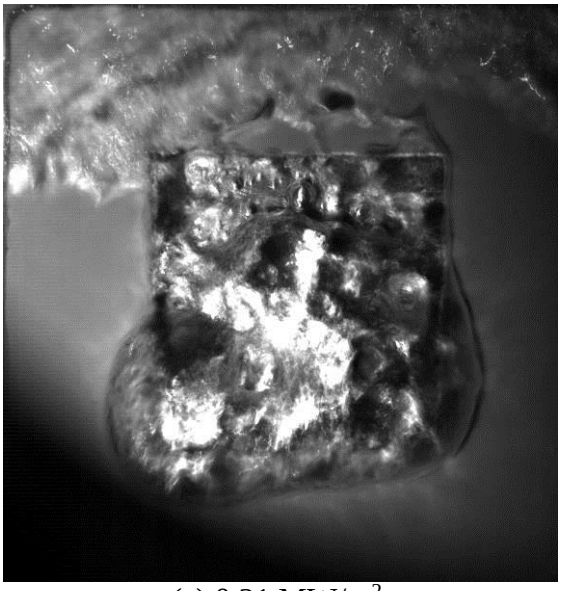

(e) 0.21 MW/m^2

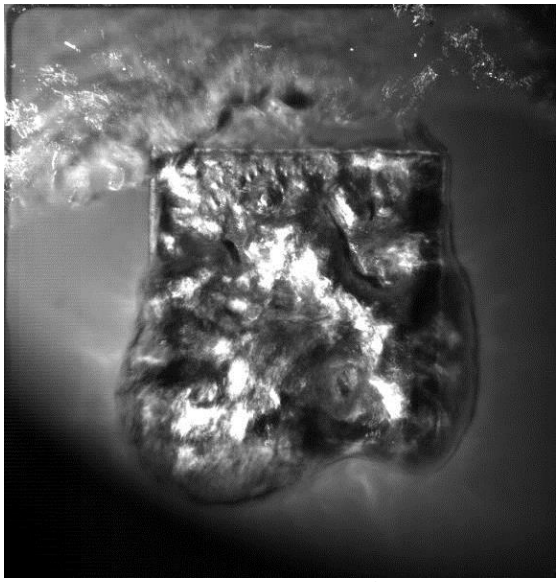

(f) 0.28 MW/m^2

Figure 4-4 (cont): Snapshots of boiling phenomenon under different heat flux in case 1.

After observing snapshots of boiling phenomenon with different heat flux, the focus moves to observe all boiling stages in one certain heat flux because it is found that the boiling process carried on with periodic circulation, especially in high heat flux. Thus, the next step is try to analyze this periodic circulation. Here, heat flux is set as 0.21 MW/m^2 and boiling stages are shown in Figure 4-5. Using image processing, three stages of the boiling process were identified: (1) vapor cover, (2) coexistence, and (3) new bubble

generation. The copper boiling surface is outlined in red (the remaining area is the PEEK). During the vapor cover stage [Figure 4-5(a)], the copper surface was completely covered in a bubble film. However, localized areas on the copper surface had a liquid-vapor mixture, which prevented initiation of the CHF (This liquid-vapor mixture area will be explained later). In these areas, a form of nucleate boiling occurred that resulted in a higher level of water replenishment (or water refluxing) on the copper surface, preventing surface dryout (the heat flux becomes critical at this point). With surface inclination, the bubble film slid along the copper surface from bottom to top. During the coexistence stage [Figure 4-5(b)], the bubble film formed during the vapor cover stage and new bubbles coexisted on the copper surface. The blue line in Figure 4-5(b) approximates the boundary between the two bubble generation stages. During the new bubble generation stage [Figure 4-5(c)], the original bubble film moved completely off the copper boiling surface (outlined in red), making room for new bubble generation. Initially, small bubbles that formed at the bottom coalesced into larger bubbles, while small bubbles that formed at the top remained separate. Eventually, all of the bubbles grew and coalesced into a single bubble film that covered the entire copper surface; this phenomenon marked the end of a single boiling process cycle and a return to the initial vapor cover stage.

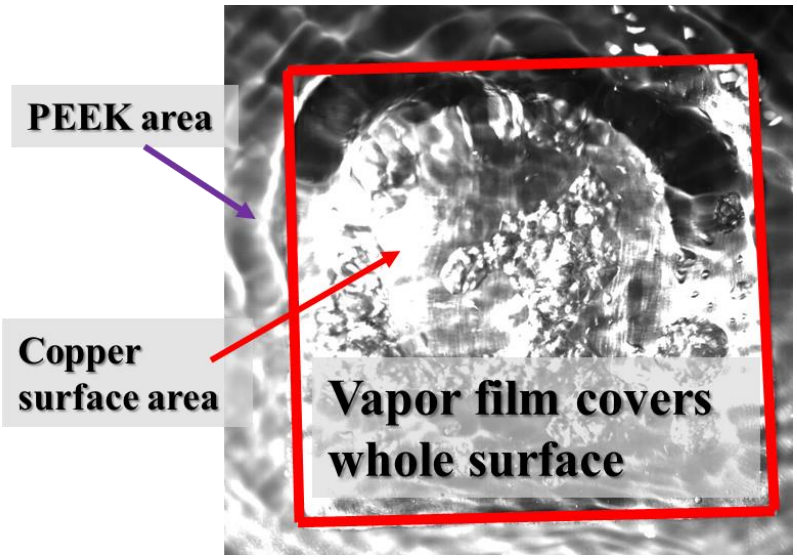

(a) Vapor cover

Figure 4-5: Three stages of the boiling process.

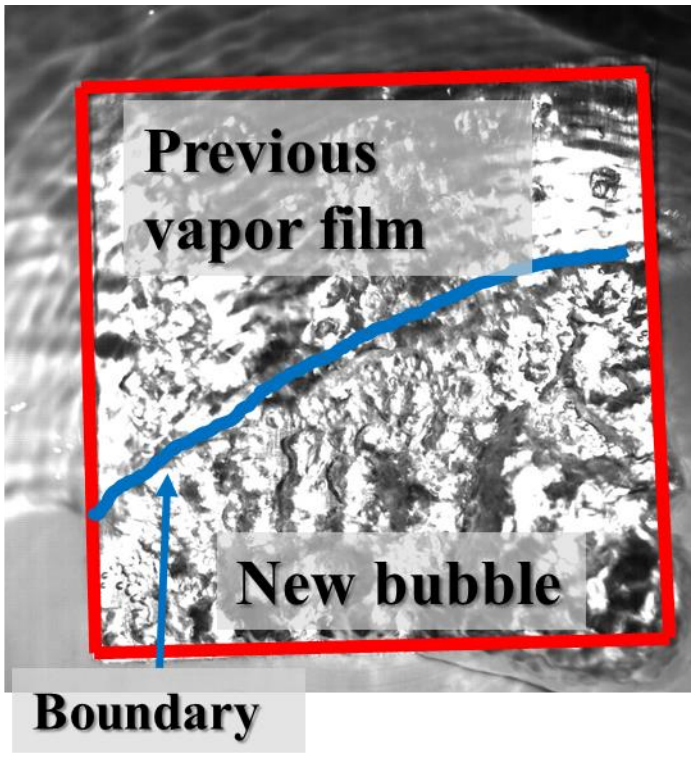

(b) Coexistence

(c) New bubble generation

Figure 4-5 (cont): Three stages of the boiling process.

As it is explained in last paragraph, in Figure 4-5 (a) stage, CHF didn't appear because of the existence of liquid-vapor mixture area, which could provide heating surface with a high level of water replenishment. However, at CHF point, heating surface was totally covered by vapor film, which means there is no space for water cooling (Figure 4-6). This caused one worse heat transfer condition and resulted in a sharp temperature increase (like temperature rise in Figure 3-16).

The formation of the liquid-vapor mixture area is explained in Figure 4-7 [31]. As it is shown, the grey means bubbles and blue parts are regarded as the coolant. In the beginning, the coolant can only vaporize at some local areas, and the vapor get together to become a huge bubble after vaporization. Next, these large bubbles keeps growing corresponding to the continuous heat input. During this period, the bubbles locating at far distance from the surface can easily expand in the horizontal direction whereas the coolant close to the surface can restrain bubble growth and inertial force of bubble generation from the heat input in g (gravity) direction. When bubbles combine at a remote place away from the surface, a large vapor film forms and encloses the coolant [31]. Therefore, the coolant can only vaporize at the original place, where the mixture of vapor and liquid is observed (Figure 4-6).

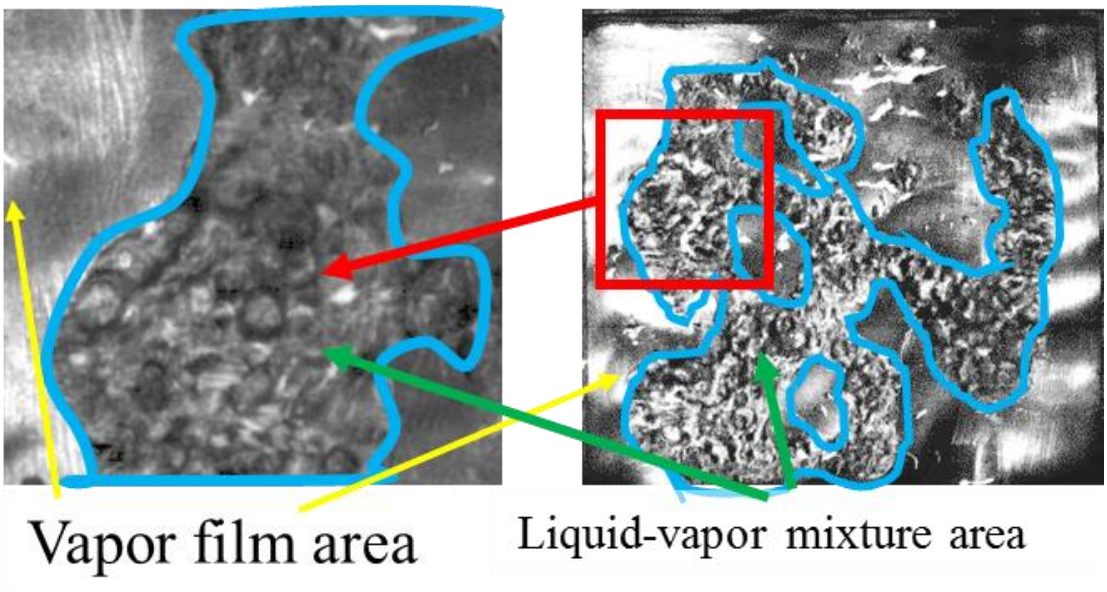

(a) Liquid-vapor appearing on heating surface

(b) Vapor fully covering heating surface

Figure 4-6: Different covering condition on heating surface [31].

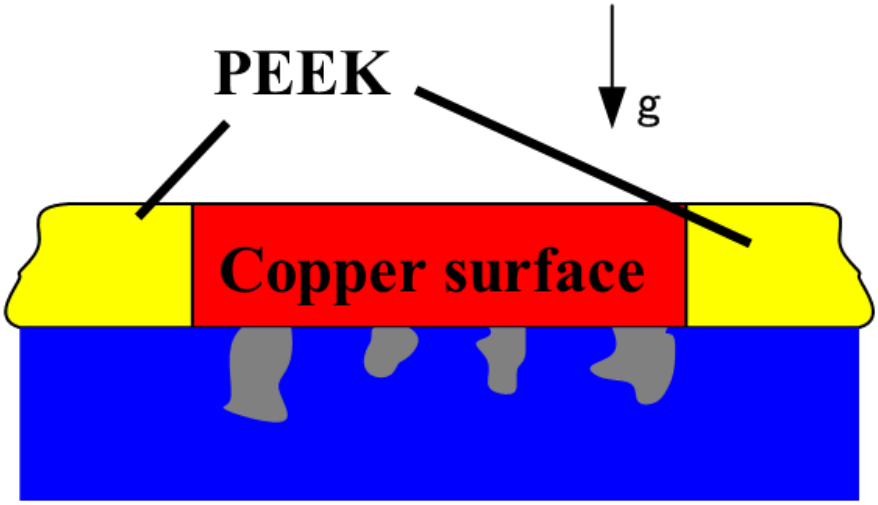

(a)

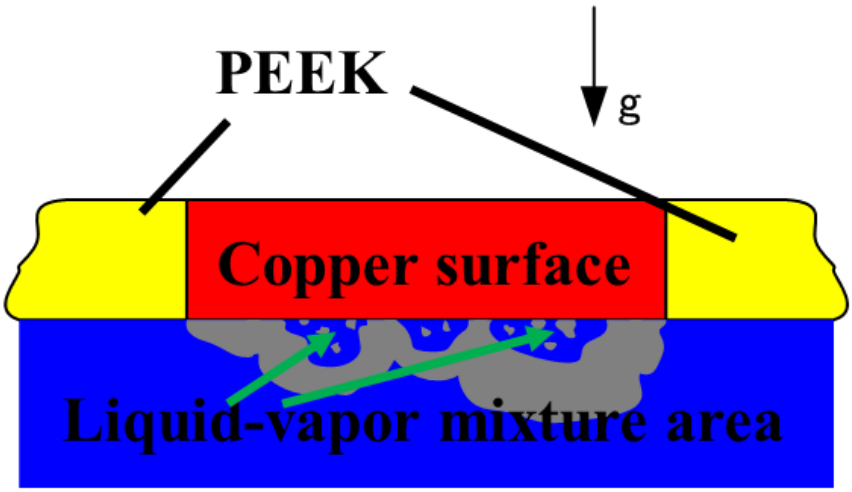

(b)

Figure 4-7: Formation of liquid-vapor mixture area [31].

4.3 Bubble Departure Frequency

In prior studies, CHF enhancement in pool boiling is as a result of these effects: (a) extended surface area, (b) nucleation site density, (c) wettability, (d) capillary wicking, and (e) wavelength crease based on the modified Zuber hydrodynamic stability model [41]. However, another effect is considered to affect CHF performance in this study. As it is explained in last section, in downward-facing pool boiling, heating surface was covered by

vapor film for some time during one boiling cycle at a high heat flux. This vapor film prevented water from approaching heating surface. Thus, one method to enhance CHF in bare surface case is to try to increase the water replenishment time during boiling, which means vapor film departure speed should be improved.

According to explanation, a new parameter is introduced, called bubble departure frequency (BDF). However, boiling condition is proceeded in advance. That is BDF is defined under the condition that heating surface is covered by only one big bubble (or vapor film) at some time during boiling period and then moving outside heating area, which is against bubble behavior at low heat flux that separate and small bubbles moving away from heating surface independently instead of getting together into one big bubble (Figure 4-8).

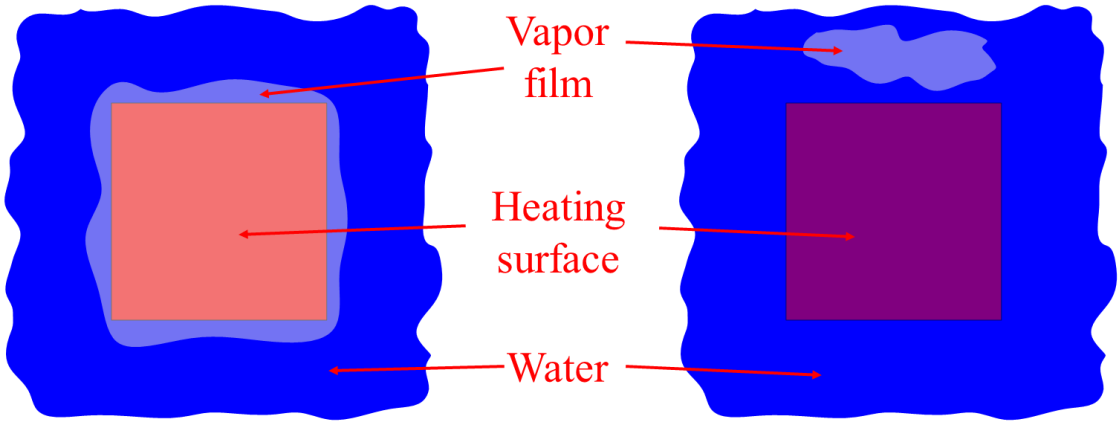

Figure 4-8: Condition for the definition of bubble departure frequency.

In this study, the BDF, expressed as the number of bubbles completed in one second [bubble/s], was calculated using the video images captured during experimentation. To enhance data reliability and precision, a minimum of 100 cycles were included for calculation. Here the BDF is used to assess bubble escaping rate (speed escaping from heating surface). More specifically, if the BDF value is bigger, it means bubble removal speed is rapid, resulting in a high level of water replenishment. Table 4-2 and Table 4-3 list different BDF of case 1-3 under similar heat flux and different BDF of case 2 and 3 near their respective CHF value, respectively. From Table 4-2, it is found that BDF shows different value as inclination angle changes. At a 5° inclination, the BDF was 4.1 bubble/s. The BDF increased as inclination increased, suggesting an increased bubble removal rate,

an increased capacity for water replenishment, and a decreased risk of CHF in a given time interval. That is the reason why CHF under 10º and 20º inclination condition will not appear around 0.25 MW/m^2 (the CHF value of bare case with 5º inclination) and is enhanced in the end. From Table 4-3, it is indicated that BDF between case 2 and 3 is small, which results in a close CHF value in these two inclination angle cases. Besides, from these two tables, BDF is largely increased, indicating a step increase in CHF value from 5º to 10º and 20º inclination angle case.

Table 4-2: Different BDF of case 1-3 under similar heat flux.

Test case	Inclination [º]	Heat flux [MW/m^2]	BDF [bubble/s]
1	5	0.25	4.1
2	10	0.23	6.6
3	20	0.26	7.6

Table 4-3: Different BDF of case 2 and case 3 near their respective CHF value.

Test case	Inclination [º]	Heat flux [MW/m^2]	BDF [bubble/s]
2	10	0.47	6.7
3	20	0.50	7.4

Figure 4-9 shows BDF value with different heat flux in both case 1 and case 2. As it is suggested BDF value is constant, regardless of heat flux, meaning that the BDF value is function of inclination angle. Because BDF can determine the final CHF value, it is concluded that CHF value is a function of inclination angle.

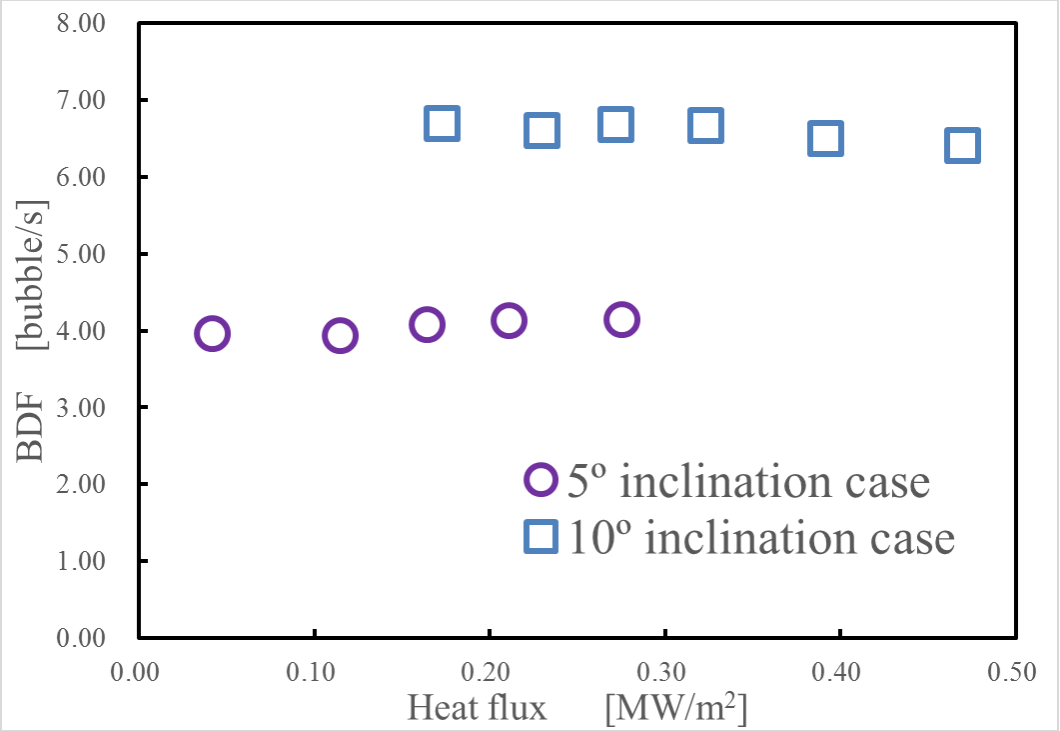

Figure 4-9: The BDF value with different heat flux in case 1 and case 2.

4.4 Chapter Summary

In this chapter, some bare surface cases are discussed, considering the inclination angle effect. Also, from video analysis, a new parameter named BDF is introduced. Then the summary is as follows.

- CHF value is a function of inclination, which means CHF goes higher when inclination angle is large.
- BDF is related to CHF performance. This is because if BDF is larger, bubble escaping rate is more rapid. Surface replenishment condition is better, which can provide surface with more water in unit time. So CHF enhances.

5. Honeycomb Surface Discussion

In this chapter, honeycomb surface experiment discussion is carried on. As one CHF enhancement method, the validity should first be confirmed. Here, solid and porous honeycomb case were used for comparison with bare surface case to clearly understand the theory of surface modification. Then, some other parameters, pore size, inclination, honeycomb structure in this study, were added to quantitatively analyze surface modification effect on CHF variation.

Based on this, work flow will be: 1) Do CHF experiments considering all cases list in chapter 3 and understand boiling phenomenon of honeycomb surface; 2) Analyze temperature distribution on the heating surface based on prior research; 3) Construct one model to explain CHF variation, including the factors that suggested in all cases; 4) After experiments and analysis, a brief summary will be given.

5.1 CHF Results and Preliminary Discussion

In this section, four different types of discussion will be taken. First, the comparison between honeycomb surface and bare surface is carried on to test whether CHF performance can be promoted. Then, experiments regarding with parameters of honeycomb plate goes after comparison. Here, the parameter will be pore size, inclination and honeycomb structure.

5.1.1 Comparison between honeycomb surface and bare surface

The aim of doing such kinds of experiments is that, 1) To see whether CHF can be enhanced by honeycomb application; 2) To study the porous surface effect compared with solid honeycomb; 3) To understand the reason for CHF enhancement.

The specific facility is shown in Figure 5-1 and experimental condition is list in Table 5-1. Here, inclination angle was only 5º, honeycomb structure (pitch/diameter) was 2.5/1.7 and pore size was 0-μm and 100-μm, respectively.

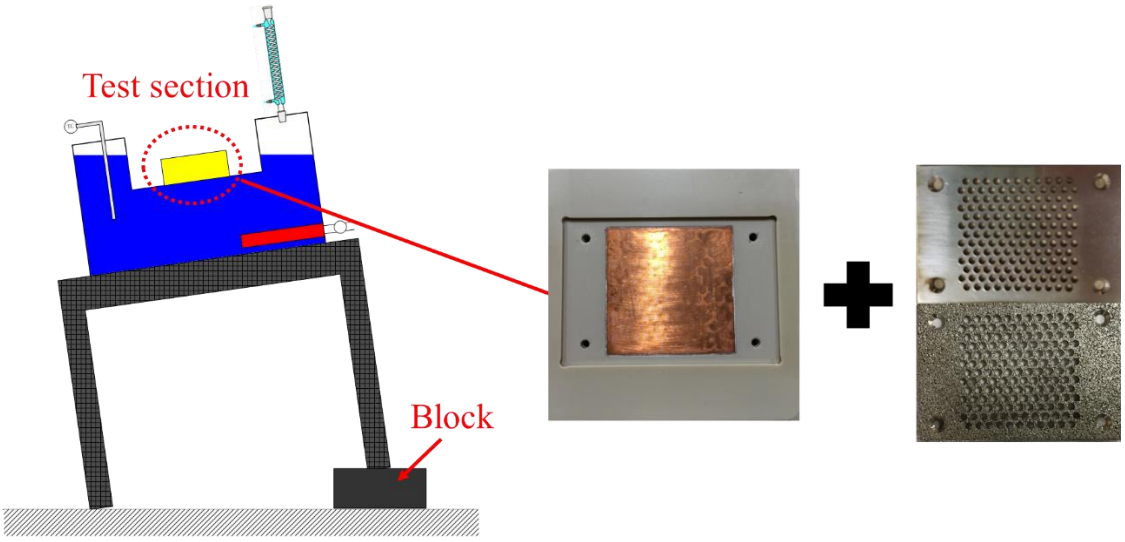

Figure 5-1: Honeycomb surface experiment facility for CHF enhancement.

Table 5-1: Experimental condition in CHF enhancement cases using honeycomb surface method.

Parameters	Value
Pressure	Atmospheric, 101325 Pa
Water temperature	100ºC
Boiling area	30 ×30 mm in square
Inclination angle	5º
Pore size	0- and 100-μm
Pitch/diameter ratio	2.5/1.7

To begin with, solid honeycomb experiment was done. Figure 5-2 shows the heat flux as a function of superheating (i.e., boiling curves) for both honeycomb and bare surface and Table 5-2 lists the CHF values measured during the downward-facing pool boiling experiments. It is obviously that CHF can be largely enhanced by application of honeycomb surface. And porous honeycomb surface can further increased CHF performance compared with solid honeycomb surface. Before understanding the reason for CHF enhancement, boiling phenomenon should first be confirmed. From boiling video, it

is ensured that bubble generation and removal is only from holes, but water refluxing path is still unknown. Thus, the first thing is to determine the path for water refluxing.

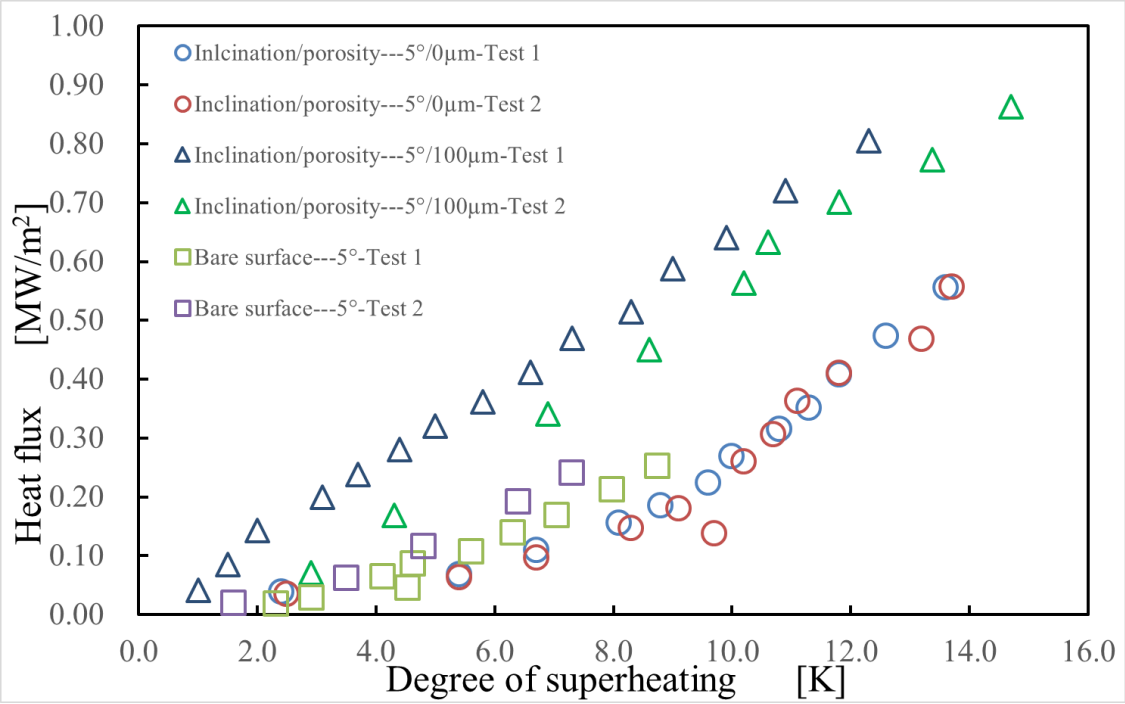

Figure 5-2: Heat flux as a function of superheating (i.e., boiling curves) for both honeycomb and bare surface.

Table 5-2: Measured CHF in downward-facing pool boiling experiments for the honeycomb surface test cases.

Test case	Surface type	Pore size [μm]	Inclination [°]	CHF [MW/m^2]
1	Bare	-	5	0.25
4	Honeycomb	0	5	0.56
7	Honeycomb	100	5	0.83

Figure 5-3 shows the possible ways for water refluxing. As it is shown, there are two potential ways, one is through gap between PEEK and honeycomb plate, the other one is through the edge of holes. So the next step is to make sure which way is correct. In this study, we used silicone to blocks the gap, because silicone was waterproof so that it is ensured that no water would penetrate through it (Figure 5-4). After doing experiment with silicone sealing, the results is shown in Table 5-3. The difference between is very small so that water refluxing through gap is negligible. The only possible way for water refluxing is only through edges of holes.

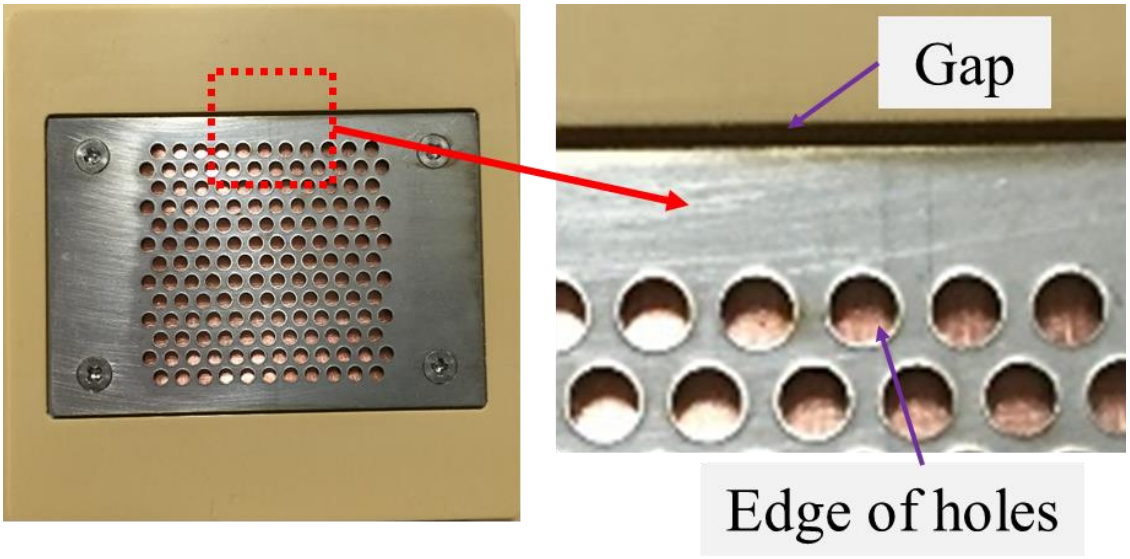

Figure 5-3: Possible ways for water refluxing: gap and edges of holes.

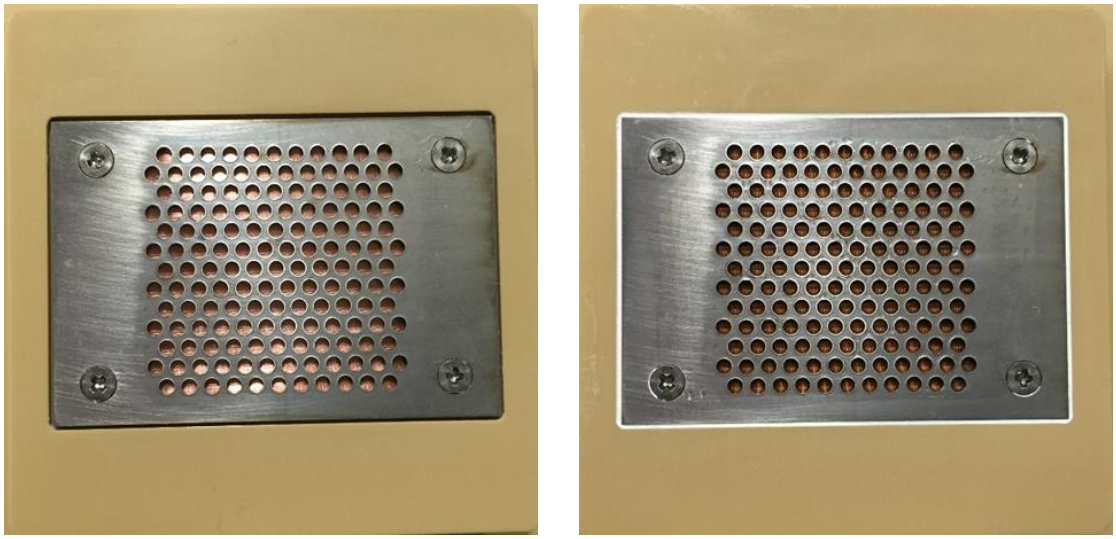

(a) without silicone paste (b) with silicone paste

Figure 5-4: Honeycomb surfaces with/without silicone paste.

Table 5-3: CHF results with/without silicone paste.

With silicone [Y/N?]	Pore size [μm]	Inclination [°]	CHF [MW/m^2]
N	0	5	0.56
Y	0	5	0.50

In test case 4, the honeycomb surface was solid with no porosity (0-μm pore size). Only the holes that formed the honeycomb structure were used as water refluxing and bubble

removal paths; the remainder of the plate was essentially waterproof. The hole-area was relatively small compared to the copper surface area. Nonetheless, the CHF value was substantially higher for test case 4 than test case 1 (the bare surface) at the same 5° surface inclination (0.56 and 0.25 MW/m^2, respectively).

Figure 5-5 provides a schematic of the water refluxing and bubble removal paths for a bare surface (test case 1) and a honeycomb surface with no porosity (0-μm pore size, test case 4). Based on the video image, bubble generation occurred across the entire copper surface in test case 1, leaving only the edges of the copper surface for water refluxing [Fig. 5-5(a)]. In test case 4, the water refluxing accessed the heating surface along the edges of the holes, while the bubbles were removed through the center of the holes [Fig. 5-5(b)]. This type of two-phase flow suggests a decreased liquid-vapor counterflow resistance [21, 30]. A decreased counterflow resistance allows more water to reach the copper surface, which subsequently increases the CHF and ultimately improves cooling effectiveness.

Another reason is regarding with bubble behavior. As it is known in Figure 5-6, in bare surface case, there exist two path for bubble growth, x-direction and y-direction. Due to the buoyance, bubbles easily get bigger along x-direction and collaborate with each other, forming a vapor film covering the heating surface. Under this condition, the heat transfer condition becomes worse. However the circumstance is quite different in honeycomb case. Because of the solid structure, bubbles can only generate in a certain area and growth direction is only through y-direction, which means bubble can easily remove out of heating area, leaving space for water refluxing. Thus, water refluxing is ensured compared with bare surface case. The increased water refluxing amount provided by the honeycomb structure, combined with the decreased counterflow resistance, increased the water refluxing and bubble removal capacities and subsequently increased the CHF.

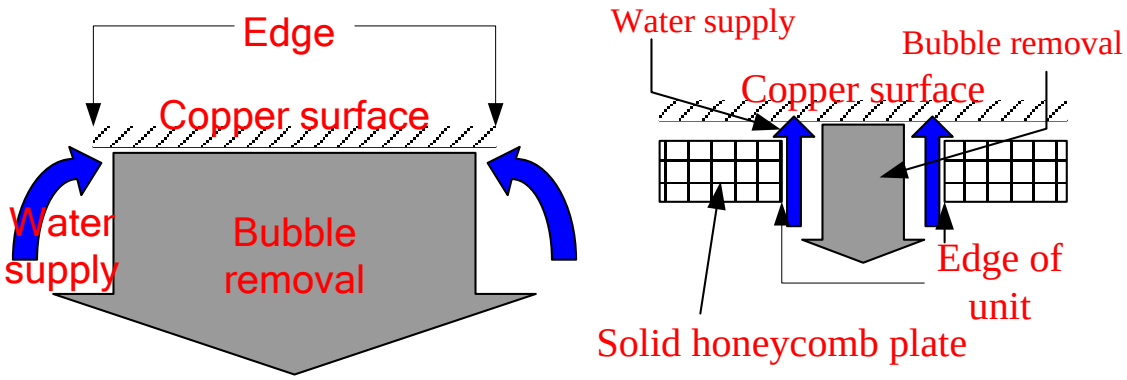

(a) bare surface

(b) honeycomb surface with no porosity (0-μm pore size)

Figure 5-5: Water refluxing and bubble removal path schematics for different surface types.

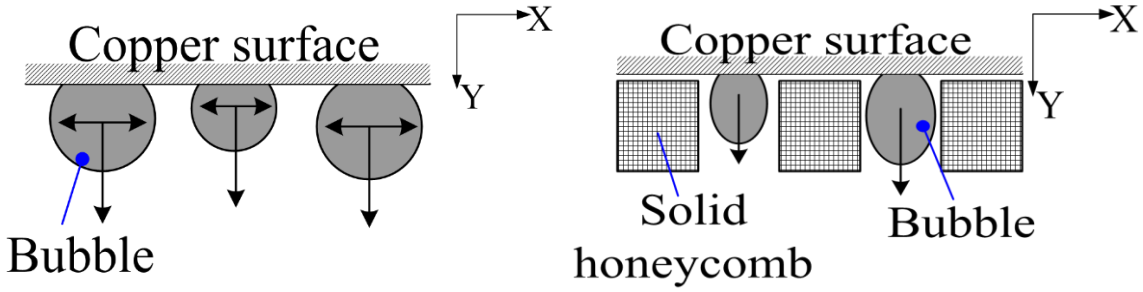

(a) bare surface

(b) honeycomb surface with no porosity (0-μm pore size)

Figure 5-6: Bubble behavior for different surface types.

Based on the results for test cases 1 (bare surface), 4 (honeycomb surface with no porosity), and 7 (honeycomb surface with a 100-μm pore size) at a consistent 5° surface inclination, the honeycomb structure mechanism was determined. During pool boiling, bubbles are removed from the holes in the honeycomb structure. After bubbles are removed, water, from both porous layer and holes, is forced to flux onto the copper surface where it absorbs heat and forms new bubbles. These new bubbles are subsequently removed from the holes in the honeycomb structure and the water refluxing process is repeated. This natural circulation process can supply a large amount of water continuously to the copper surface, subsequently increasing the CHF. Figure 5-7 provides a schematic of this natural water refluxing-bubble removal circulation process for a porous honeycomb surface.

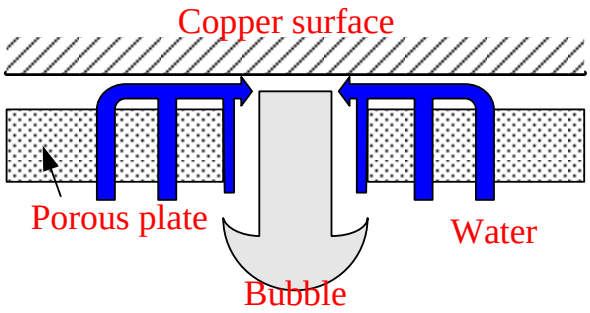

Figure 5-7: Natural water refluxing-bubble removal circulation process schematic for a porous honeycomb surface.

When comparing the honeycomb surface test cases 4 (0-µm pore size) and 7 (100-µm pore size), the results indicated a lower degree of superheating for the porous honeycomb surface at the same heat flux. The results from the downward-facing pool boiling experiments indicated higher CHF values for the porous honeycomb surface test cases (100-µm pore size) relative to the honeycomb surface test case with no porosity (0-µm pore size). The hydrophilic pores absorbed water, increasing the water refluxing to the copper surface through this alternate path and subsequently increasing the CHF. Figure 5-8 depicts differences in the boiling patterns for the honeycomb surface test cases 4 (0-µm pore size) and 7 (100-µm pore size). In test case 4, few holes generated bubbles. Comparatively, in test case 7, nearly all holes generated bubbles. This observable difference suggests that porous surfaces increase water refluxing capacity, increase the CHF, and increase overall system cooling effectiveness.

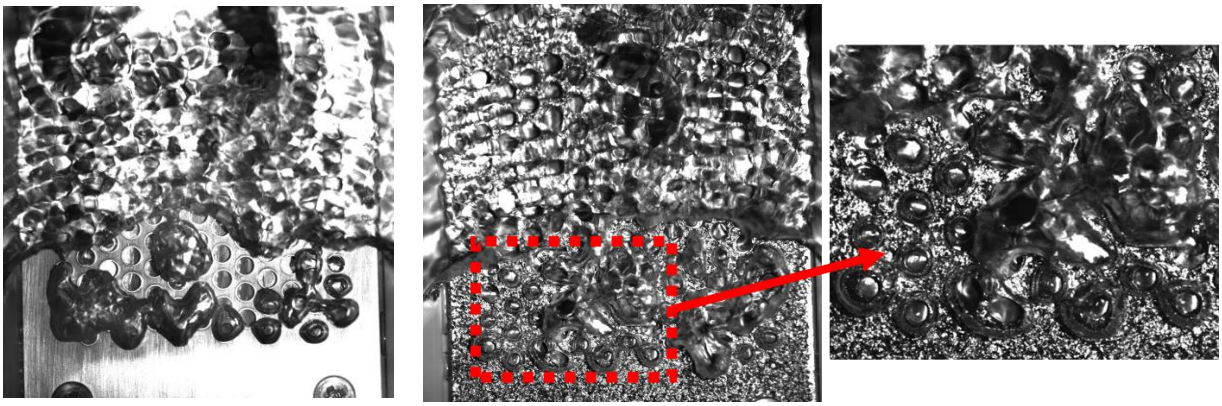

(a) case 4 (b) case 7

Figure 5-8: Quantities of holes utilized for boiling in case 4 and case 7.

5.1.2 Pore Size Effect

Then, experiments regarding with honeycomb parameters are determined. In this section, honeycomb surface with different pore size is discussed. The aim is to see whether CHF can be affected by present pore size.

The specific facility is shown in Figure 5-9 and experimental condition is list in Table 5-4. Here, inclination angle was only 5º, honeycomb structure (pitch/diameter) was 2.5/1.7 and pore size was 5-μm, 20-μm and 100-μm, respectively.

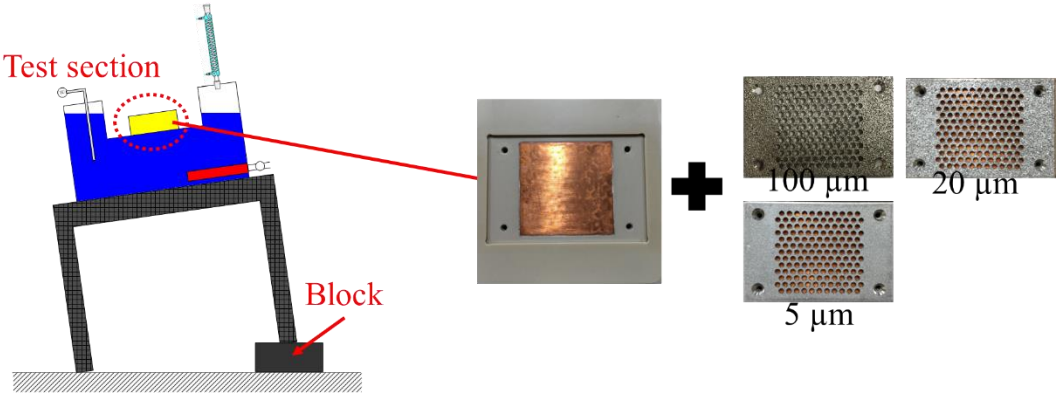

Figure 5-9: Pore size effect experiment facility in honeycomb cases.

Table 5-4: Experimental condition in pore size effect cases.

Parameters	Value
Pressure	Atmospheric, 101325 Pa
Water temperature	100ºC
Boiling area	30 ×30 mm in square
Inclination angle	5º
Pore size	5-, 20- and 100-μm
Pitch/diameter ratio	2.5/1.7

Table 5-5 lists the results of CHF value with different pore size in 5º inclination case and Figure 5-10 shows the heat flux as a function of superheating (i.e., boiling curves). Through the table and figure, it is found that CHF value is almost same indicating no CHF enhancement by effect of pore size and the superheating is also similar at the same heat flux within these three case. Thus, it is concluded that in present case, pore size has on effect on CHF performance.

Table 5-5: Results of CHF value with different pore size in 5º inclination case.

Test case	Surface type	Pore size [μm]	Inclination [°]	CHF [MW/m^2]
5	Honeycomb	5	5	0.79
6	Honeycomb	20	5	0.83
7	Honeycomb	100	5	0.83

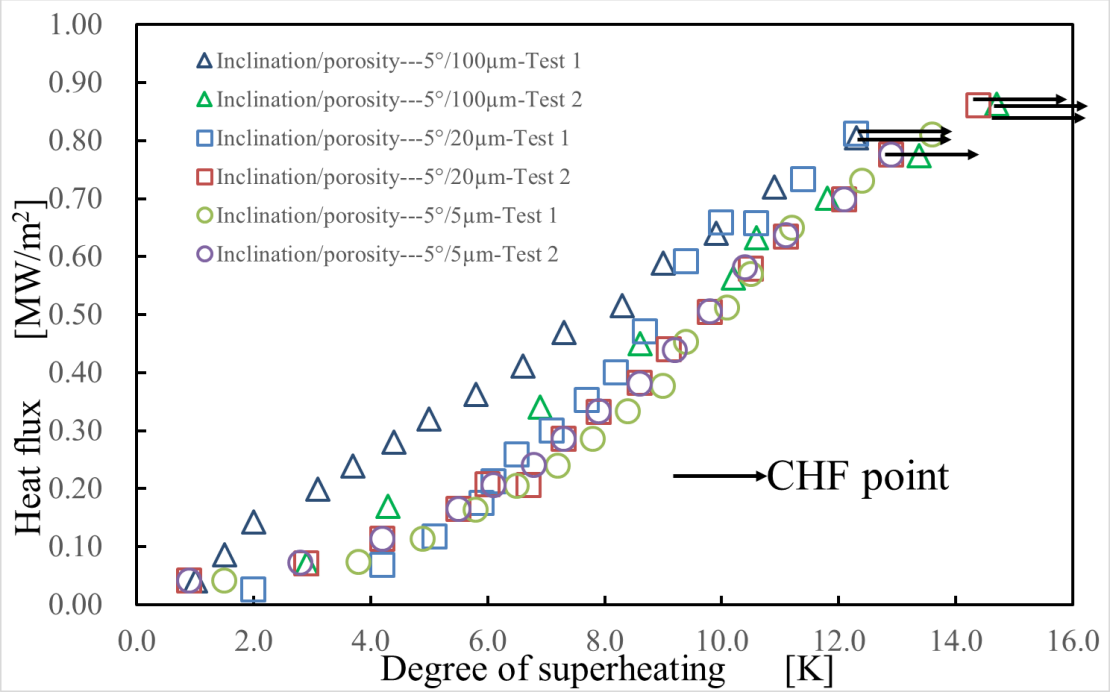

Figure 5-10: Heat flux as a function of superheating (i.e., boiling curves) with different pore size.

5.1.3 Inclination Effect

In this section, honeycomb surface with different pore size is discussed. The aim is to see inclination effect on CHF performance.

The specific facility is shown in Figure 5-11 and experimental condition is list in Table 5-6. Here, inclination angle was 5º, 10º and 20º (this angle will be changed by using block), honeycomb structure (pitch/diameter) was 2.5/1.7 and pore size was only 100-μm.

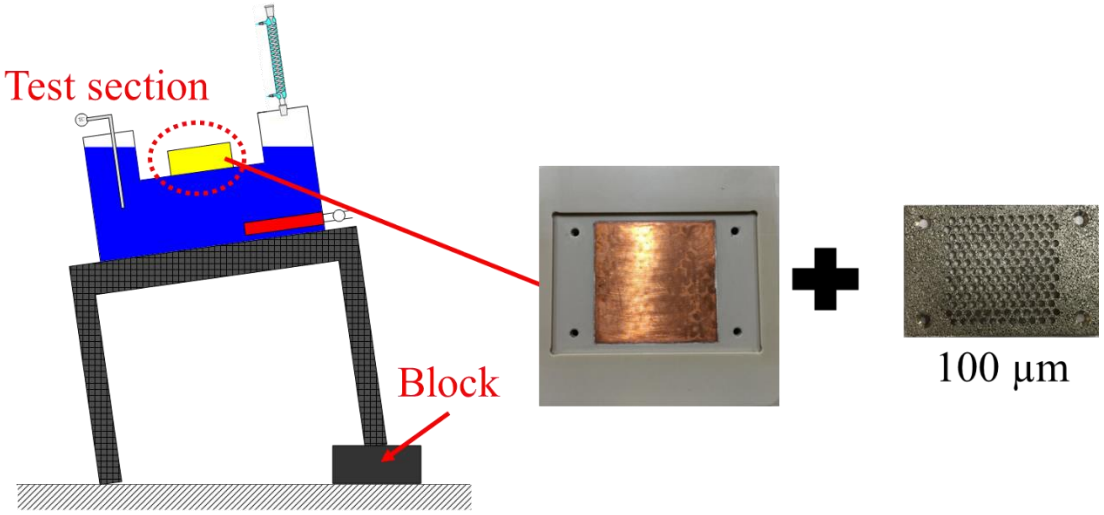

Figure 5-11: Inclination effect experiment facility in honeycomb cases.

Table 5-6: Experimental condition in inclination effect cases.

Parameters	Value
Pressure	Atmospheric, 101325 Pa
Water temperature	100ºC
Boiling area	30 ×30 mm in square
Inclination angle	5º, 10º, 20º
Pore size	100-μm
Pitch/diameter ratio	2.5/1.7

Table 5-7 lists the results of CHF value with different inclination for both honeycomb surface and bare surface case and Figure 5-12 shows the heat flux as a function of superheating (i.e., boiling curves). Through the table and figure, it is found that CHF value is increased as inclination angle. However, the enhancement is within gradual trend as inclination compared with bare surface case, which means enhancing percentage is decreasing as inclination angle becomes larger (Figure 5-13).

Table 5-7: Results of CHF value with different inclination for both honeycomb surface and bare case.

Test case	Surface type	Pore size [μm]	Inclination [°]	CHF [MW/m^2]
7	Honeycomb	100	5	0.83
8	Honeycomb	100	10	0.91
9	Honeycomb	100	20	1.00
1	Bare	-	5	0.25
2	Bare	-	10	0.47
3	Bare	-	20	0.50

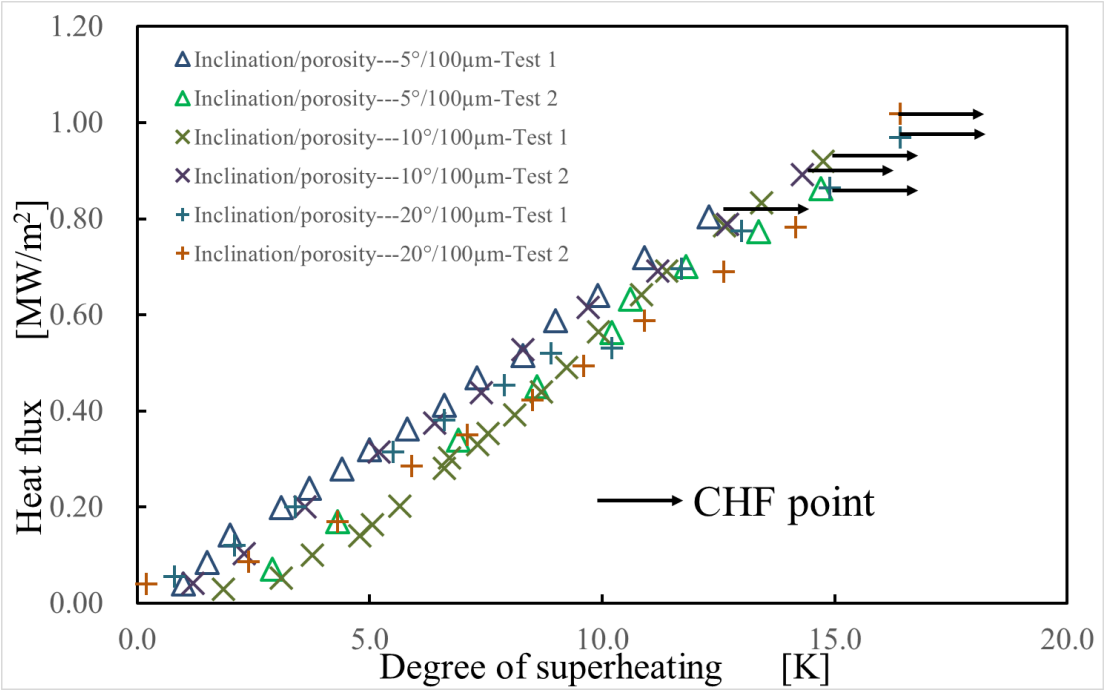

Figure 5-12: Heat flux as a function of superheating (i.e., boiling curves) in inclination effect case.

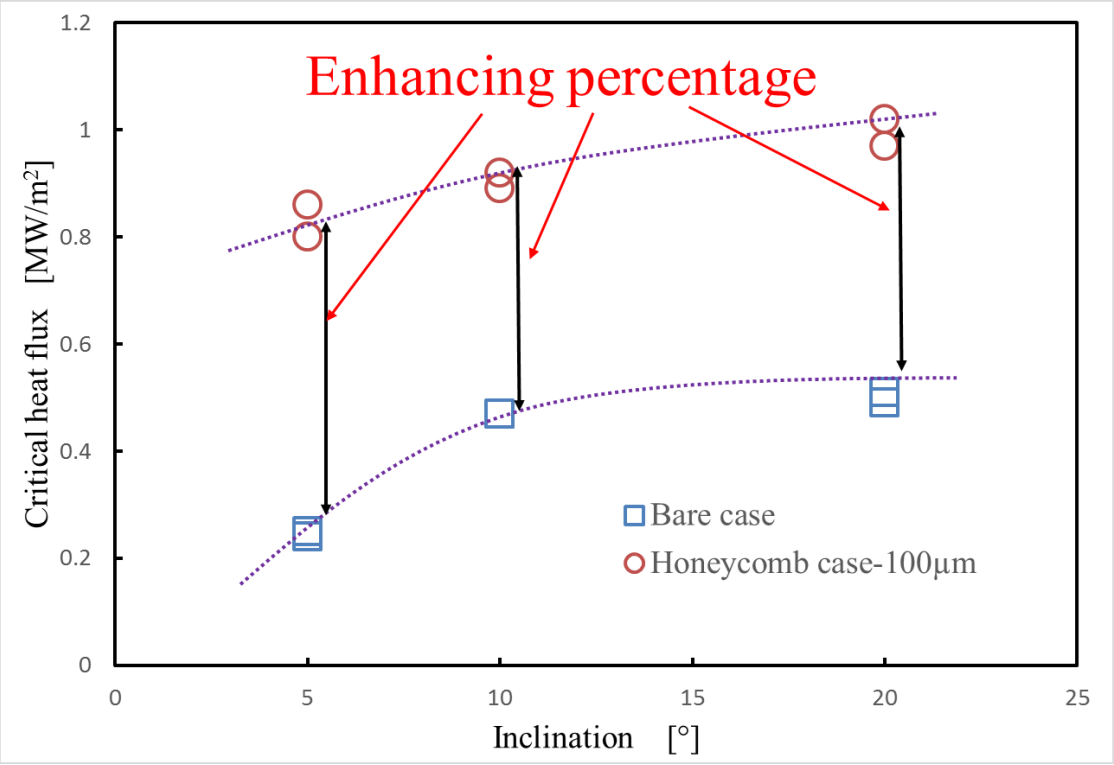

Figure 5-13: Enhancing percentage variation trend between bare surface and honeycomb surface as inclination.

As it is mentioned in last chapter, inclination can affect surface wettability. That is when inclination is higher, surface wettability goes higher. And similar condition was observed in honeycomb surface case (Table 5-7). According to this phenomenon, BDF of honeycomb surface cases were also calculated, which is list in Table 5-8. Compared with BDF in bare surface case, the value in honeycomb surface case increases gradually, which suggested one gradual surface wettability as inclination angle and one slow CHF value increase in the end. Due to these two different CHF variation trend in honeycomb surface and bare surface cases, the enhancing percentage shows a decreasing trend as inclination angle increases.

Table 5-8: BDF results for both honeycomb surface and bare surface with different inclination angle.

Inclination angle [°]	BDF [bubble/s]	
	Bare surface	Honeycomb surface
5	4.1	4.2
10	6.7	5.3
20	7.4	6.1

5.1.4 Honeycomb Structure Effect

In this section, honeycomb surface with different pore size is discussed. The aim is to see honeycomb structure effect on CHF performance. More specifically, honeycomb structure means two parameters in this study. One is pitch (or center distance), defined as Δt. The other one is diameter of hole, defined as d.

The specific facility is shown in Figure 5-14 and experimental condition is list in Table 5-9. Here, inclination angle was only 5°, pore size was 100-μm. Besides, five different types of honeycomb plate were chosen. The pitch/diameter ratio were 2.5/1.7, 3.0/1.7, 1.8/1.0, 4.2/2.4, 4.0/1.7, respectively.

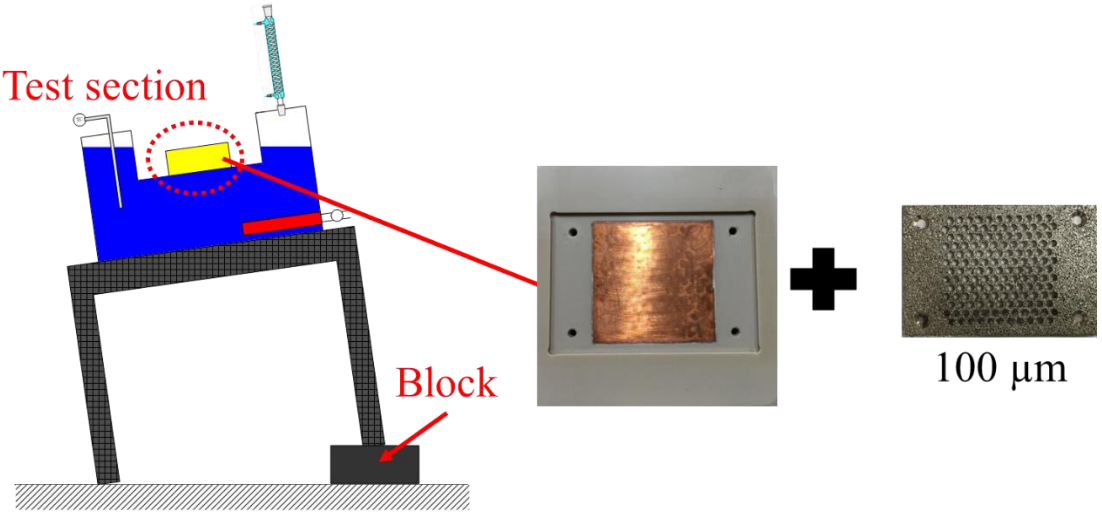

Figure 5-14: Honeycomb structure effect experiment facility in honeycomb cases.

Table 5-9: Experimental condition in inclination effect cases.

Parameters	Value
Pressure	Atmospheric, 101325 Pa
Water temperature	100ºC
Boiling area	30 ×30 mm in square
Inclination angle	5º
Pore size	100-μm
Pitch/diameter ratio	2.5/1.7, 3.0/1.7, 1.8/1.0, 4.2/2.4, 4.0/1.7, 2.1/1.7

Here, another new parameter will be introduced, which is hole-area ratio, defined as γ. Equation is shown as following:

$$\gamma = \left(\frac{1}{4} n\pi d^2 / A_{Cu}\right) \tag{5-1}$$

Where, n means quantities of holes in honeycomb plate, π refers to ratio of a circle's circumference, d indicates diameter of hole and A_{CU} means the area of copper surface.

Table 5-10 lists the results of CHF value with different with different honeycomb structure, Figure 5-15 shows the heat flux as a function of superheating (i.e., boiling curves) in case 7 and case 10-14, Figure 5-16 shows the heat flux as a function of hole-ratio. Through figure, it is shown that as hole-ratio increases, CHF value appears with an increasing trend (0.41 MW/m^2 @ 0.14 vs 0.75 MW/m^2 @ 0.25 vs 0.83 MW/m^2 @ 0.36). When hole-ratio is same, no obvious CHF difference is found.

Table 5-10: Results of CHF value with honeycomb structure.

Test case	Structure [$\Delta t/d$]	Hole-ratio	Inclination [°]	CHF [MW/m^2]
7	2.5/1.7	0.36	5	0.83
10	4.0/1.7	0.17	5	0.41
11	4.2/2.4	0.26	5	0.75
12	3.0/1.7	0.25	5	0.75
13	1.8/1.0	0.24	5	0.73
14	2.1/1.7	0.51	5	0.77

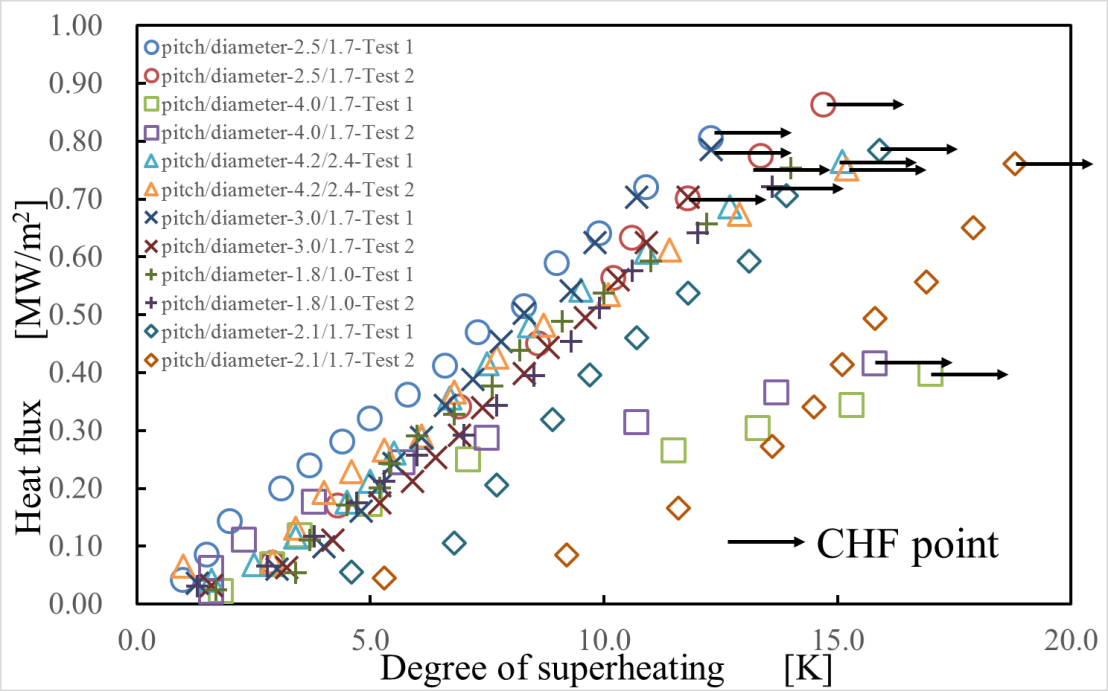

Figure 5-15: Heat flux as a function of superheating (i.e., boiling curves) in honeycomb structure case.

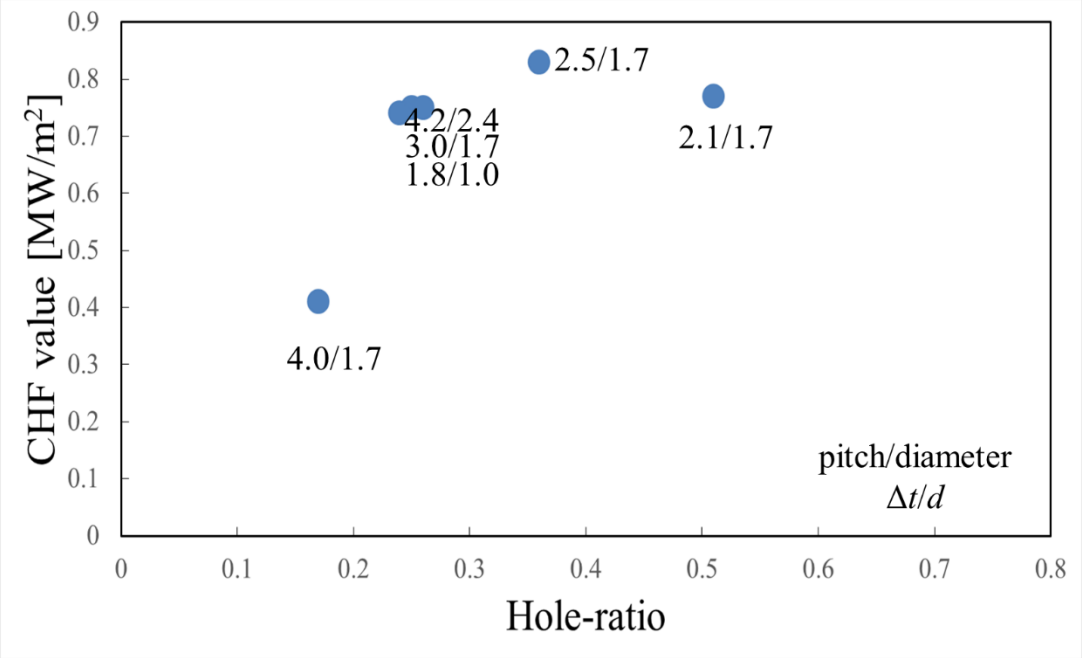

Figure 5-16: Heat flux as a function of hole-ratio.

5.1.5 Summary of Honeycomb Cases

According to these experiments, it can be concluded that: 1) honeycomb surface can improve CHF performance due to natural circulation caused by the structure type. Then, porous honeycomb surface can further improve CHF compared with solid honeycomb case; 2) present pore size has no effect on CHF performance; 3) Inclination promotes CHF value, but the enhancement is lower compared with bare surface case; 4) CHF increases as hole-ratio. The former three findings can be depicted and shown in Figure 5-17.

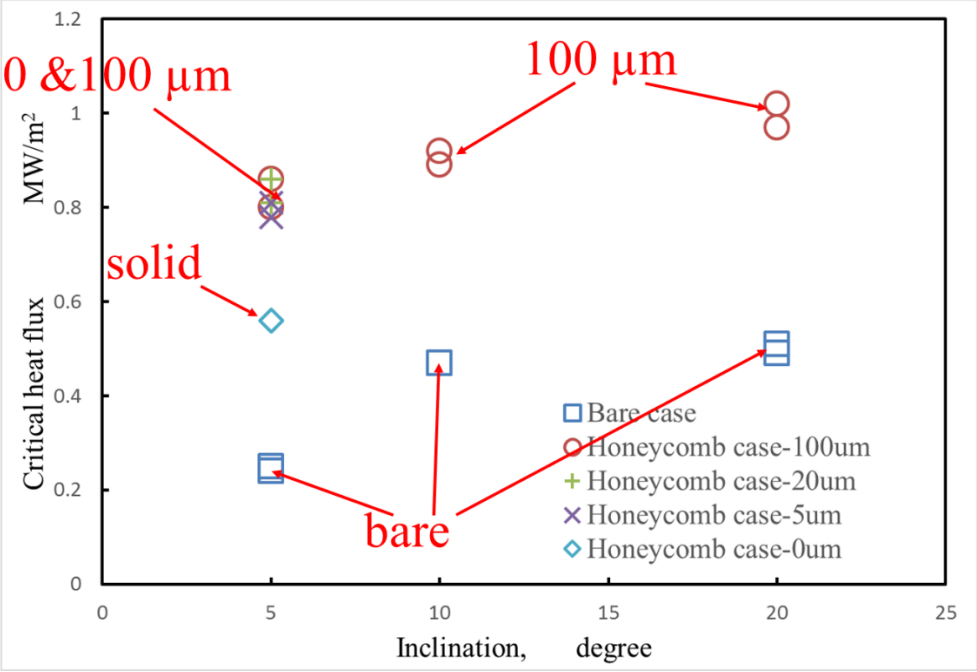

Figure 5-17: CHF value comparison between bare surface case and honeycomb case.

5.2 Honeycomb CHF Model

From Section 5.2, it is known that CHF can increase as boiling area (or hole-area). So the next step is to quantitatively analyze CHF variation trend.

5.2.1 CHF Variation Trend

5.2.1.1 Previous Study

Researcher Mori studied the Porous honeycomb by changing width of vapor escape channel, which is defined as d_v [23]. In that study, CHF variation as a function of d_v is given in Figure 5-18 [23]. As it is shown, CHF decreases as d_v increases. However, the hole area is one parameter that is used for discussion. So we should know relationship between width and hole area. In Mori's study, the honeycomb plate was circular. For calculation, the circular ship is equivalent to square shape. And the side length of square shape is A mm. So hole area, A_h, can be calculated through the following equation.

$$A_h = \left(\frac{A}{0.4+d_v}\right)^2 * (d_v)^2 = A^2 * \left(\frac{1}{\frac{0.4}{d_v}+1}\right)^2 \quad (5\text{-}1)$$

Through calculation, it is found when the width becomes bigger, hole area will go larger. So the trend that CHF value as a function of hole-area is clearly understood. It is that CHF decreases as inclination.

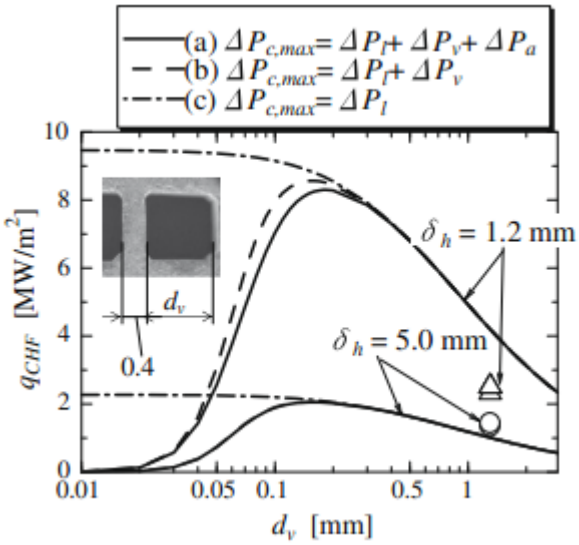

Figure 5-18: CHF value as a function of width [23].

5.2.1.2 Present Study

In present study, the CHF trend is completely different from previous study. It is that the CHF value increases as hole-area, which has been shown in Figure 5-16 (Section 5.1). As

mentioned before, the extended boiling area is regarded as one reason for CHF enhancement, which is against the CHF results of researcher Mori. However, based on his model, CHF should show the decreasing trend. Here it is assumed that the factor, extended boiling area, should be modified.

5.2.2 Explanation for CHF Variation

For honeycomb surface boiling, Mori suggested one model. Figure 5-19 [23] gives the schematic diagram of steam and water flows in a honeycomb porous plate. During the boiling, liquid can be absorbed toward heating surface within the porous medium by capillary force, and vapor generated inside holes will escape through it. In this model, the pressure head, here it is capillary pressure, compensates for the pressure losses along the vapor-liquid path. The equation is that:

$$\Delta p_{c,max} = \Delta p_l + \Delta p_v + \Delta p_a \quad (5\text{-}2)$$

Where $\Delta p_{c,\max}$ is capillary pressure, Δp_l and Δp_v are frictional pressure drops caused by the liquid flow in the porous medium and the vapor flow through the channels, respectively, and Δp_a is the accelerational pressure drop caused by phase change from liquid to vapor.

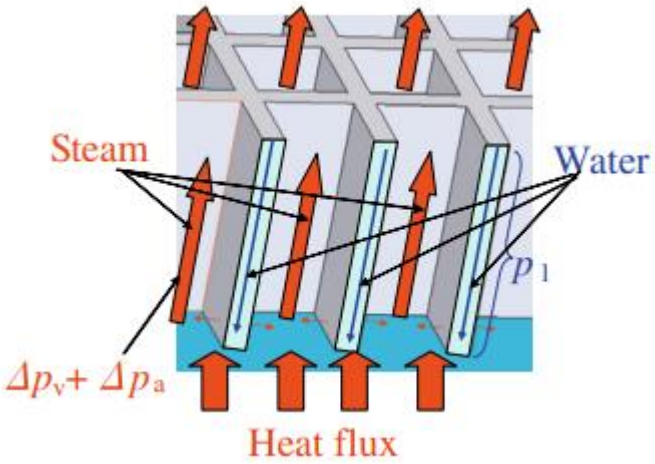

Figure 5-19: Schematic diagram of steam and water flows in a honeycomb porous plate [23].

Here, we use mass transfer conservation to analyze the boiling phenomenon and regard honeycomb plate as one controlled volume system. During the experiment, water was going inside to approach heating surface and vapor was escaping outside from holes. However, mass flow rate of water fluxing and bubble removal should be equal due to mass transfer conservation. Take temperature variation of one case for example (Figure 5-20). Before CHF appearance, there existed two types of temperature stages. One is called constant stage, which means mass flow rate of water refluxing and bubble removal were equal and constant corresponding to the unchanged temperature curves. The other one is called increasing stage, which means both mass flow rate increased with same pace. When CHF happened, it meant the two mass flow rate were forced to sharply decrease to one relatively low level (for comparison, it is set as almost 0 in Figure 5-20). This is because under CHF situation heating surface is totally covered by a vapor film with no water refluxing. Also, from video, it is observed that after CHF only a little amount of vapor were coming from holes (Figure 5-21), indicating that mass flow rate of vapor flow and water refluxing is quite slow. So it is known that both mass flow rate reached the maximum that just before CHF appearance. For future explanation and calculation, the mass flow rate of last constant period is supposed to be the maximum mass flow rate point. Besides, it is found that heat flux is appropriate to mass flow rate, which means the larger heat flux is the higher CHF value is.

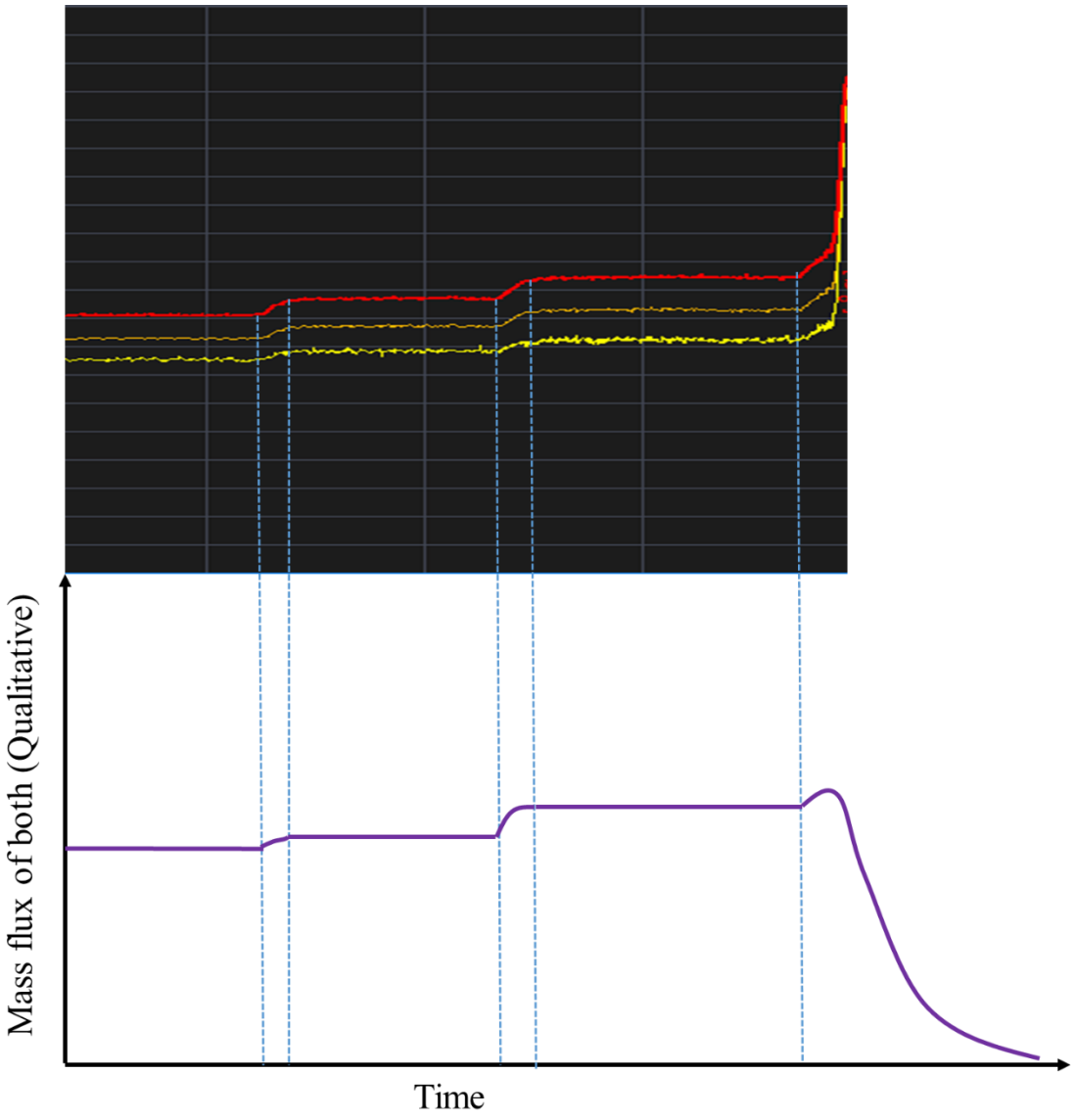

Figure 5-20: Temperature variation during experiment and its corresponding mass flow rate variation (qualitative).

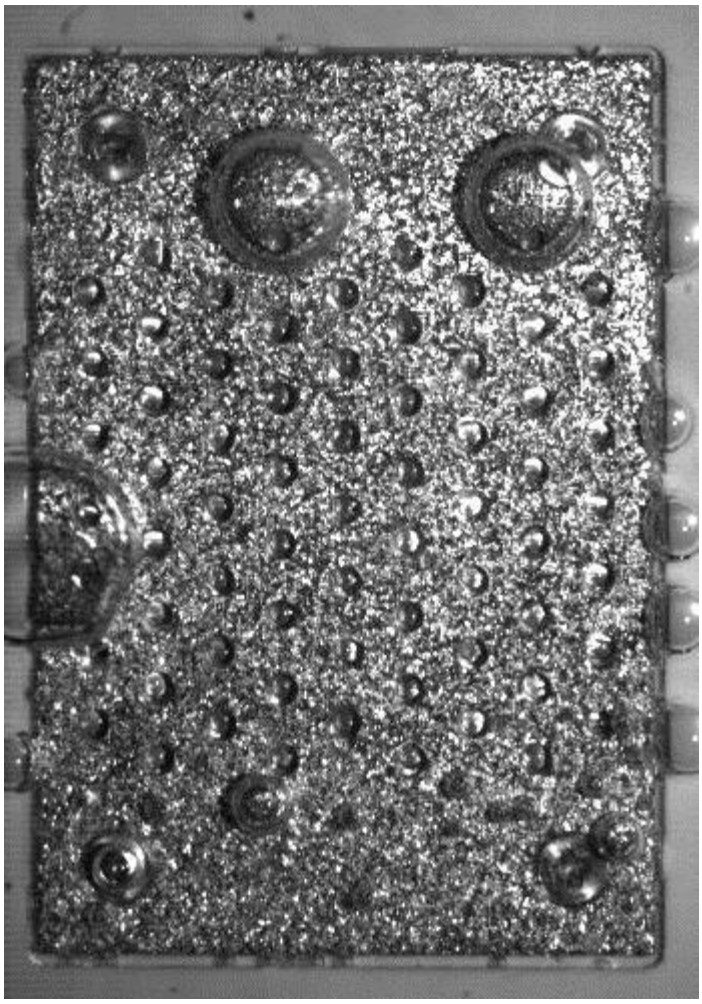

Figure 5-21: Vapor phenomenon after CHF appearance.

Before explaining the CHF trend, some other definitions should be determined in advance. They are the available bubble removal mass flow rate (defined as $m_{a,\,br}$) and available water refluxing mass flow rate (defined as $m_{a,\,wr}$). After definition, mass flow rate variation will be like that. When there is one thermal input, there comes with one corresponding water refluxing and bubble removal mass flow rate to cool down this power. Then if power input is increased, both mass flow rate will increase to meet the new cooling ability. And this situation exists until one mass flow rate reaches the available mass flow rate. If thermal power continue to increase, there will be not enough water refluxing mass flow rate or bubble removal mass flow rate so that heating surface will be covered by vapor film, causing CHF appearance.

Based on Mori's model, the capillary force shows non-relationship with porous surface area, but the available water reflux mass flow rate is relevant to the porous surface area. That is if the area is big, mass flow rate will be large. When considering about available bubble removal mass flow rate, it should be related to the hole-area. More specifically, the bigger the hole-area is, the larger available bubble removal flux it is. In a word, as hole-area increases, the available water refluxing mass flow rate is decreasing while the available bubble removal mass flow rate is increasing correspondingly. After knowing this, CHF trend in present study and Mori's study is understood.

Figure 5-22 shows presumptive available mass flow rate for both water refluxing and bubble removal. As it is shown, water refluxing is decreasing as hole-area ratio while bubble removal is increasing as hole-area ratio. Here hole-area ratio means the occupied percentage of hole-area on heating surface area. In Mori's study, hole-area ratio is very big (more than 0.57) [24] so that the available mass flow rate of water refluxing is smaller than that of bubble removal. During the boiling, as mass flow rate increases as thermal power input ascends, the available mass flow rate of water refluxing was first reached, which means in higher hole-area ratio case, the water refluxing mass flow rate is more important. Also the available mass flow rate shows decreasing trend as hole-area ratio so that CHF will decrease. However, in present study, hole-area ratio is small so that the available mass flow rate of bubble removal is lower than that of water refluxing, being the important factor that affects CHF value. According to the increasing trend of bubble removal mass flow rate trend, CHF shows an increasing scenario. When the both available mass flow rate are equal, it is supposed that CHF reaches the maximum. This point is called turning point, which means CHF increases first and then decreases.

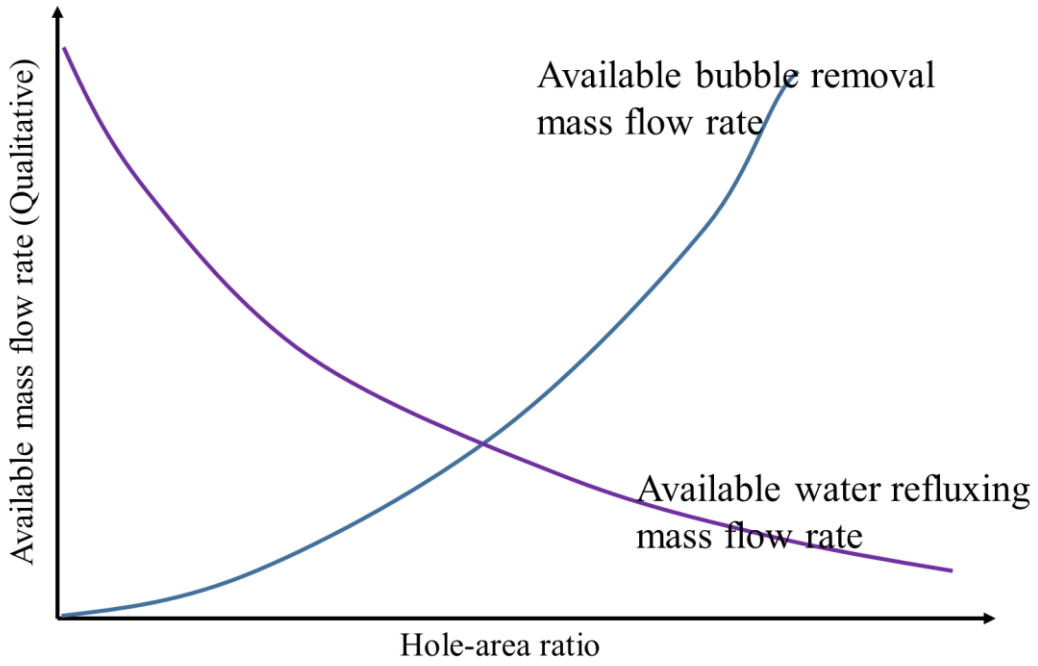

Figure 5-22: Presumptive available mass flow rate for both water refluxing and bubble removal.

When CHF happens, the both mass flow rate reaches the maximum. However, it is different from the available mass flow rate. To better differentiate them, another two parameters are introduced, maximum bubble removal mass flow rate (defined as $m_{m,\,br}$) and maximum water refluxing mass flow rate (defined as $m_{m,\,wr}$). Under the condition that hole-area ratio is small, when CHF appears, the maximum bubble removal mass flow rate is equal to the available mass flow rate of bubble removal. Or if hole-area ratio is large, the maximum water refluxing mass flow rate is equal to the available mass flow rate of water refluxing at CHF point. After knowing that quantitative analysis will be given.

5.2.3 CHF Variation Model (Formulation)

As it is mentioned in last section, the two available mass flow rate will determine the CHF variation. So the formulation of CHF variation trend is try to analyze these mass flow rate. In this study, the mass flow rate is decided by pressure balance. So the first aim is to clearly understand pressure balance during boiling.

5.2.3.1 Pressure balance in porous honeycomb surface cases

In this study, both solid and porous honeycomb surface cases were carried on for experiments. Because most of experiment cases were regarding with porous honeycomb case, so the study process will start with solid case. And the pressure balance is based on the model of Mori (In equation 5-2, the maximum capillary pressure is equal to pressure drop of water penetration, vapor escaping and acceleration pressure drop during phase change. If the plate is solid, it means capillary pressure is equal to 0.) [23].

Before constructing pressure balance the first thing is to understand boiling circulation inside porous honeycomb. In real boiling, the fluid flow is like the path shown in Figure 5-5(b). That was water refluxed through the edge of holes and approached the heating copper surface to cool down it. Then vapor got together and moved outside through the center of holes. To clearly observe the flow path, we transfer this U-type path to a linear path, which is shown in Figure 5-23. As it is shown, the fluid is flowing within three kinds of zones, water zone (the path for water refluxing), boiling zone (for cooling down heating surface) and the last zone, vapor zone (the path for vapor escaping. As it is shown in Figure 5-7, for porous honeycomb surface case there exist two paths for water refluxing. One is through the edge of holes and the other one is through porous surface. Based on this, the zone classification is clear. There are two channels in water zone, porous channel and hole-channel respectively. Porous channel is the room for water absorption by porous surface and hole-channel is the space for water refluxing through holes. Both channels provides boiling zone with water.

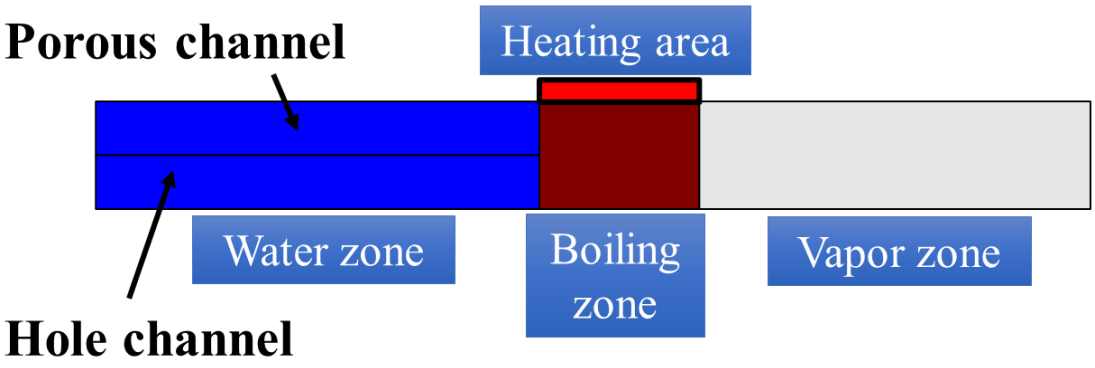

Figure 5-23: Three different zones in one control volume of porous honeycomb surface case.

First focus on the pressure balance of vapor escaping from holes. As it is known, vapor escaping will cause pressure loss so that there must be one pressure head to compensate this energy loss. From Figure 5-23, in this system, the only energy input is thermal power, so it is assumed that the thermal power compensates for vapor flow pressure loss. Cho et al [44-46] introduce one force named bubble growth force in their study. Due to the only energy input, the bubble growth behavior can only be determined by this power. As the bubble growing up, it will expand and move outside holes, forming the vapor flow. Because of vapor flow, pressure loss appears. Based on this, it is concluded that pressure drop of vapor flow inside holes is due to bubble growth and this growth is caused by thermal power input. The bubble growth force F_{du} is given in the following. When divided by hole-area, the pressure head by bubble growth is known.

$$F_{du} = -\rho_f \pi r_b^2 \left(\frac{3}{2} C_s \dot{r_b}^2 + r_b \ddot{r_b}\right) \tag{5-3}$$

Where ρ_f means liquid density, r_b means radius of bubble, C_s means shear lift coefficient.

The next is to focus on pressure balance of water refluxing side. As it is known, the pressure of one point consists of two parts, dynamic pressure p_d and hydraulic head p_h. The equation is given in the follow (equation 5-4). In equation 5-5, it is known that dynamic pressure p_d is related with density and velocity.

$$p = p_d + p_h \tag{5-4}$$

$$p_d \propto \rho v^2 \tag{5-5}$$

Due to the thermal power input, the pressure at the inlet of vapor zone is enhanced compared with pressure at the outlet of water zone. The increased pressure Δp_{wr} can be calculated through the pressure value of these two location. Also, these two location is same in real boiling case (this is because vapor area is where water is boiling) so that hydraulic head is similar. The only difference is in the dynamic pressure term. Because the water refluxing will cause pressure loss, the increased pressure Δp_{wr} will compensate it.

After this, the pressure balance in water refluxing side is understood. More specifically, the thermal power input gives bubble one force called bubble grow force, propelling bubble to become bigger and moving outsides the holes and this pressure head by power input is compensating pressure loss of vapor escaping. In the meantime, thermal power increased the pressure, providing water refluxing with motivation. And pressure balance equation is list in the following.

$$\Delta p_{du} = \Delta p_v \tag{5-6}$$

$$p_{wr} = \Delta p_{l,h} + \Delta p_{l,p} \tag{5-7}$$

Where, Δp_{du} is the pressure head due to bubble growth force, Δp_v is frictional pressure drop caused by the vapor flow through the holes, $\Delta p_{l,h}$ is frictional pressure drop caused by water flow through holes, $\Delta p_{l,p}$ is frictional pressure drop caused by water flow through porous surface and p_{wr} is the increased pressure caused by thermal power input.

From the analysis, the function of thermal power is known. On one hand it can increase the pressure to activate water refluxing. On the other hand it can force on bubble propelling vapor escaping.

5.2.3.2 Available mass flow rate calculation

In last section, several kinds of pressure difference are known. They are Δp_v, p_{wr}, $\Delta p_{l,h}$, $\Delta p_{l,p}$, Δp_{du}. Based on equation 5-7, available mass flow rate of water can be calculated. However, the pressure head Δp_{du} is difficult to calculate. Thus, available mass flow rate of vapor will be calculated based on present experiment study. Here it is supposed that the available mass flow rate of vapor escaping is only related with hole-area, which means mass flow rate is bigger at larger hole-area (Figure 5-24), and the relation is proportional.

Thus, according to CHF results, the available mass flow rate is determined. The calculating process is as follows.

1) Confirm the relation between CHF and vapor mass flow rate (see equation 5-8);

2) Plot vapor mass flow rate data into one figure, set x-axial as hole-area ratio (Figure 5-24);

3) Make one fitting curve based on present data;

Relation between CHF and bubble removal mass flow rate is depicted in the following. Because in present study, CHF is determined by bubble removal mass flow rate so this flux can be regarded as the available mass flow rate of vapor escaping.

$$m_{a,br} = \frac{q_{CHF}}{h_{fg}} \tag{5-8}$$

Where $m_{a,\,br}$ means the available mass flow rate of bubble removal, q_{CHF} means critical heat flux and h_{fg} means latent heat.

Figure 5-24 shows maximum bubble removal mass flow rate at CHF point as a function of hole-area ratio and its fitting curve. Regarding with the fitting equation, x means hole-area ratio and y means expected maximum bubble removal mass flow rate at CHF point. The goodness of fitness is 0.9391. Based on this, the equation is decided. As it is suggested in previous paragraph, the maximum bubble removal mass flow rate is also available bubble removal mass flow rate.

$$m_{a,br} = 0.001 * \gamma + 2E - 5 \tag{5-9}$$

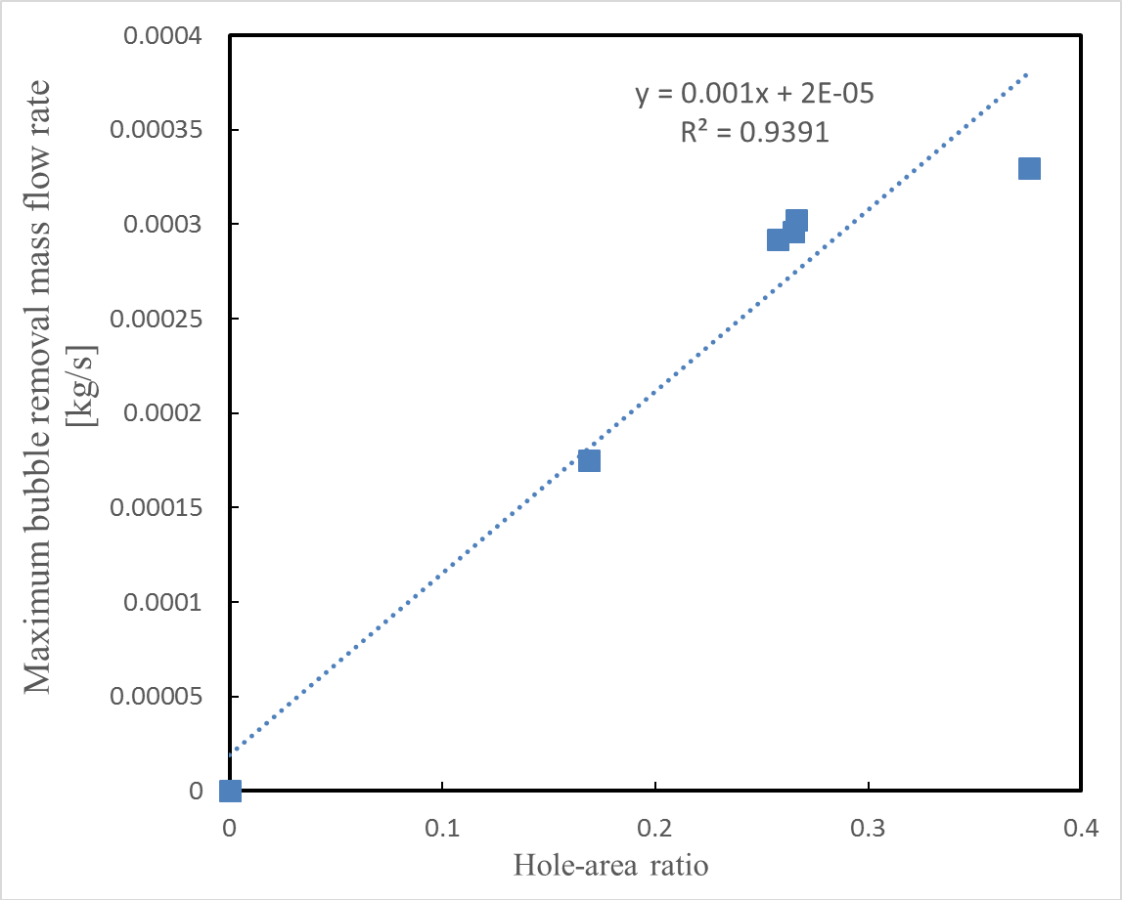

Figure 5-24: Maximum vapor mass flow rate at CHF point as a function of hole-area ratio and its fitting curve.

From Figure 5-24, it is also known that the mass flux should be constant. Through calculation, the available mass flux of bubble removal is 1.2 kg/m^2 s. the calculating equation is list in the following.

$$G_{a,br} = m_{a,br}/A_h \quad (5\text{-}10)$$

Where, $G_{a,br}$ is available mass flux of bubble removal, $m_{a,\,br}$ is the available mass flow rate of bubble removal and A_h means hole-area.

The next step is try to analyze the available mass flow rate of water refluxing. According to equation 5-7, the available mass flow rate of water refluxing can be decided. To calculate these pressure term in equation 5-7, equation 5-11, 5-12, 5-13 are given [47, 49, 50]. Through calculation based on experiment, Reynold number of water refluxing

through holes is less than 1000, so equation of frictional pressure drop caused by water flow through holes was chosen inside laminar regime.

$$p_{wr} = \left(\frac{1}{\rho_v} - \frac{1}{\rho_l}\right) * G^2 \quad (5\text{-}11)$$

$$\Delta p_{l,h} = \frac{\mu_l \delta_h}{K A_p \rho_l} * (\alpha m) \quad (5\text{-}12)$$

$$\Delta p_{l,p} = \frac{32 \mu_l \delta_h}{\rho_l A_h d^2} [(1-\alpha)m] \quad (5\text{-}13)$$

Where, ρ_v is vapor density, ρ_l is water density, G is mass flux of bubble removal, μ_l is viscosity of water, δ_h is thickness of honeycomb plate, K is permeability, A_p is porous-area, α is one coefficient, m is mass flow rate of water refluxing, d is diameter of holes.

Because the aim is to calculate available water refluxing mass flow rate, some parameters will be used with the available value. More specifically, $G_{a,br}$ replaces G, $m_{a,wr}$ replaces m. Regarding with coefficient α, it means the contribution of CHF value through porous surface in total CHF value. In this study, α is 0.33 and here we suppose it is a constant value in different hole-area ratio.

Through calculation, the available water refluxing mass flow rate is plot in Figure 5-25. Also in this figure the available bubble removal mass flow rate is added. As it is shown, at low hole-area ratio range, the available water refluxing mass flow rate is much larger than available bubble removal mass flow rate. So final CHF value is determined by available bubble removal mass flow rate. As hole-area ratio increases, CHF increase. However, bubble removal flow rate is still lower. This condition continues until both available mass flow rate reaches the same level. Here, we call it crossing point. Regarding with this crossing point, it is supposed that CHF reaches the maximum. After crossing point, available bubble removal mass flow rate is larger than available water refluxing mass flow rate. And in this stage water refluxing mass flow rate will become the key issue to affect final CHF performance. Based on this, the CHF value should decrease. Though model calculation, the crossing point is at the hole-area hole with 0.406.

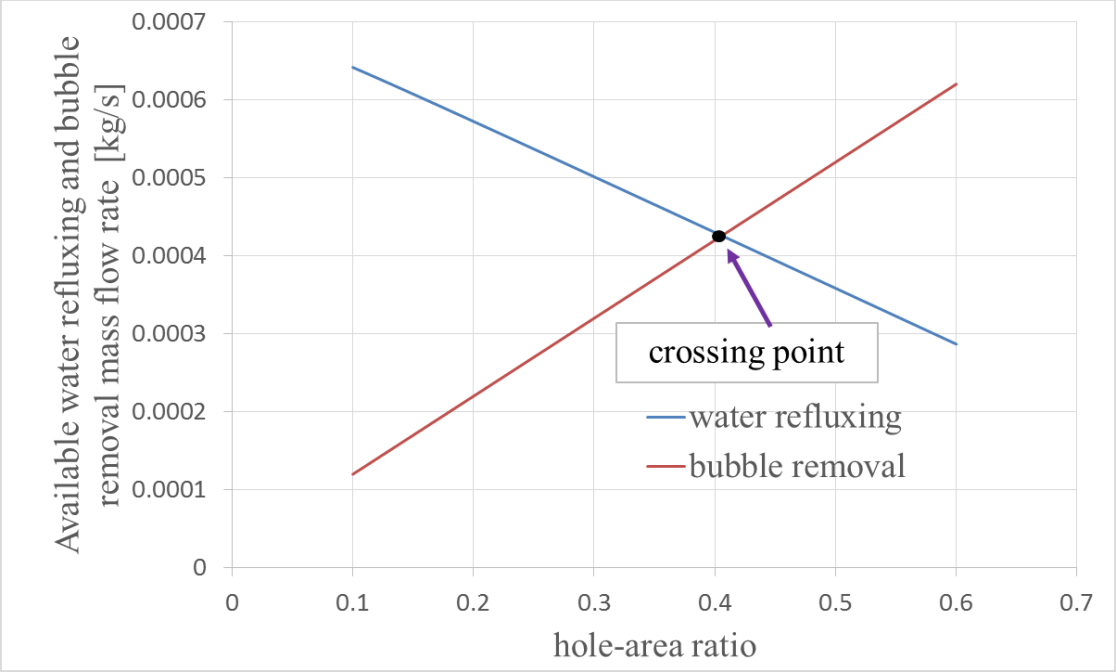

Figure 5-25: Available water refluxing and bubble removal mass flow rate as a function of hole-area ratio.

As it is shown in Figure 5-16, CHF value at hole-area 0.51 is about 0.77 MW/m^2, which is lower than CHF value at hole-area ratio 0.37 (0.83 MW/m^2). This means turning point is in the range from 0.37 to 0.51. And this crossing point calculation results is in this range, indicating that these mass flow rate curve can be used to depict CHF variation trend.

From the comparison between formulation and experiment data, it is found that pressure balance method can be used in downward-facing pool boiling.

5.3 Other Discussion

In this study, other kinds of experiment (for example, pore size effect and same hole-area ratio with different diameter experiment cases) were carried on. According to available mass flux suggested last section, here a brief explanation for CHF variation is given.

In pore size effect experiment, the hole-area ratio is same so we believed that available bubble removal mass flow rate is same. However, in this hole-area ratio range, available

water refluxing mass flow rate is larger than available bubble removal mass flow rate. And it also shows the trend in 5 μm and 20 μm cases. Thus, CHF didn't change when changing pore size.

Also, in same hole-area ratio with different diameter experiment cases. It is believed that in downward-facing pool boiling, how to remove bubble is one key issue to affect CHF. This is because, in downward-facing, bubbles are preferred to attach heating surface due to buoyance. That is the reason why CHF shows no difference with different honeycomb structure.

5.4 Chapter Summary

In this chapter, some honeycomb surface cases are discussed, considering solid and porous surface effect, pore size effect, inclination angle effect and honeycomb structure effect. In this study, we focus on CHF enhancement thus the discussion will first summarize CHF results and then explain CHF variation theoretically.

Figure 5-17 shows CHF value comparison between bare surface case and honeycomb case about the three former effect results. As it is shown, the solid honeycomb can increase CHF value compared with bare surface, and porous honeycomb surface can further enhance CHF value to a high level of cooling ability. And in all inclination cases, porous honeycomb surface can promotes CHF compared with bare surface cases. When dealing honeycomb surface with different pore size, it shows the same value. Regarding with inclination effect, it performs that CHF value can increase as inclination.

Figure 5-16 shows critical heat flux as a function of hole-area ratio. As it is shown, when hole-area ratio is lower, CHF value shows an increasing trend. However, CHF value seems to decrease a little (0.77 MW/m^2 at hole-area ratio, slightly lower than 0.83 MW/m^2 at hole-area ratio 0.37).

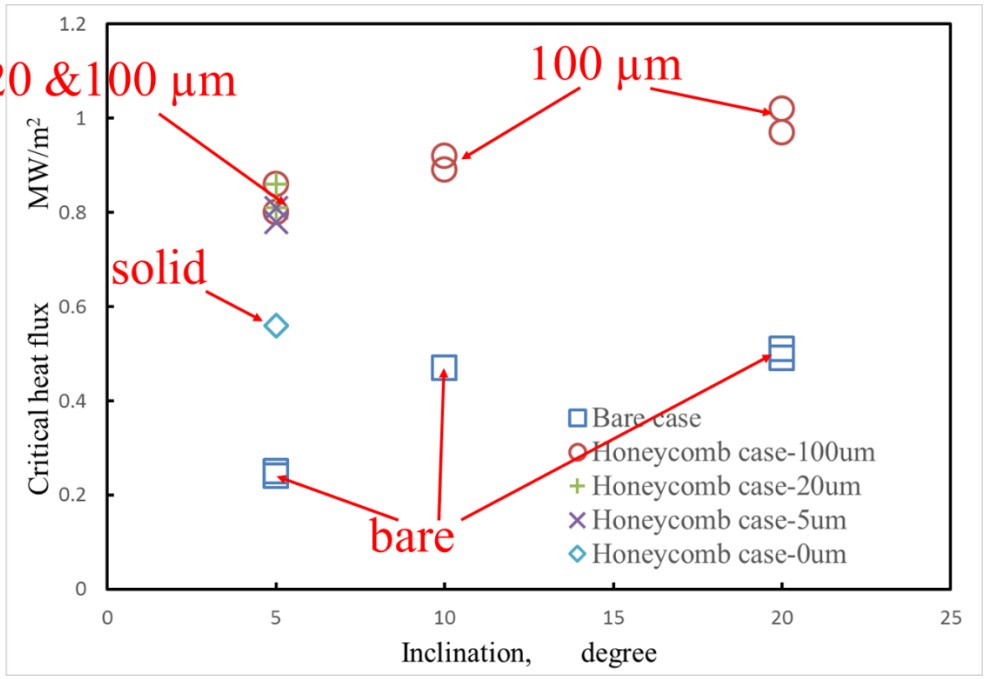

Figure 5-17: CHF value comparison between bare surface case and honeycomb case.

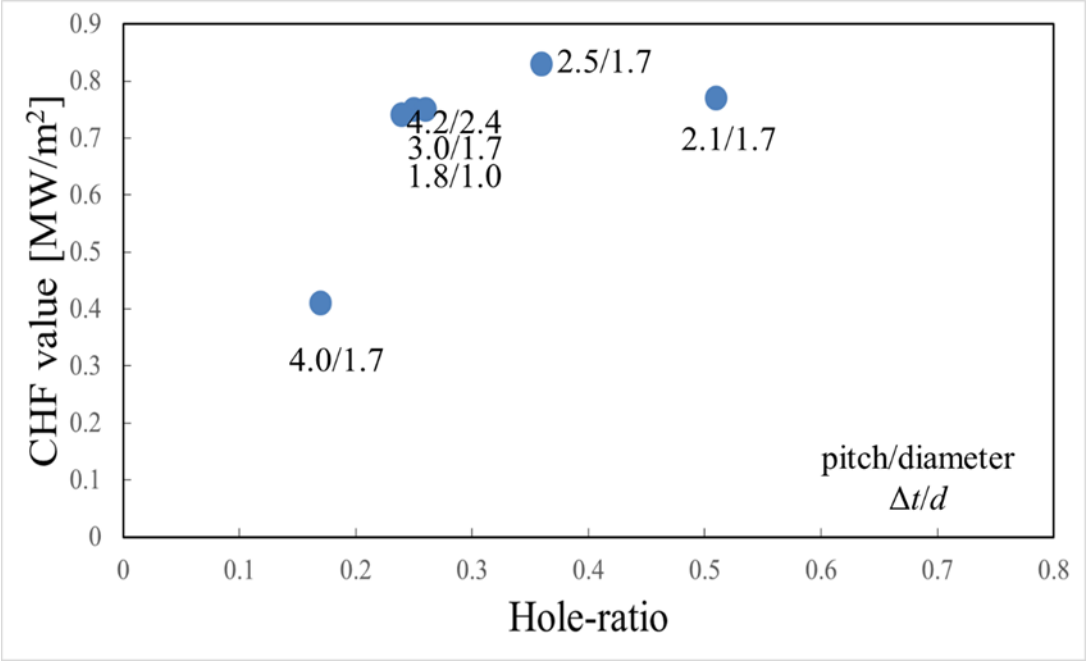

Figure 5-16: Heat flux as a function of hole-ratio.

After these findings according to CHF results, the theoretical explanation is given.

- The reason for CHF enhancement after apply one solid honeycomb plate is that the structure can separate phase flow path and reduce liquid-drag resistance [21]. Besides, the restricted bubble behavior by solid structure is another reason for CHF enhancement. When applying porous honeycomb surface plate instead of solid one, CHF is further increased due to the additional water refluxing path through porous surface, which means the heat transfer condition is improved.
- CHF performance is determined by the balance of water refluxing and bubble removal, which means the lower value decides the final CHF value. Based on pressure balance model suggested in this study, the available water refluxing and bubble removal mass flow rate were calculated. In lower hole-area ratio, bubble removal flow rate keeps increasing but still lower than water refluxing flow rate. So CHF is decided by bubble removal flow rate and keeps increasing. When both flow rate are same it means CHF reaches the maximum and will decrease, because after that water refluxing flow rate will be lower than bubble removal flow rate, determining CHF performance. That is the reason at large hole-area ratio the CHF value is lower than the CHF at a lower hole-area ratio. Through calculation, it is predicted that the crossing point of honeycomb in this study is about 0.41.
- When keeping hole-ratio same, CHF shows similar results. This is because how to remove bubble is one important issue in downward-facing pool boiling, resulting an unchanged CHF performance.
- CHF value is a function of inclination, which means CHF goes higher when inclination angle is large. Inclination can change BDF and BDF is related to CHF. This is because if BDF is larger, bubble escaping rate is more rapid. Surface replenishment condition is better, which can provide surface with more water in unit time. So CHF enhances.

6. Irradiation Effect Discussion

In this chapter, irradiation effect experiment was carried on. As one CHF enhancement method, the validity should first be confirmed. Here, both bare and honeycomb surface experiments were done to compare with the data in chapter 4 and chapter 5. According to prior research, RISA effect boosted CHF enhancement on oxidized metals. Thus, this effect on pure metal (bare surface) and honeycomb surface need to be understood. Also, two irradiation sources were introduced to test whether source has some different effect on CHF performance.

Based on this, work flow will be: 1) Do droplet test by irradiation; 2) Do bare surface experiments and analyze experiment data; 3) Do honeycomb surface experiments and analyze experiment data; 4) After experiments and analysis, a brief summary will be given.

Some contents of this chapter have already been published. [31]

6.1 Droplet Test

Before start of droplet test, the aim should be first confirmed. There are 3 points regarding with this aim. It is 1) Confirm hydrophilicity of both bare and porous honeycomb surface by irradiation; 2) Differentiate two irradiation effect, gamma irradiation and electron beam irradiation; 3) Prepare for pool boiling experiment.

To test the effect of irradiation, a porous plate (similar to the honeycomb material) and a copper plate (similar to the copper block material) were irradiated using the gamma-ray source. A new set of porous and copper plates were also irradiated using the electron-beam source. These materials were irradiated to observe the change in hydrophilicity by performing droplet tests before and after irradiation. As mentioned earlier, previous RISA experiments showed an increase in hydrophilicity after irradiation. An increase in surface hydrophilicity would allow more water availability to the surface during boiling. To

quantitatively analyze hydrophilicity, one parameter named contact angle was introduced (Figure 6-1). The calculation way is that, 1) Take one profile of droplet attaching to a surface; 2) Set the edge of interface between droplet and surface as one contact point; 3) Set two sides, one side is along the interface, the other side is tangent to contour of droplet; 4) Define the intersection angle as contact angle.

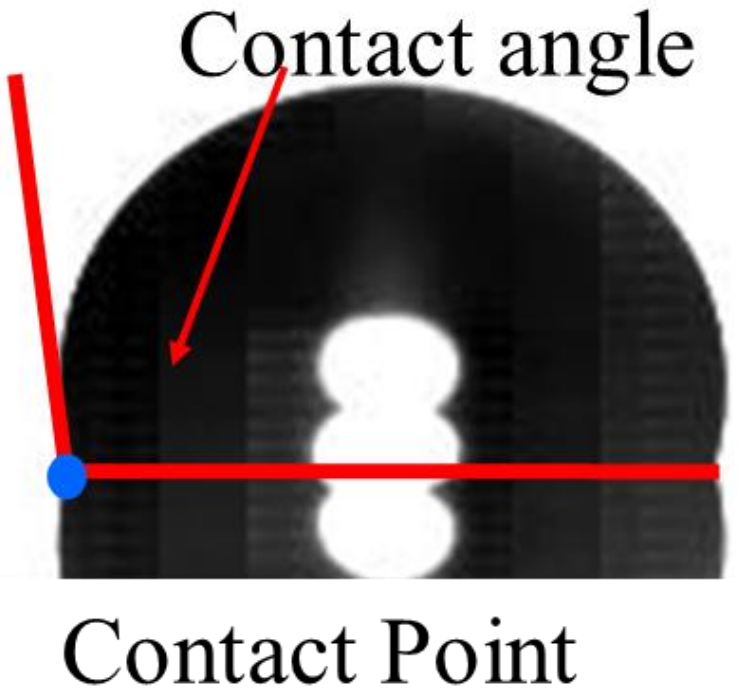

Figure 6-1: Definition of contact angle.

In the recent tests, if the post-irradiated droplet angle was decreased compared to the pre-irradiated one, the hydrophilicity was considered to have been enhanced. If there was no change in the droplet angle after irradiation, the hydrophilicity was considered to remain unchanged. The total dose for each source was ~1000 kGy.

6.1.1 Droplet Test without Irradiation

Before irradiation, surface response without irradiation is given. Figure 6-2 and Figure 6-3 show snapshots of the contact angle on copper surface and 100 µm porous surface, respectively. As it is shown, the contact angle was big and it was almost the same level when dropping on the surface (this is observed from video captured during droplet test).

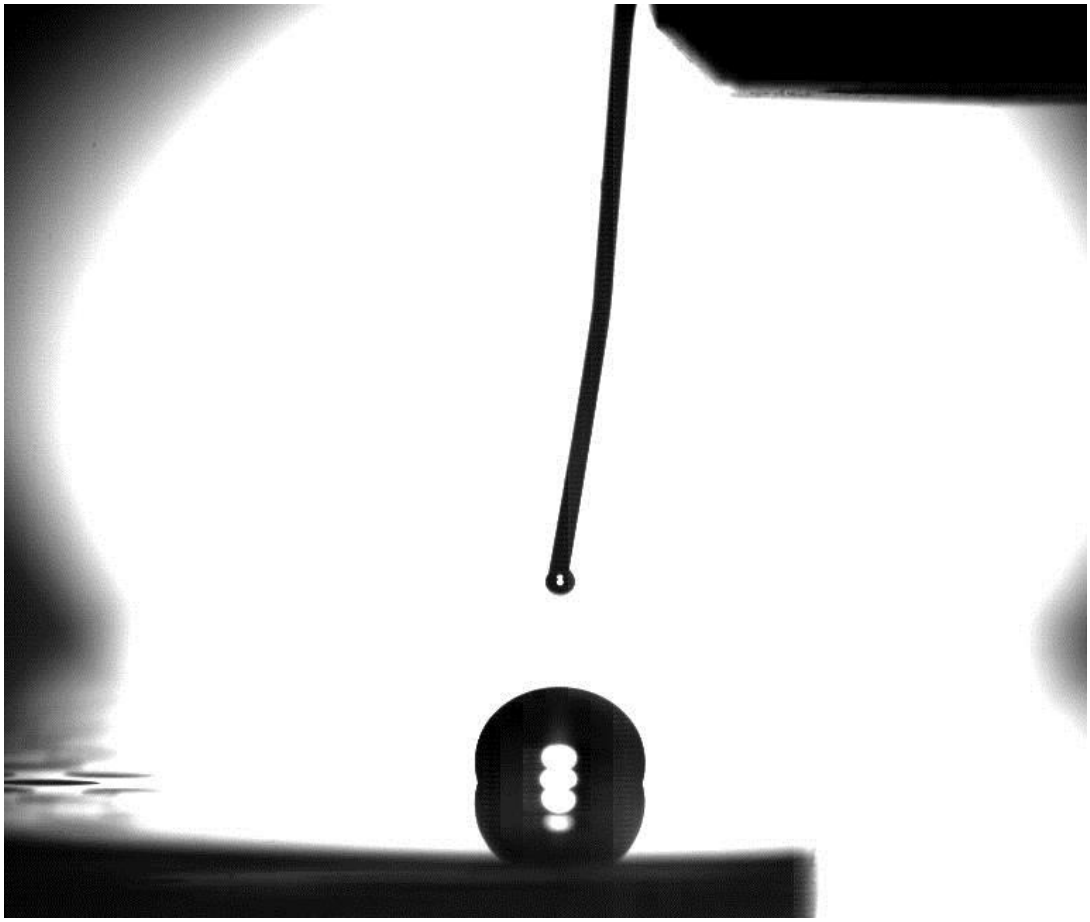

Figure 6-2: Snapshots of the contact angle on copper surface.

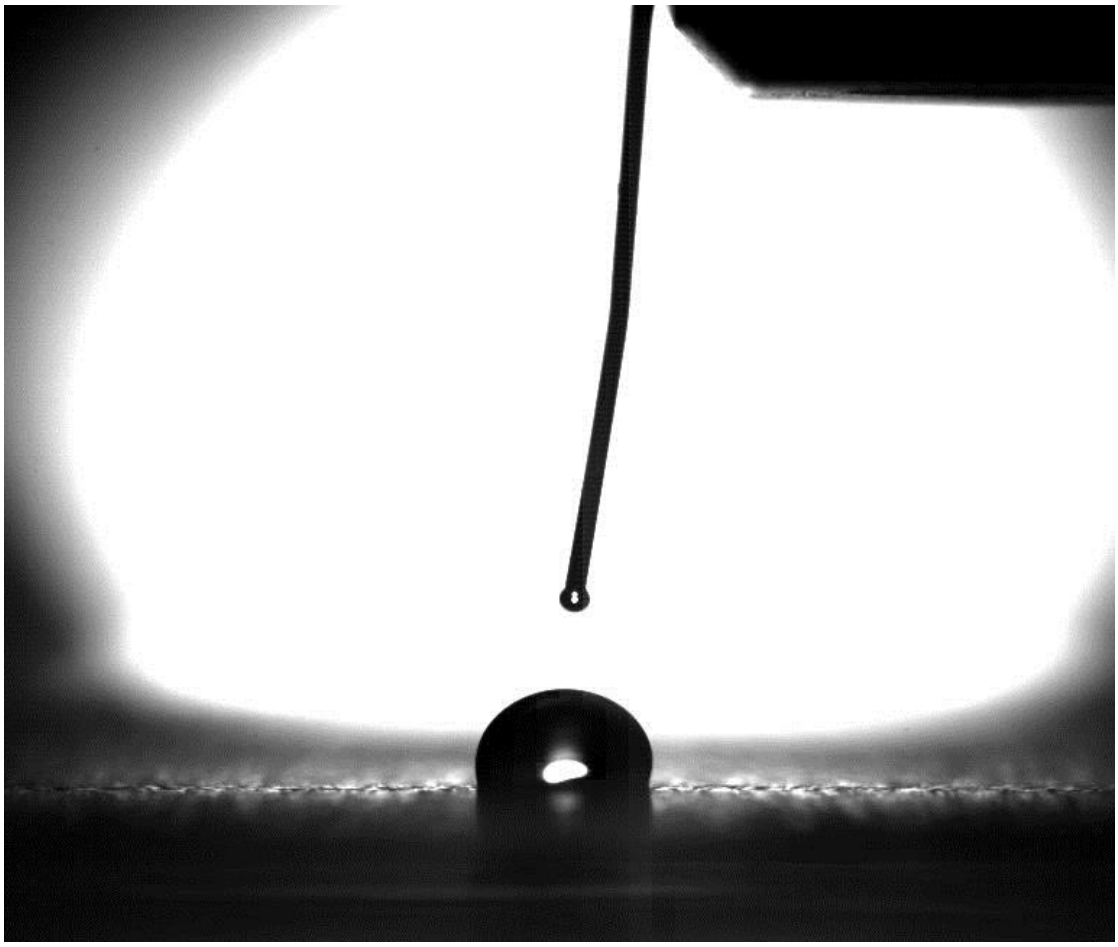

Figure 6-3: Snapshots of the contact angle on 100 μm surface.

6.1.2 Droplet Test with Irradiation

However, after irradiation the phenomenon is quite different from non-irradiation case. In this study, both irradiation source, gamma-ray irradiation and electron-beam irradiation source were chosen. So there is need to show both droplet behavior by irradiation. Figure 6-4 shows the snapshots of contact angle on copper surface and 100 μm porous surface by gamma-ray irradiation and Figure 6-5 shows the snapshots of contact angle on copper surface and 100 μm porous surface by electron-beam irradiation. Even though the sources were different, decreasing trend of contact angle was similar. More specifically, contact angle on copper surface decreases to a very low level (about 15º on copper surface vs 30º on 100 μm porous surface) while the angle value decreased to 0º on both case. To clearly observe contact angle behavior, some snapshots of droplet variation in one case is given in

Figure 6-6. From the figure, it is confirmed that the capillary ability is largely increased. Table 6-1 lists the average static contact angles of lest side and right side before and after irradiation (1000 kGy). This work was carried on and developed by Stalder et al. [42-43], which they implemented droplet test video into image processing software and measure the values. Droplet tests were performed at least three times for each material to get the repeatability. From figure and table, it is shown that irradiation improved the surface hydrophilicity due to the decreased contact angle.

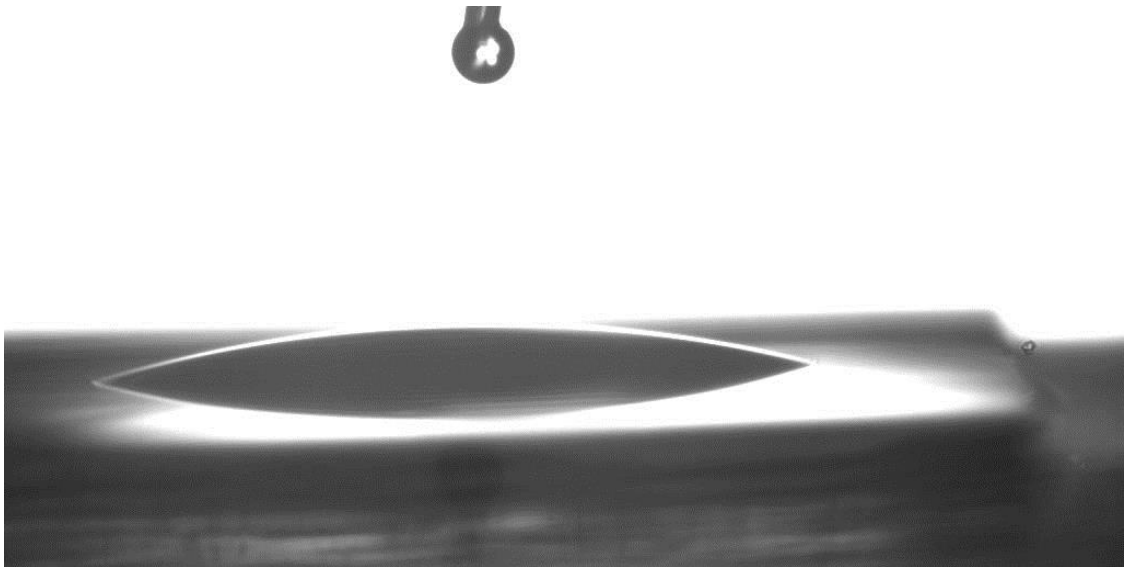

(a) on copper surface

(b) on 100 μm porous surface

Figure 6-4: Snapshots of contact angle on copper surface and 100 μm porous surface by gamma-ray irradiation.

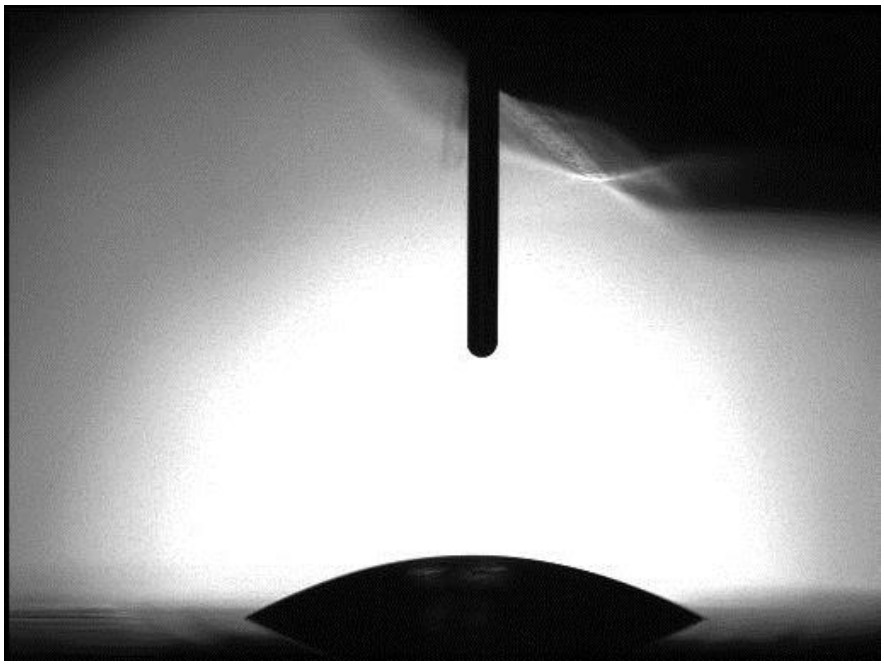

(a) on copper surface

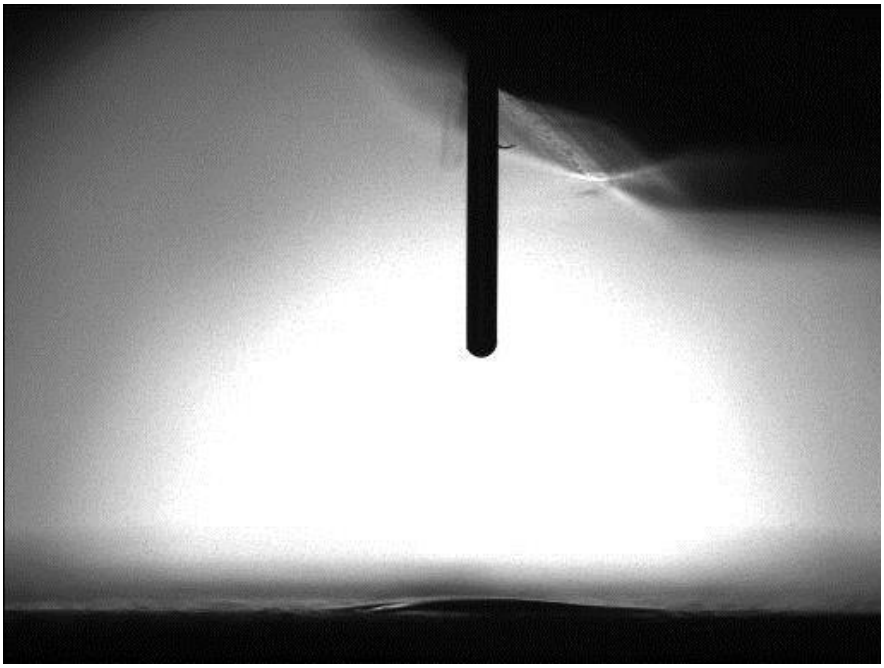

(b) on 100 μm porous surface

Figure 6-5: Snapshots of contact angle on copper surface and 100 μm porous surface by electron-beam irradiation.

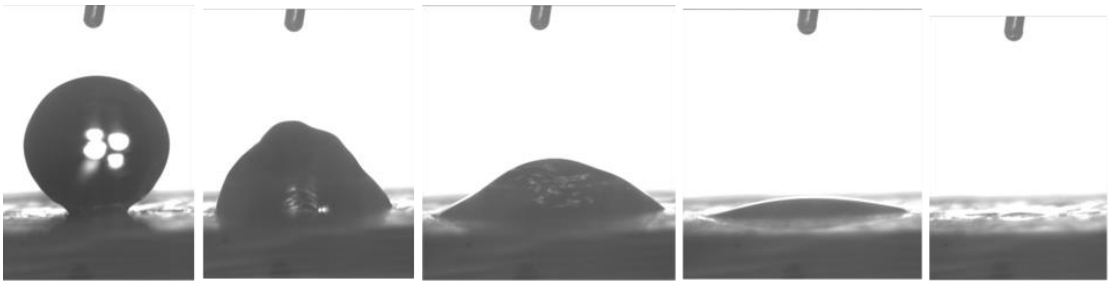

Figure 6-6: Time lapse (≈44 ms) of droplet on porous plate after gamma irradiation [31].

Table 6-1: Average static contact angles of left side and right side before and after irradiation (~1000 kGy) [31].

	Before Irradiation		**After Irradiation (Gamma Ray)**		**After Irradiation (Electron Beam)**	
	left	*right*	*left*	*right*	*left*	*right*
Porous plate	91°	95°	0°	0°	0°	0°
Copper plate	99°	98°	15°	15°	29°	33°

6.1.3 Summary of Droplet Test

After droplet test, here comes the summary. From video and table, it is found that both irradiation sources can improve hydrophilicity based on the decreased contact angle. Also the sources (including gamma-ray and electron-beam) has same effect when keeping dose rate same.

After knowing this, the next step is try to do the pool boiling experiment to test surface hydrophilicity on CHF performance. First, we will start with bare surface case and then deal with honeycomb surface cases.

6.2 Bare Surface Results and Discussion

The aim of doing bare surface with irradiation effect is that 1) confirm irradiation effect on CHF performance; 2) differentiate two irradiation effect; 3) understand the combination of

irradiation and inclination effect on CHF performance; 4) discover the reasons for CHF enhancement.

The specific facility is shown in Figure 6-7 and experimental condition is list in Table 6-2. Here, inclination angle was only 5º, 10º and 20º. Irradiation source included gamma-ray and electron-beam. And dose amount were selected with 0, 300, 1000 and 3000 kGy (0 kGy is used for comparison with irradiated ones).

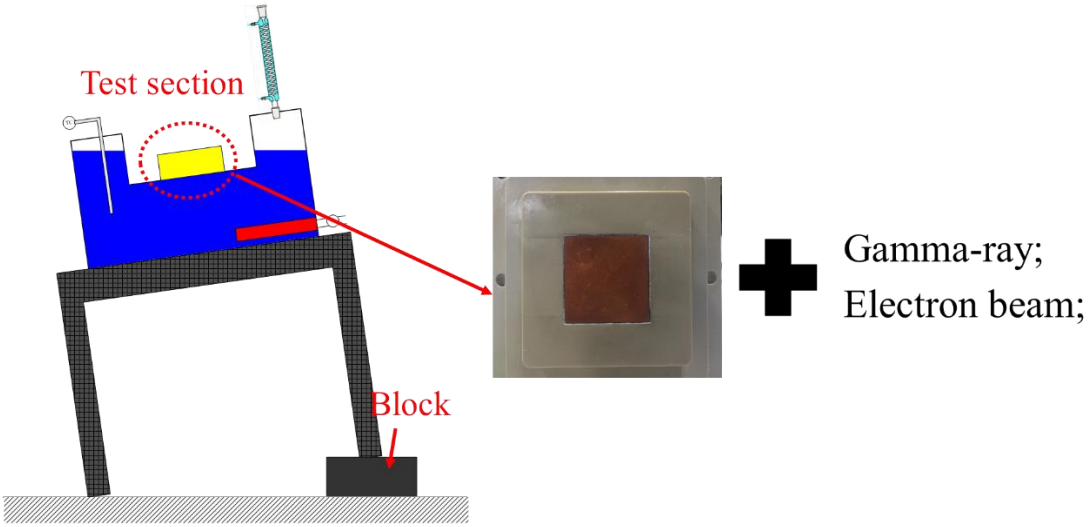

Figure 6-7: Experiment facility of irradiation effect on bare surface.

Table 6-2: Experimental condition in CHF enhancement cases using honeycomb surface method.

Parameters	Value
Pressure	Atmospheric, 101325 Pa
Water temperature	100ºC
Boiling area	30 ×30 mm in square
Inclination angle	5º, 10º, 20º
Dose amount	0, 300, 1000, 3000 kGy

According to the BDF calculation in Chapter 4, the value in 10º and 20º case is much higher than that in 5º case. So discussion will start with 5º case first.

6.2.1 5º Inclination Case Discussion

In 5º inclination case, both gamma-ray and electron-beam irradiation effect were done. So in the following discussion, both will be explained. Through the results, we first should know whether CHF can be enhanced. And then it is necessary to clearly understand whether dose source has effect.

6.2.2.1 Results and discussion of heat transfer after gamma-ray irradiation

After irradiation, the CHF value showed some increase (Table 6-3). Specifically, the CHF in bare case after irradiation increases from 0.25 to 0.41 MW/m^2, showing an enhancement with almost 64%. Regarding with "start time" in Table 6-3, it is the time needed for experiment preparation [31]. To make CHF results reliable and obtain better experiment repeatability, start time is tried to be kept similar. Also the CHF value in this table is an average, because the repeatability should be kept to make sure that data is reliable.

Table 6-3: CHF value of bare surface at 5º inclination with gamma-ray irradiation [31].

Case	Condition	Total dose (kGy)	Start time	CHF value (MW/m^2)	Enhancement
Case 1	BARE(0)	0		0.25	
Case 15	BARE(1)	1020	50 min	0.41	64.0% (+0.16)

NOTE: start time refers to time interval between stopping radiation and starting experiment. And 0 means non-irradiation and 1 means surface with irradiation.

Figure 6-8 shows Heat flux as a function of superheating (i.e., boiling curves). Both the heat flux and the superheat increase. A video of instant boiling is captured using the camera (Figure 6-9). However, these snapshots are different from previous ones (like Figure 4-4). Because the previous ones focus on bubble generation, which can clearly see the boiling condition at different heat flux. And Figure 6-9 tries to explain the vapor-liquid mixture area, which is used for future explanation about the reason for CHF enhancement by irradiation.

In Figure 6-9(d), the left part is magnification of red zone in the right part. As it is shown in this picture, the copper surface is covered by two different phases at the same time. More specifically, some portion is covered by a mixture of liquid and vapor looking like uneven things on the surface. The other portion is fully covered with vapor film (Figure 6-9(d)). In the area covered with the mixture of liquid and vapor, a form of nucleate boiling keeps happening which can leads to a higher level of water replenishment towards heating surface. Also from Figure 6-9, there exists one trend. That is when the heat flux increases and approaches the CHF, the vapor-liquid mixture area increases and reaches a maximum whereas vapor film occupies the whole copper surface, leaving no space for mixture area appears in CHF point. From this figure it is also found that the vapor-liquid mixture area increases as heat flux increases and it reaches the maximum before reaching CHF point.

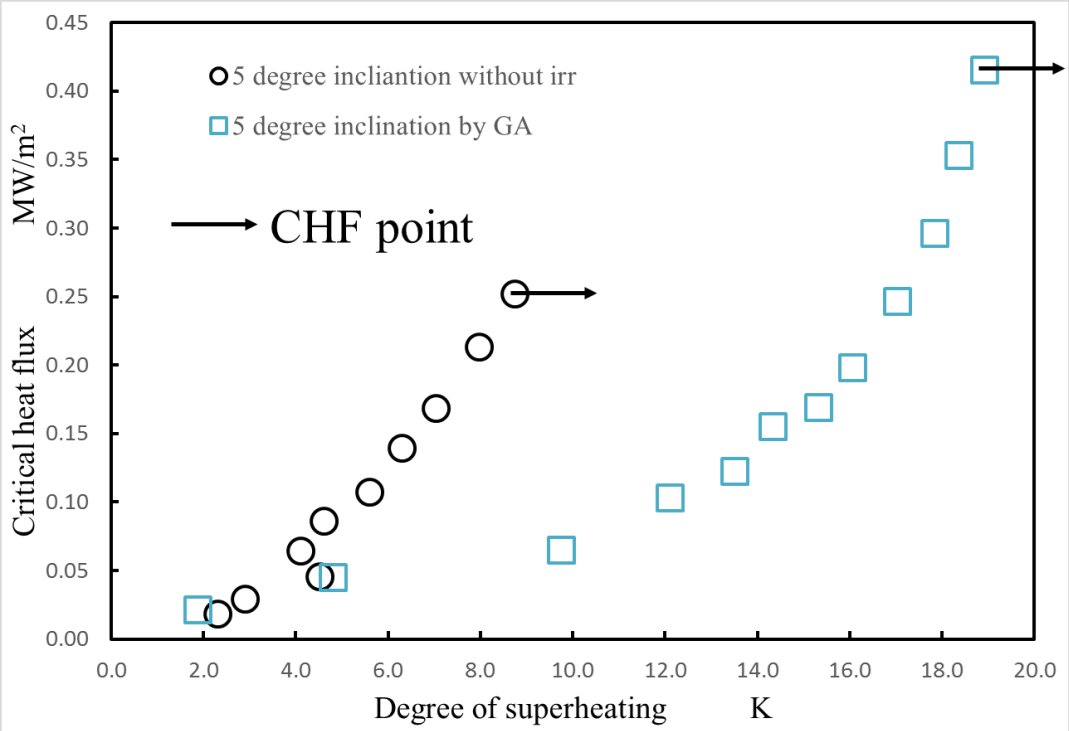

Figure 6-8: Heat flux as a function of superheating (i.e., boiling curves) for cases 1 and 15.

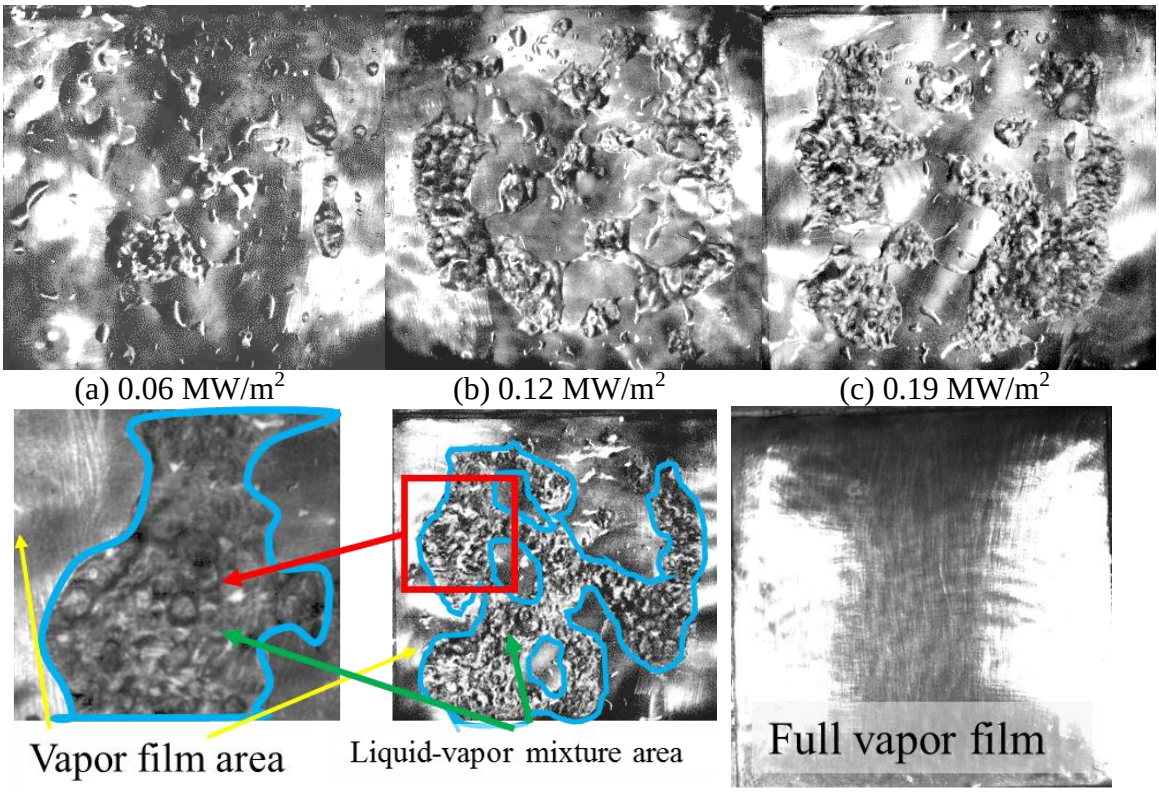

(a) 0.06 MW/m^2 (b) 0.12 MW/m^2 (c) 0.19 MW/m^2

(d) near CHF (e) CHF point

Figure 6-9: Snapshots of copper surface for different heat fluxes in case 1 [31].

After irradiation, the boiling phenomenon is quite different (Figure 6-10). Here, for comparison, heat flux is selected as similar as that in bare surface without irradiation (Figure 6-9(d)). The left part of is the magnification of the red zone in the right part. As it is shown, the vapor-liquid mixture area almost covers the whole heating surface indicating that this kind of area can be largely increased after irradiation. This is because after irradiation, the hydrophilicity is enhanced (approval from droplet test) and therefore the more area can be used for nucleation boiling. With the increased mixture area, boiling heat transfer condition becomes better so that cooling ability is promoted, resulting in a delay in CHF appearance. Besides, the increased rewetting of surface results in larger superheat as in the case of nanoparticles [16].

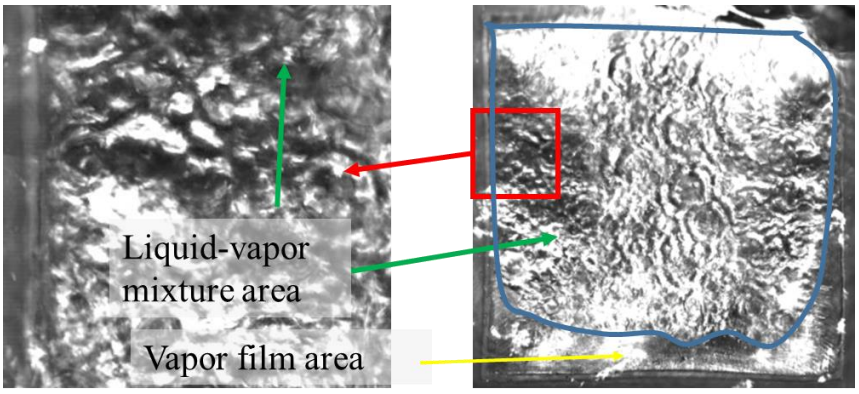

Figure 6-10: Snapshot of copper surface with 0.25 MW/m^2 heat flux in case 15 [31].

6.2.2.2 Results and discussion of heat transfer after electron-beam irradiation

The electron-beam irradiation experiment is conducted to check whether the CHF can be enhanced using an electron source. To the best of the authors' knowledge, such experiments have not been performed previously. In the gamma-ray irradiation experiment, a dose of only 1000 kGy was applied. A similar dose was also applied in the electron-beam experiments, with the addition of a lower dose (300 kGy) and a higher dose (3000 kGy) for comparison. Table 6-4 lists all experimental cases with their CHF values for the electron-beam experiments. In this series of experiments, controlled tests (without irradiation) were conducted for better comparison. Here start time is also kept. The experimental results indicate that electron-beam irradiation also shows enhancement. Case 16 shows almost the same value as before (case 1 shows a value of 0.28 MW/m^2). After 1000 kGy dose irradiation, the increased value was also similar (+0.14 MW/m^2 and +0.16 MW/m^2, respectively). However, when the dose is decreased to 300 kGy, the CHF decreases to the non-irradiated level. Figure 6-11 shows the boiling curve for cases 16, 17 and 18. As shown in this figure, the boiling curves well fit each other under the same condition, suggesting the repeatability of the results.

Table 6-4: CHF value under different conditions with electron-beam irradiation at 5° inclination.

Case	Condition	Total dose (kGy)	Start time	CHF value (MW/m^2)	Enhancement
Case 1	BARE(0)	0		0.28	
Case 16	BARE(1)	300	64 min	0.26	7.1% (-0.02)
Case 16	BARE(1)	300	63 min	0.31	10.1% (+0.03)
Case 17	BARE(1)	1000	70 min	0.42	50.0% (+0.14)
Case 17	BARE(1)	1000	58 min	0.43	53.6% (+0.15)
Case 18	BARE(1)	3000	~60 min	0.42	50.0% (+0.14)
Case 18	BARE(1)	3000	~60 min	0.44	57.1% (+0.14)

NOTE: start time refers to interval between starting experiment and stopping radiation. And 0 means non-irradiation and 1 means surface with irradiation.

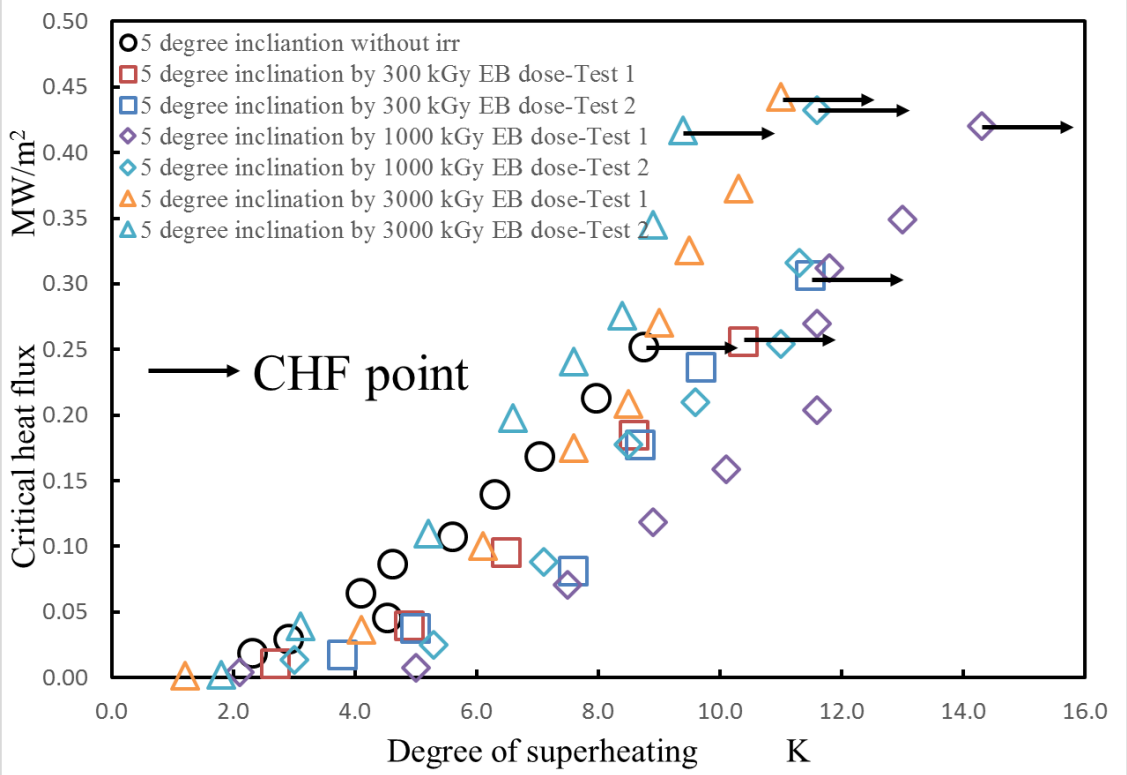

Figure 6-11: Heat flux as a function of superheating (i.e., boiling curves) for cases 1, 16 17 and 18.

During the boiling process, a boiling area was observed in these cases as well. Image processing was used to analyze the boiling area, and the original light source and parameter settings were the same for all cases. When choosing similar heat flux, the snapshots are

shown in Figure 6-12. The images show the complete boiling surface, and the silicone (square shaped) at the edge of each picture indicates the edge of the copper block. On the copper surface, the white area inside red zone is the vapor-liquid mixture area, and the black area is where a vapor film covers the copper surface. In Figure 6-12 (a) and (b), the mixture area is almost the same. This means that although the surface is irradiated, the lower dose has little effect on the surface modification. However, after 1000-kGy irradiation, the mixture area increases and covers almost the entire surface. It is believed that the increased mixture area promotes boiling heat transfer and enhances the CHF in the end. From both gamma irradiation and electron beam irradiation results, 1000-kGy dose can modify copper surface, increasing mixture area and largely improving heat transfer condition. Thus this leads to an enhancement in CHF value by irradiation. In Figure 6-12 (c), the vapor-liquid mixture area is almost occupied the whole copper surface, which means there is no additional space for bubble generation. That is the reason that CHF cannot be further enhanced.

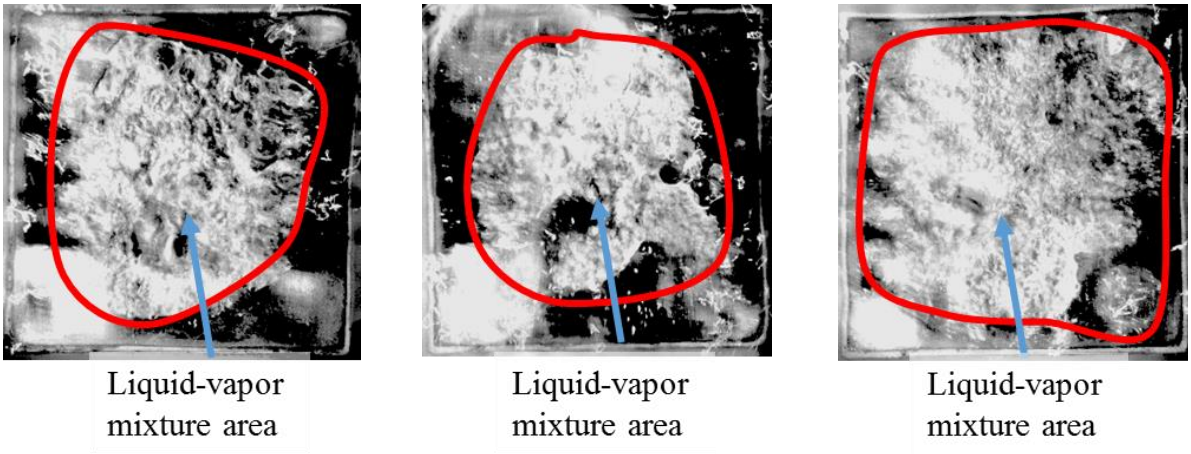

(a) Non-irradiated case with heat flux of 0.21WM/m^2

(b) 300-kGy case with heat flux of 0.24 WM/m^2

(c) 1000-kGy case with heat flux of 0.25 WM/m^2

Figure 6-12: Snapshots of copper surface with similar heat fluxes under different dose rate conditions (5º inclination, electron-beam irradiation) [31].

After knowing this, it is necessary to understand the formation of increased vapor-liquid mixture area. Through video analysis, it is also found that at high heat flux, the boiling is carried on with periodic circle. And in one cycle, a big vapor will move outside copper surface once. Thus, the BDF is also available in irradiation experiment. Table 6-5

list the BDF values with different dose amount. As it is shown, the BDF values are similar so that it is supposed that dose amount cannot affect BDF or even the final CHF value. In another word, irradiation and bubble film removal ability is irrelevance.

Table 6-5: BDF value under different conditions with electron-beam irradiation at 5º inclination.

Inclination angle, º	Irradiation source	Dose amount, kGy	BDF, bubble/s	Heat flux, MW/m^2
5	no	0	4.14	0.28
5	Electron-beam	300	4.37	0.26
5	Electron-beam	1000	4.11	0.27
5	Electron-beam	3000	4.11	0.27

In previous paragraph, the formation of area is observed at high heat flux. So we try to observe single bubble behavior at low heat flux. Figure 6-13 shows the bubble behavior under different conditions with electron-beam irradiation at 5º inclination (low heat flux). When the surface is without irradiation, bubble behavior is like that. Some quite bubbles were generating on heating copper surface and the quantities is a lot. Also, similar phenomenon is observed on 300 kGy case. The bubbles were small and numbers were large. According to this phenomenon, the size of vapor-liquid mixture area was in same level, showing no enhancement in CHF value. However, in 1000 and 3000 kGy cases, bubble behavior changed. The bubbles were very big compared with low dose amount case and non-irradiation case. Besides, only a few bubbles were appearing on heating surface, indicating an increased hydrophilicity. Based on this, an increased vapor-liquid mixture was found at high heat flux.

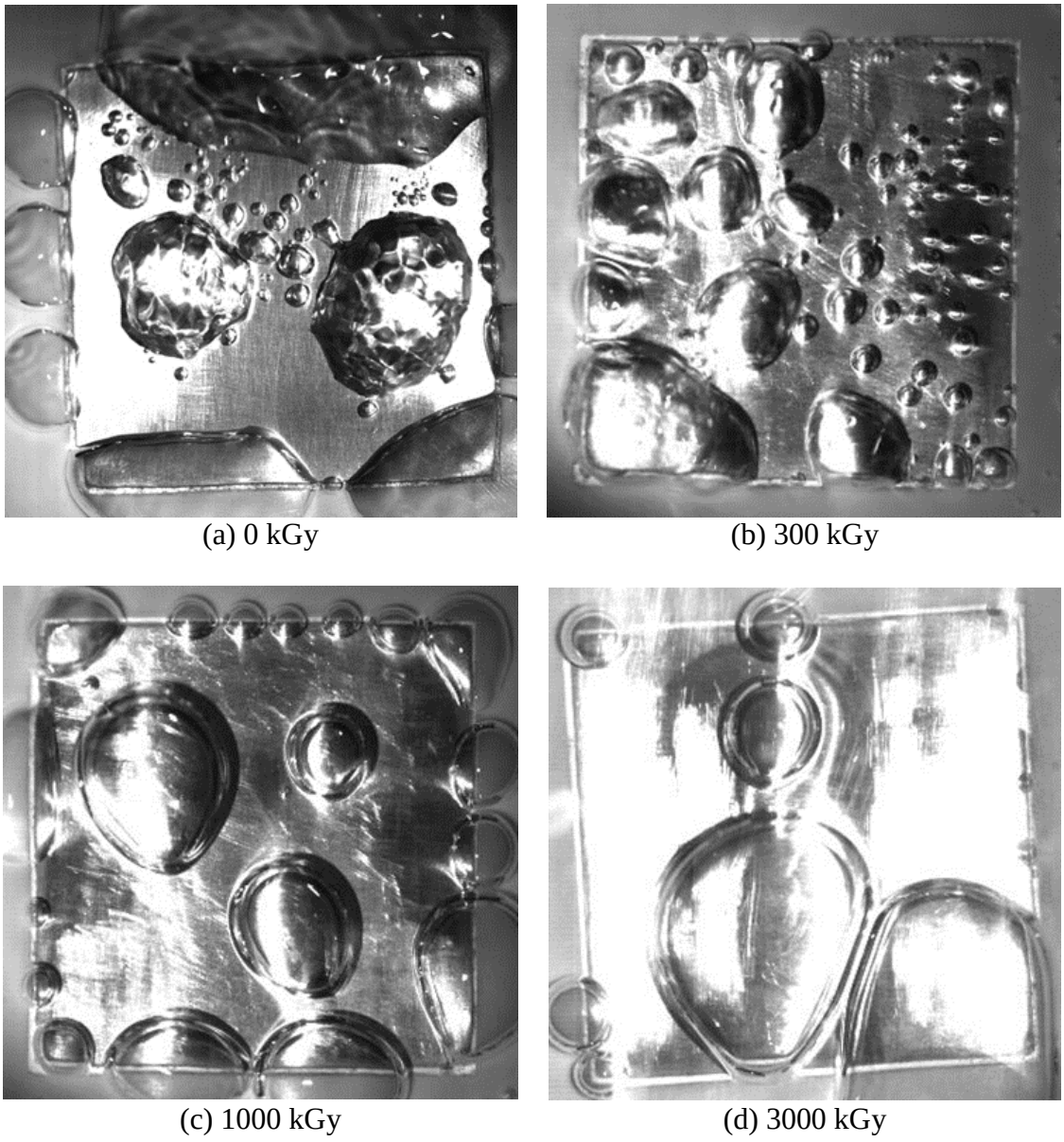

(a) 0 kGy (b) 300 kGy

(c) 1000 kGy (d) 3000 kGy

Figure 6-13: Bubble behavior under different conditions with electron-beam irradiation at 5º inclination (low heat flux).

6.2.2.3 Summary of reasons for CHF enhancement

In prior studies, CHF enhancement in pool boiling is as a result of these effects: (a) extended surface area, (b) nucleation site density, (c) wettability, (d) capillary wicking, and (e) wavelength crease based on the modified Zuber hydrodynamic stability model [41]. From this study, the increased vapor-liquid mixture area were both captured in gamma-ray and electron-beam irradiation experiments. In Figure 4-7, the formation of this area is

already explained. In this area, boiling is happening so that this area is also called nucleation sites. Because the nucleation site area is enlarged, it means boiling area is getting bigger. According to increased boiling area, heat transfer conditions becomes better so that CHF can be delayed.

The conclusion can be made that irradiation can enhance nucleation site area, further improving heat transfer condition, which will result in an increased CHF performance in the end. Also the dose source has no different effect on CHF value if dose amount is kept same.

After knowing that irradiation can promote nucleation site area, the next step is to check whether CHF value can be enhanced by irradiation in 10º and 20º inclination case.

6.2.2 10º and 20º Inclination Case Discussion

In last section, the aim of doing 10º and 20º inclination experiment is clear. Because it is found the dose source has no effect, in higher inclination case only electron-beam irradiation method was selected.

6.2.2.1 Results of 10º inclination case

After irradiation, the CHF value showed no increase (Table 6-6). Specifically, the CHF of the bare case without irradiation is 0.47 MW/m^2 and CHF after 1000 kGy is 0.45 MW/m^2. Figure 6-14 shows a heat flux as a function of superheating (i.e., boiling curves) for cases 2 and 19.

Table 6-6: CHF value under different conditions with electron-beam irradiation at 10º inclination.

Case	Condition	Total dose (kGy)	Start time	CHF value (MW/m^2)	Enhancement
Case 2	BARE(0)	0		0.47	
Case 19	BARE(1)	1000	~60 min	0.45	4.3% (-0.02)

NOTE: start time refers to interval between starting experiment and stopping radiation. And 0 means non-irradiation and 1 means surface with irradiation.

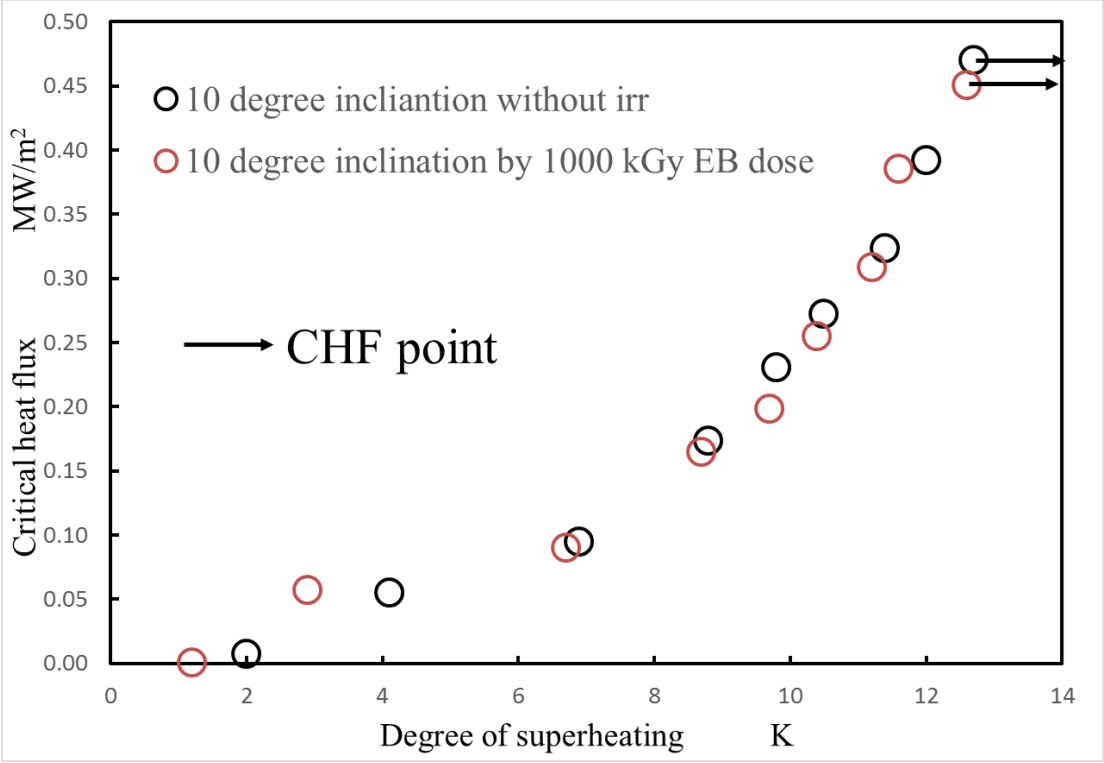

Figure 6-14: Heat flux as a function of superheating (i.e., boiling curves) for cases 2 and 19.

6.2.2.2 Results of 20º inclination case

After irradiation, the CHF value showed no increase (Table 6-7). Specifically, the CHF of the bare case without irradiation is 0.50 MW/m^2 and CHF after 1000 kGy is 0.43 MW/m^2. Figure 6-15 shows a heat flux as a function of superheating (i.e., boiling curves) for cases 3 and 20.

Table 6-7: CHF value under different conditions with electron-beam irradiation at 20º inclination.

Case	Condition	Total dose (kGy)	Start time	CHF value (MW/m^2)	Enhancement
Case 3	BARE(0)	0		0.50	
Case 20	BARE(1)	1000	~60 min	0.43	14.0% (-0.07)

NOTE: start time refers to interval between starting experiment and stopping radiation. And 0 means non-irradiation and 1 means surface with irradiation.

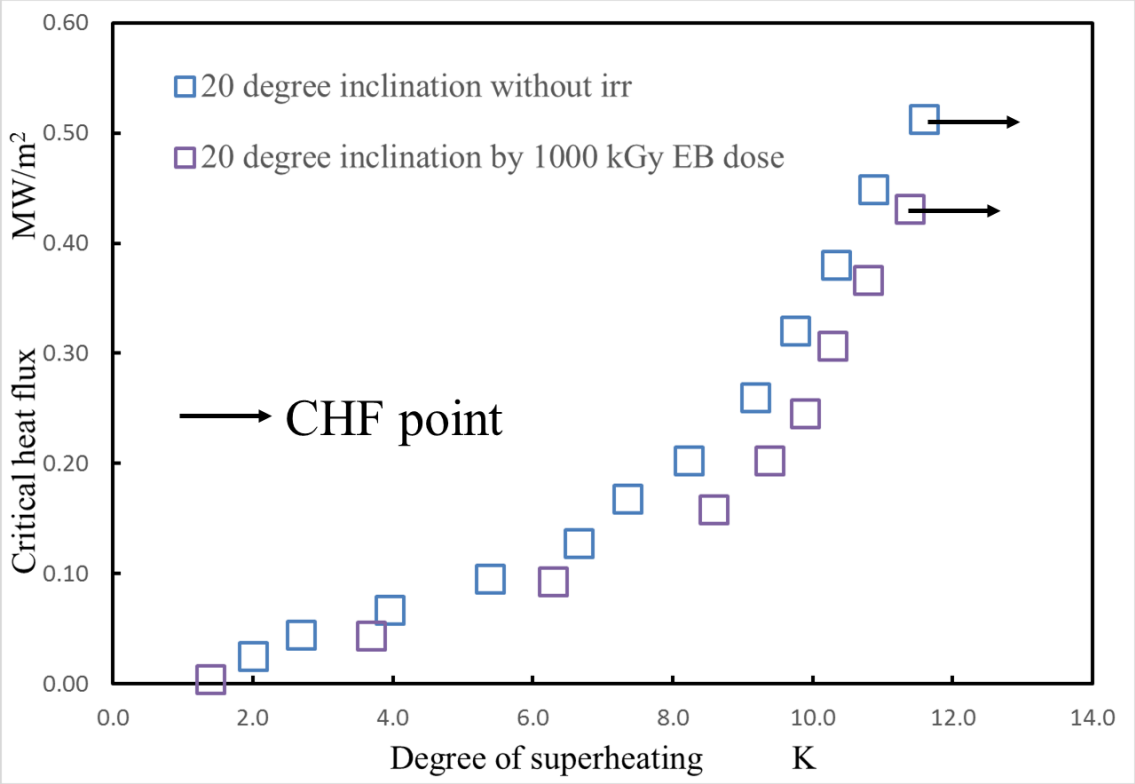

Figure 6-15: Heat flux as a function of superheating (i.e., boiling curves) for cases 3 and 20.

6.2.2.3 Discussion of CHF results.

From Table 6-6 and Table 6-7, it is found that CHF cannot be enhanced by inclination. From droplet test and video capture in 5º inclination case, surface hydrophilicity was supposed to be increased and the nucleation site area during boiling should be increased. However this improvement cannot result in promoting CHF performance. Here the author believed that the bubble film departure frequency (or bubble film removing speed) is one key issue that caused this unchanged CHF results.

Figure 6-16 shows the snapshots of bubble film condition in both 5º and 20º inclination case under 1000 kGy dose amount. For comparison, the shooting range was set within same area and the size copper surface was set same. As it is shown, area inside yellow curves is the N^{th} bubble film and area inside green curves is $(N-1)^{th}$ bubble film. So only one generation was found in 5º inclination case whereas two bubble film generation was found in 20º inclination case. Thus, it is concluded that bubble film removing speed in 20º

inclination case was rapid (4.1 bubble/s @ 5º vs 7.4 bubble/s @ 20º). When the removing speed became fast, it means time consuming of bubble film covering period was decreasing. Due to this short covering period, effect of vapor-liquid mixture area (nucleation site area) descends, resulting no further CHF enhancement. In another word, the bubble film removal was so speedy that there was not enough time for high level of water replenishment in the mixture area.

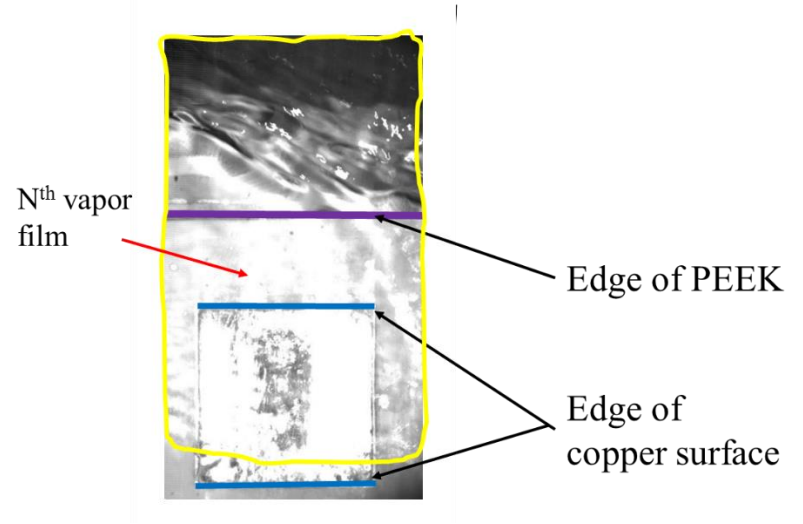

(a) 5º inclination case

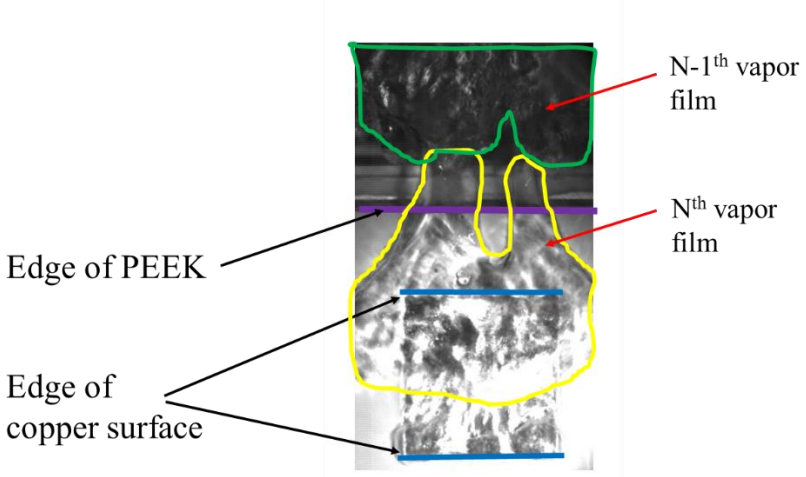

(b) 20º inclination case

Figure 6-16: Snapshots of bubble film condition in both 5º and 20º inclination case under 1000 kGy dose amount.

Also, the BDF of 10º and 20º inclination case after irradiation was calculated and the results are list in Table 6-8. From the table, it is found that irradiation cannot affect BDF, which shows same phenomenon with 5º inclination case. Combined with suggestion in Chapter 4, it is known that BDF can only be determined by inclination rather than irradiation.

Table 6-8: BDF value under different conditions at 10º and 20º inclination.

Inclination angle, º	Irradiation source	Dose amount, kGy	BDF, bubble/s	Heat flux, MW/m^2
10	No	0	6.7	0.47
10	EB	1000	6.5	0.45
20	No	0	7.4	0.50
20	EB	1000	7.1	0.43

6.2.3 Summary of Bare Surface Cases by Irradiation

In this study, both gamma-ray and electron-beam irradiation were selected for CHF enhancement study. In electron-beam irradiation experiment, inclination effect was also chosen as one factor to test the irradiation phenomenon. Through the results, it can be found that:

1) After irradiation, the bubble becomes very big (due to the increased hydrophilicity) compared with non-irradiation case. Because of this changing, at high heat flux (it means the heat flux that can force a big bubble film appearing on heat surface) an increased vapor-liquid mixture area is observed. So it is concluded that irradiation can improve nucleation site area, promoting heat transfer condition. And this is the key issue that result in CHF enhancement;

2) CHF enhancement is only found in 5º inclination case rather than 10º and 20º inclination case. This is because at higher inclination, the bubble film departure frequency is much larger than that in 5º. So the effect of vapor-liquid mixture area is weaken by this shorted bubble film covering period, leading to an unchanged CHF performance.

6.3 Honeycomb Surface Results and Discussion

First the theory of honeycomb is given. Because it is already explained in last chapter, a brief introduction is descripted here. During boiling, water will be absorbed through porous surface and approaching heating surface to keep it wet. Also water refluxing can be realized through the holes. After that, the water will vaporizes and grows inside the hole-shaped channel. When the bubbles become big enough, they will come out of holes and cover the porous surface of the honeycomb. Only water inside the porous layer can be supplied to the boiling surface during this time. After the bubble film is removed, the next water refluxing will carry on. This can complete one heat transfer cycle (Figure 6-17). Because more water can be used for cooling, the CHF in the honeycomb case is increased. Mori et al. [23] found that honeycomb structure can provide two separate path for both water refluxing and bubble removal, decreasing the flow friction.

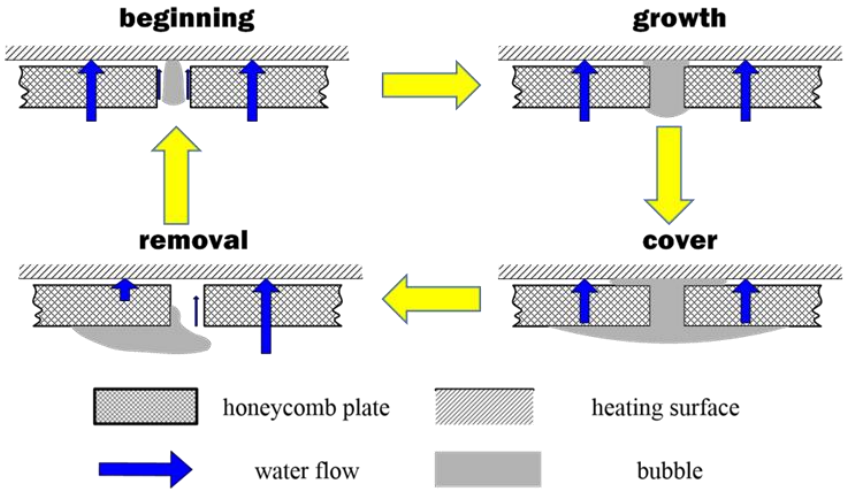

Figure 6-17: Water refluxing cycle in honeycomb structure [31].

The aim of doing such kinds of experiments is that, 1) To Confirm irradiation effect on CHF performance; 2) To differentiate two irradiation effect; 3) To see combination of irradiation and inclination effect on CHF performance; 4) To understand the reasons for CHF enhancement.

The specific facility is shown in Figure 6-18 and experimental condition is list in Table 6-9. Here honeycomb structure (pitch/diameter) was 2.5/1.7, pore size was only 100-μm, inclination angle were 5º, 10º and 20º, respectively.

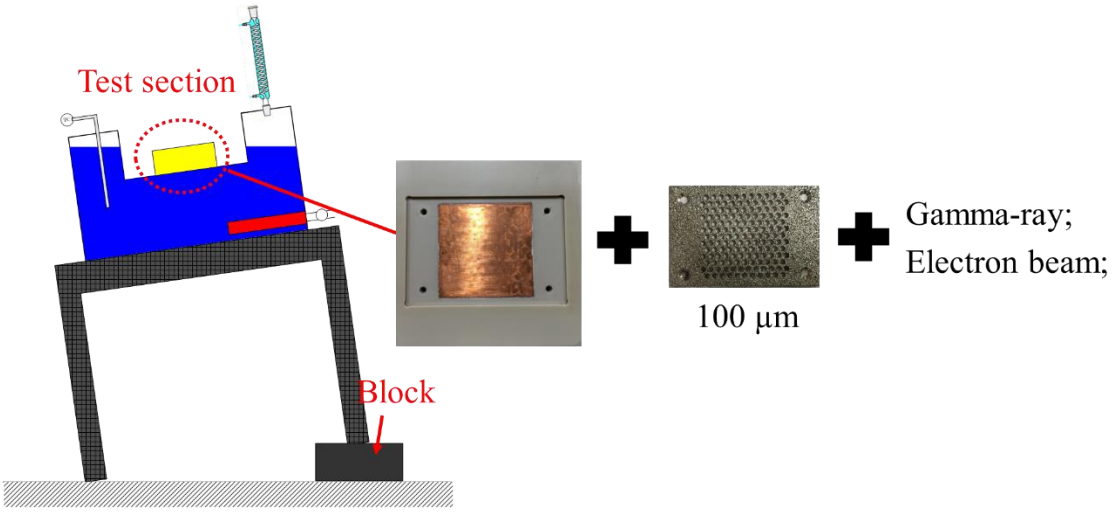

Figure 6-18: Honeycomb surface within irradiation effect experiment facility for CHF enhancement.

Table 6-9: Experimental condition in CHF enhancement cases using honeycomb surface and irradiation method.

Parameters	Value
Pressure	Atmospheric, 101325 Pa
Water temperature	100ºC
Boiling area	30 ×30 mm in square
Inclination angle	5º, 10º and 20º
Pore size	100-μm
Pitch/diameter ratio	2.5/1.7
Dose amount	0, 1000 and 3000 kGy
Dose source	Gamma-ray and Electron-beam

6.3.1 Gamma-ray Irradiation results

Table 6-10 shows the CHF results after irradiation. Figure 6-19 shows heat flux as a function of superheating (i.e., boiling curves) for cases 7 and 21. From the results, no CHF enhancement was observed. Here irradiation in case 21 means both copper surface and honeycomb were irradiated.

Table 6-10: CHF results of honeycomb surface cases by gamma-ray irradiation.

	Inclination angle, °	Test section	Porous size, μm	Dose amount, kGy	CHF value, MW/m^2
Case 7	5	Porous HC	100	0	0.83
Case 21	5	Porous HC	100	1000	0.87

NOTE: HC means honeycomb plate.

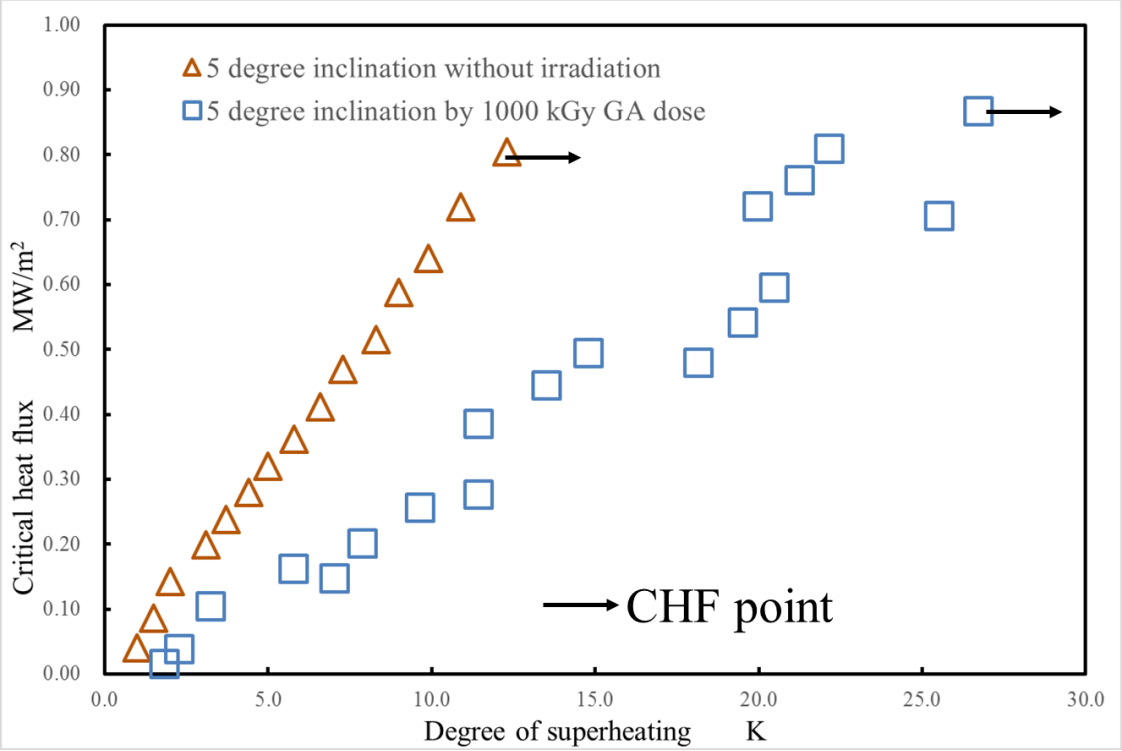

Figure 6-19: heat flux as a function of superheating (i.e., boiling curves) for cases 7 and 21.

6.3.2 Electron-beam Irradiation Results

Table 6-11 shows the CHF results after irradiation. Figure 6-20 shows heat flux as a function of superheating (i.e., boiling curves) for cases 7, 22, 23, 24 and 25. From the results, no CHF enhancement was observed even with higher dose or higher inclination. Here irradiation in case 22-25 means both copper surface and honeycomb were irradiated.

Table 6-11: CHF results of honeycomb surface cases by electron-beam irradiation.

	Inclination angle, °	Test section	Porous size, μm	Dose amount, kGy	CHF value, MW/m^2
Case 7	5	Porous HC	100	0	0.83
Case 22	5	Porous HC	100	1000	0.87
Case 8	10	Porous HC	100	0	0.91
Case 23	10	Porous HC	100	1000	0.87
Case 24	10	Porous HC	100	3000	0.85
Case 9	20	Porous HC	100	0	1.00
Case 25	20	Porous HC	100	1000	1.02

NOTE: HC means honeycomb plate.

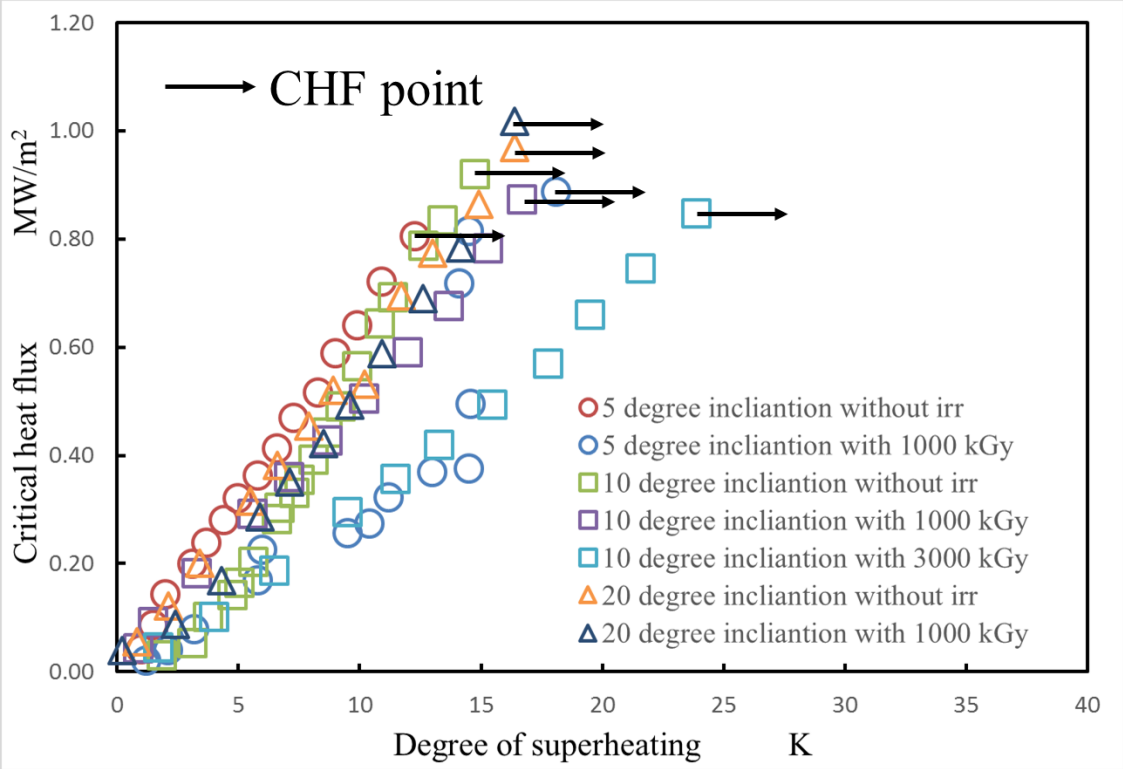

Figure 6-20: Heat flux as a function of superheating (i.e., boiling curves) for cases 7, 22, 23, 24 and 25.

6.3.3 Results Discussion

From the results, no CHF enhancement was observed no matter what the inclination, irradiation dose and dose source were set. Also we test the BDF value. Here only 5°

inclination case was calculated for comparison. At CHF point, the values were 4.30 (non-irradiation) and 4.17 (by 1000 kGy irradiation), respectively. Besides, BDF at lower heat flux was calculated. Through comparison these values fit each well, showing the same variation trend (Figure 6-21). So it is concluded that in honeycomb case, irradiation cannot affect BDF either.

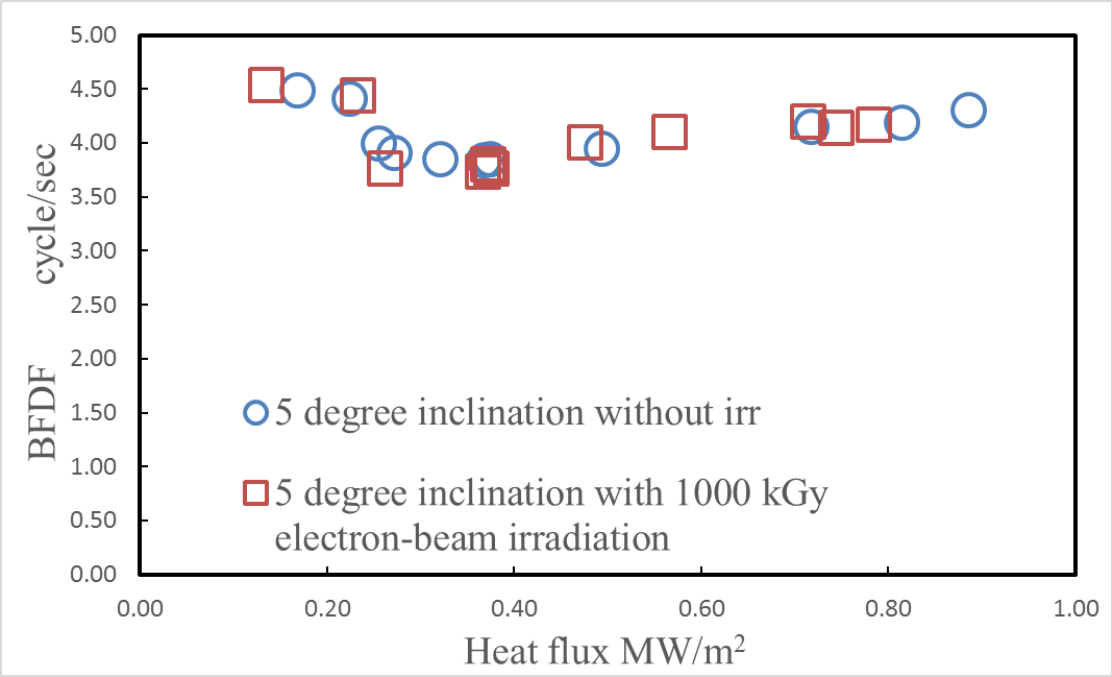

Figure 6-21: BDF value variation in case 7 and 22.

As it is indicated in last chapter, available water refluxing mass flow rate is calculated. Because the irradiation strength is not strong so that it is believed that electron-beam irradiation cannot change honeycomb plate structure, which means the mass flow rate cannot be changed. Besides, the pitch/diameter ratio was 2.5/1.7 and the hole-ratio is about 37%. Regarding with this ratio, it is believed that the available bubble removal mass flow rate is lower than that of water refluxing, which means bubble removal is key issue to determine the final CHF value. Considering that both water refluxing and bubble removal mass flow rate remain unchanged, the CHF results of honeycomb cases by irradiation will keep constant instead of increasing.

6.4 Chapter Summary

In this chapter, both bare surface and porous honeycomb surface by irradiation cases are discussed. Also, inclination effect is added into consideration. All the CHF results are plot into one figure to see the variation trend (Figure 6-22). At the upper part is honeycomb CHF results. As it is shown, no CHF enhancement is observed in all cases. In another word, the dose source and dose amount has no effect on CHF performance. CHF only increases as inclination.

At the bottom part there appears the results of bare surface cases. In 5º inclination, CHF enhancement is found. Also, both gamma-ray and electron-beam irradiation can improve it and the extent of enhancement is same, indicating that it is the dose that promotes CHF value instead of dose source. When dose amount is lower (300 kGy for example), no CHF enhancement is found. In 10º and 20º inclination, no CHF enhancement is observed.

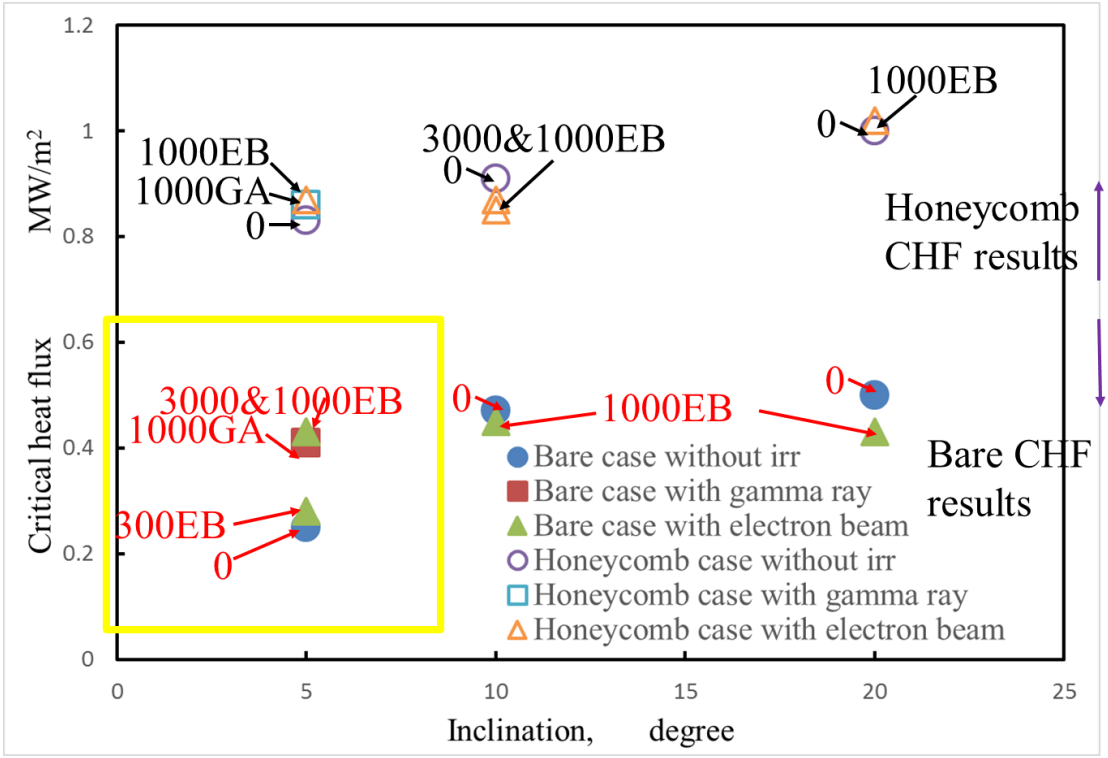

Figure 6-22: Comparison of CHF value with/without irradiation at different inclination angle.

Based on this figure, the summary is as follows.

- After irradiation, the hydrophilicity of the materials increases and the contact angle decreases compared with those in the non-irradiated case. When keeping the dose rate constant, the enhancement by either gamma-ray irradiation or electron-beam irradiation is approximately the same.
- In 5º degree inclination case, the bubble is getting bigger and the vapor-liquid mixture area is largely increased after irradiation. That is the reason for CHF enhancement. Here, this mixture area is called nucleation site area. So it is found that irradiation can increase nucleation site area, which is one reason for CHF improvement studied by previous research.
- In 10º and 20º inclination case, no CHF enhancement is found. This is because bubble film removal frequency is so speedy that it weakens the effect of vapor-liquid mixture area which can keep the surface cooling down.
- In honeycomb surface cases, no CHF enhancement is observed. This is because irradiation cannot change honeycomb plate structure to change water refluxing mass flow rate. Further, bubble removal mass flow rate is key issue in this type of honeycomb structure, which determines the final CHF value. These two factors results in unchanged CHF results.
- Irradiation cannot affect BDF value. In another word, surface wettability is only decided by inclination angle.

7. Conclusion and Future Plan

7.1 Main conclusions

For the development of NPPs in the future, the thermal power should be largely increased, which means there is a need for improvement of cooling ability correspondingly to keep melting corium in-vessel retention for sake of potential severe accident. To reach the aim of keep the integrity of reactor pressure vessel, one effective method is to enhance CHF of ex-vessel. In this study, two methods, honeycomb surface and irradiation methods, were chosen for CHF enhancement discussion. In the following, the test results are given. Meanwhile, combined with CHF enhancement theory, theory for CHF improvement by using present two methods are explained.

Based on honeycomb and irradiation experiment, the findings are list as follows:

- In bare surface case, CHF increases as inclination, which means the higher inclination it is the larger CHF value it shows;
- In honeycomb surface cases, a) solid honeycomb surface can enhance CHF compared with bare surface case. Moreover, porous honeycomb surface cam further enhance CHF performance; b) present pore size has no effect on CHF value; c) CHF also increases as inclination going up; d) CHF value increases as hole-area ratio;
- In irradiation cases, a) irradiation reduces contact angle, increasing surface hydrophilicity. Also, at same dose amount extent of angle decreasing is similar which means source type has no effect; b) in 5° bare surface case, CHF can be largely enhanced by high dose irradiation. Besides, source type has similar effect on CHF performance; c) in 10° and 20° bare surface case, CHF cannot be enhanced; d) in all honeycomb surface case, irradiation cannot affect CHF performance;

Based on experiment findings, the discussion is given in the following.

- Inclination can affect BDF, one factor that can determine the speed of bubble removal from heating surface. More specifically, at high inclination, bubble removal speed is rapid so that BDF is larger. Under this circumstance, surface replenishment condition becomes better, which can provide surface with more coolant in unit time. In both bare and honeycomb surface, BDF becomes larger with increasing inclination.
- Separate phase circulation and bubble behavior restricted by honeycomb structure are the reason for CHF enhancement by application of honeycomb. Besides, additional water refluxing path can also enhance CHF performance.
- Pressure balance model can be used in downward-facing pool boiling. Through the comparison between formulation and experiment, it is known that CHF value is a balance of water refluxing and bubble removal mass flow rate, which means the lower value can determine the final CHF performance. In this study, according to formulation water refluxing mass flow rate decreases as hole-area ratio while bubble removal mass flow rate increases as hole-area ratio. So CHF can reaches the maximum when both mass flow rate are equal. Besides, this crossing point of both water refluxing and bubble removal mass flow rate curve is at the hole-area ratio 0.41.
- Irradiation can increase nucleation site area. If the nucleation site area is big, the level of water replenishment toward heating surface is larger, causing an improved heat transfer condition. That is the reason for CHF enhancement.
- From both surface modification method, it is found in downward-facing, bubble removal is dominant to determine CHF. This is reason why CHF is similar with same hole-ratio even though diameter is different and the reason why irradiation cannot enhance CHF in honeycomb surface case.

From the discussion based on experiment results, some conclusions can be made and these can provide some reference for future IVR design.

1) Pressure balance can be applicable in downward-facing boiling and CHF is a function of hole-ratio. With given parameter of honeycomb plate, the higher CHF region can be predicted;

2) Irradiation can increase nucleation site area, which is one reason for CHF enhancement. For future design, one of enhancing CHF method is try to increase nucleation site area;

3) How to remove bubble is key issue in downward-facing pool boiling. To enhance CHF, first try to increase bubble removal ability.

7.2 Future Work

This studies introduces two different methods that can enhance CHF value compared with bare surface case. In parallel, the theoretical explanation has been given to illustrate the reason for CHF enhancement. However, there is still a need for further study and some part should be modified more reasonably. The following lists the future work plan.

1) Regarding with irradiation study, this study only gives some qualitative analysis to explain the reason for CHF enhancement, such as contact angle decreasing or nucleation site area increasing after irradiation. The next step is try to construct relation between dose amount and size of nucleation site area. Meanwhile, two irradiation dose sources had been used for study. Even though CHF performance is same on bare surface cases, the boiling curve shows different increasing trend. Because of this, there is a need to study the irradiation effect on surface. The preliminary proposal is try to use SEM to scan the surface to observe the differences.

2) In present study, only the increasing trend as hole-area ratio increasing was observed based on experiment data. However, as the model indicates a decreasing CHF trend should appear at high hole-area ratio. So the next step is try to manufacture porous honeycomb plate with larger hole-area ratio. Then do the experiment to check the CHF decreasing trend.

3) Try to modify the available water refluxing and bubble removal mass flow rate model in this study. For now, the available bubble removal mass flow rate model is calculated and made through fitting approaching method, which is based on experiment results. According to previous study, this flow rate can be affected by some force on bubble

(bubble grow force for example [44-46]). Thus, the consideration of using these forces to construct available bubble removal mass flow rate is taken. Besides, in pressure balance explanation the pressure variation by gravity haven't been considered. So we try to improve our model to fit the experiment data.

Acknowledgement

I am very appreciated to have a chance to interact with people who made mu studies and life in Japan enjoyable.

I would like to thank Professor Koji Okamoto for helping me to finish my doctoral course in the University of Tokyo. I am very grateful for his help, assistance and especially the guidance and encouragement during the time when I was faced with some troubles.

I would like to thank the committee members for taking the time out of their busy schedules to attend my final defense and providing me with lots of suggestions to complement and improve my studies.

I would like to thank Project Associate professor Nejdet Erkan and Lecturer Masahiro Kondo for all comments during my studies and assistance during the experiments.

I would like to thank all my friends and colleagues who gave me advice during the studies, especially Dr. Byeongnam Jo, Dr. Abdul Khan, Dr. Penghui Chai, Dr. Hongyang Wei, Miss Yang Wu, Mr. Qian Zhou, Mr. Laishun Wang, Mr. Kai Wang, and Mr. Shota Ueda.

I would like to thank the staff at the department of Nuclear Engineering and Management at the University of Tokyo for help me with various procedures in daily life, especially Ms. Hisako Komatsu, Ms. Mari Morishita and Ms. Tamami Nabeshima. With their help, my life in Japan becomes comfortable.

I would like to thank my Japanese Teacher Ami Nakamura who made me get easier to know the Japanese culture and enjoy the life in foreign country.

Finally, I am very thankful to my family and my girlfriend for providing their support and encouragement to help me finish my doctoral course.

APPENDIX

Appendix-A Inclination Angle Setting

In this study, three different inclination angles were chosen for CHF enhancement study. They were 5º, 10º and 20º, respectively. Here we use inclined cover and blocks which can tilt the support to reach the aim. First, the inclined cover and blocks are introduced.

Figure A-1 shows both plain cover and inclined cover utilized in this study. Regarding with inclined cover, the tilting angle is 10º, which can be directly used for 10º inclination experiment case.

(a) plain cover

(b) inclined cover

Figure A-1: Two covers that are utilized in this study.

Besides, the blocks were used to tilt the support to reach higher inclination (e.g. 20º). Figure A-2 gives the picture of experimental facility with 5º inclination. As it is shown, blocks are put under support to tilt support.

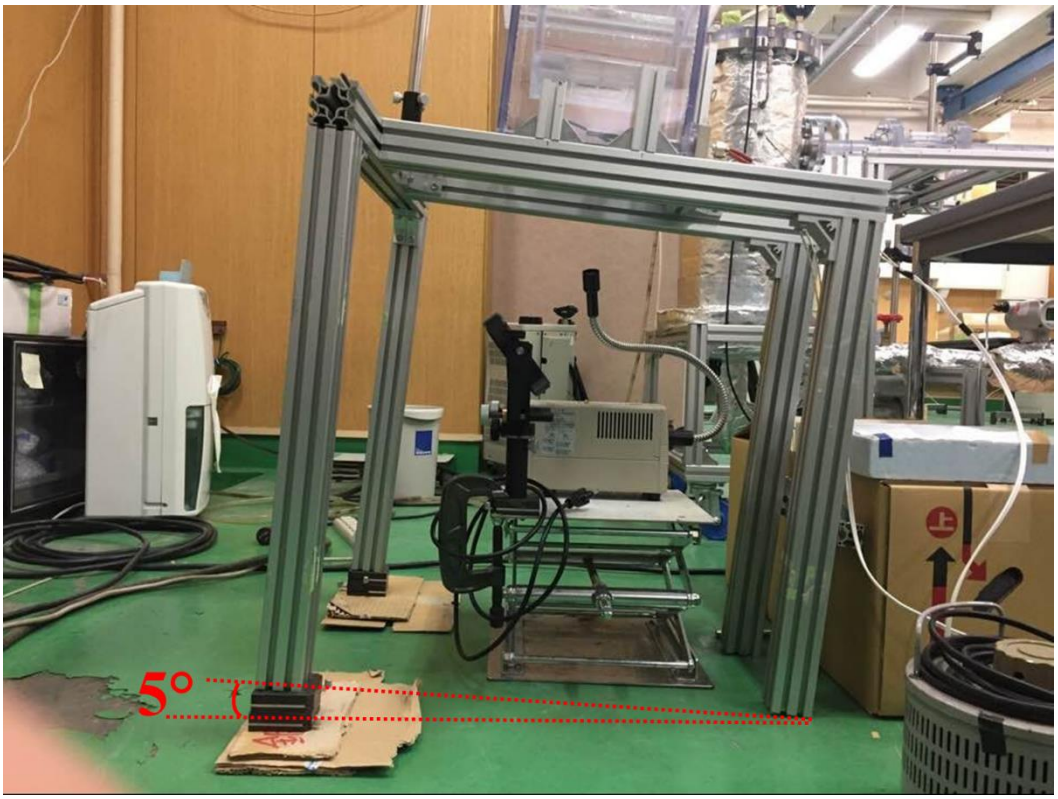

Figure A-2: Experimental facility with 5º inclination.

After using the combination of cover and block, the different inclination angle can be realized. Table A-1 shows the combination method to reach expected angle.

Table A-1: Combination method to reach 5º, 10º and 20º.

Expected inclination angle, º	Cover type	Tilting angle by blocks, º
5	Plain cover	5
10	Inclined cover	0
20	Inclined cover	10

Appendix-B Surface Polishing Procedures

The following steps show the surface polishing procedures.

1) Remove previous applied silicone attaching to the surface after taking test section out of cover.

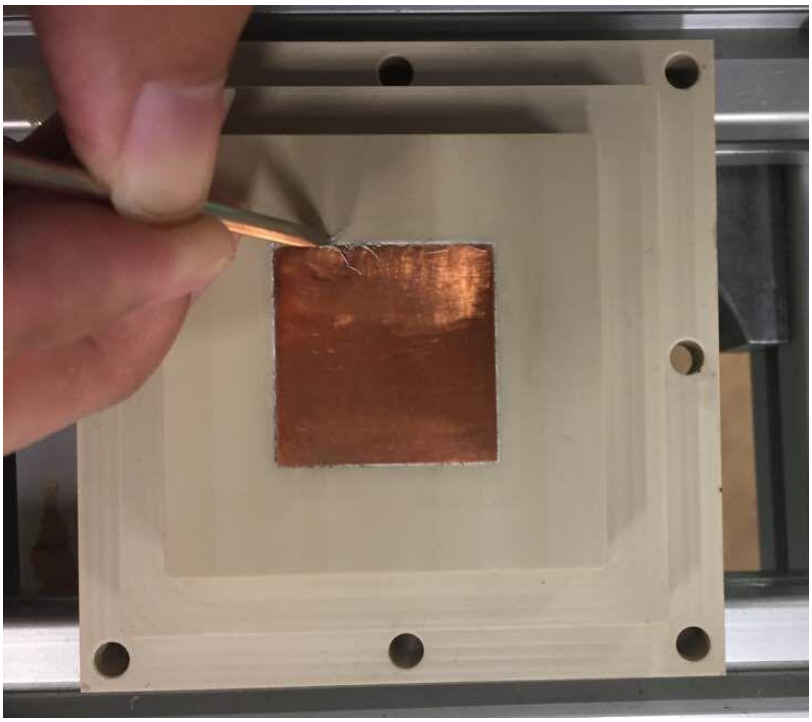

2) Apply new silicone to the gap between copper block and PEEK.

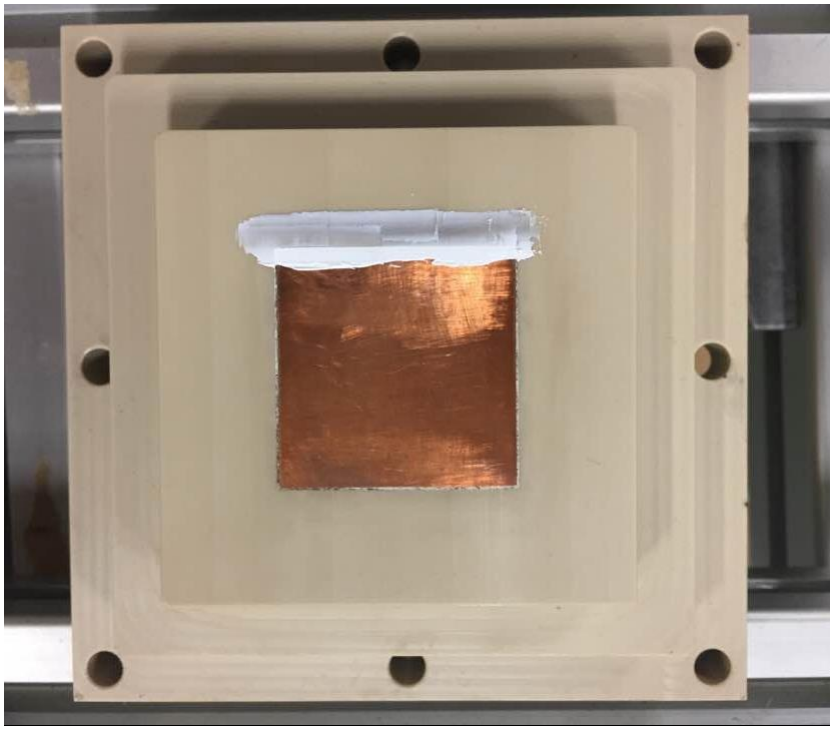

3) Remove the additional silicone attaching on copper surface and PEEK.

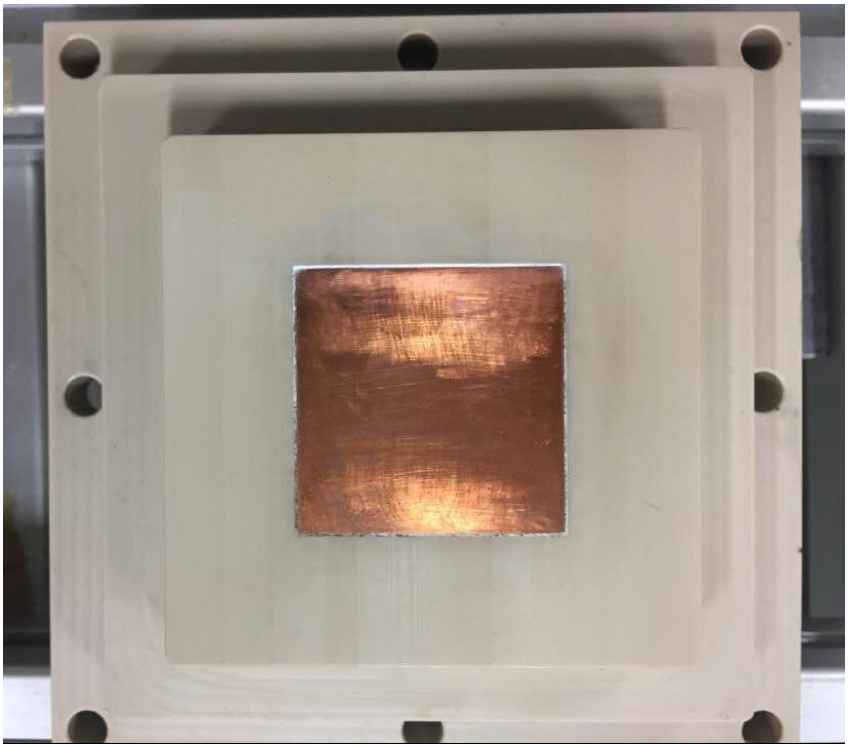

4) Apply oil on copper surface.

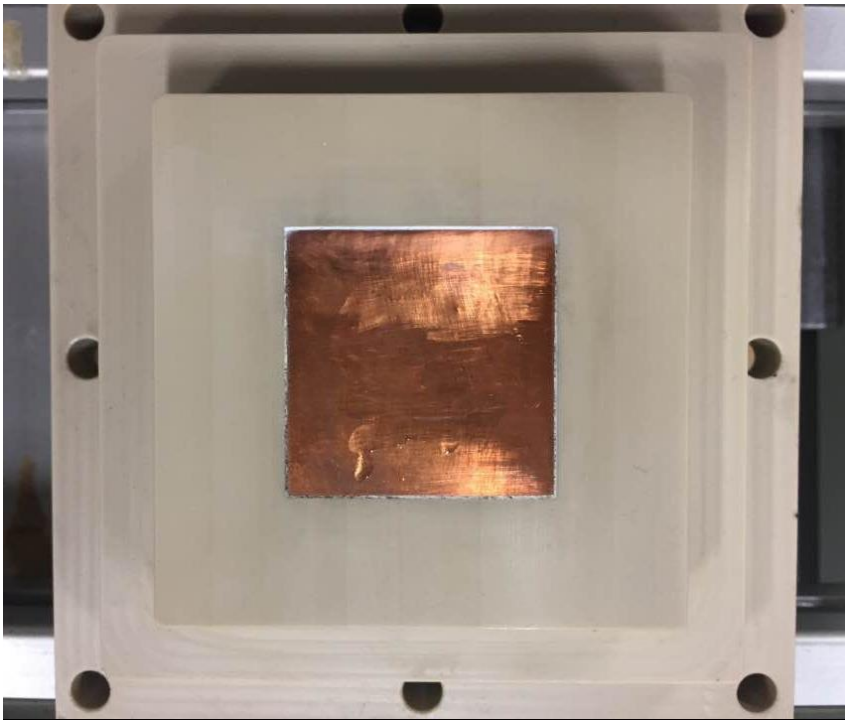

5) Use P1200 sandpaper to polish copper surface.

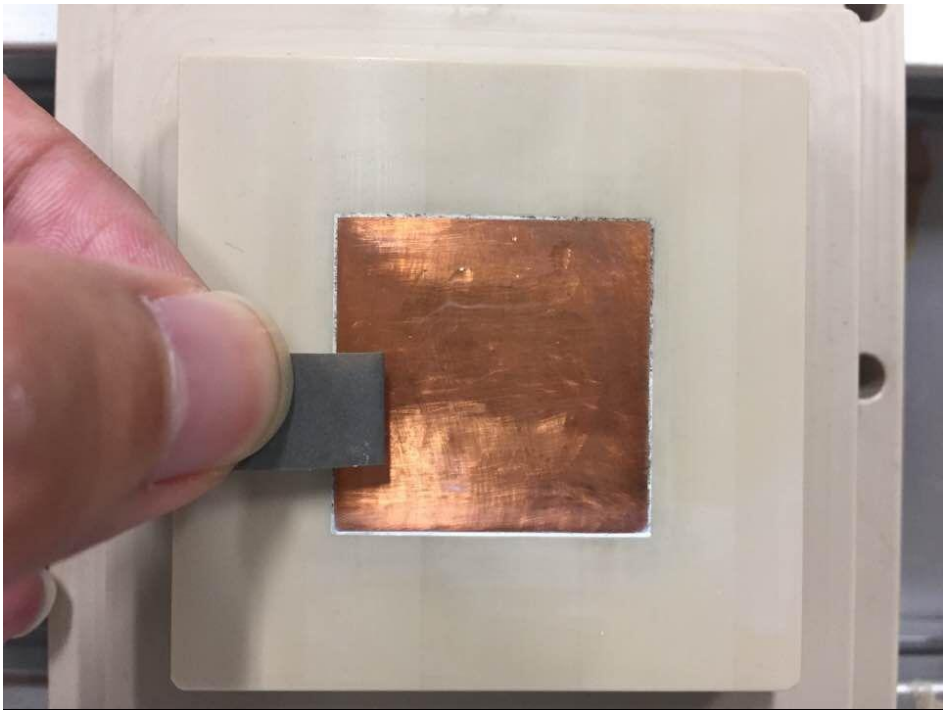

6) Wipe off the residual oil and use acetone to clean surface.

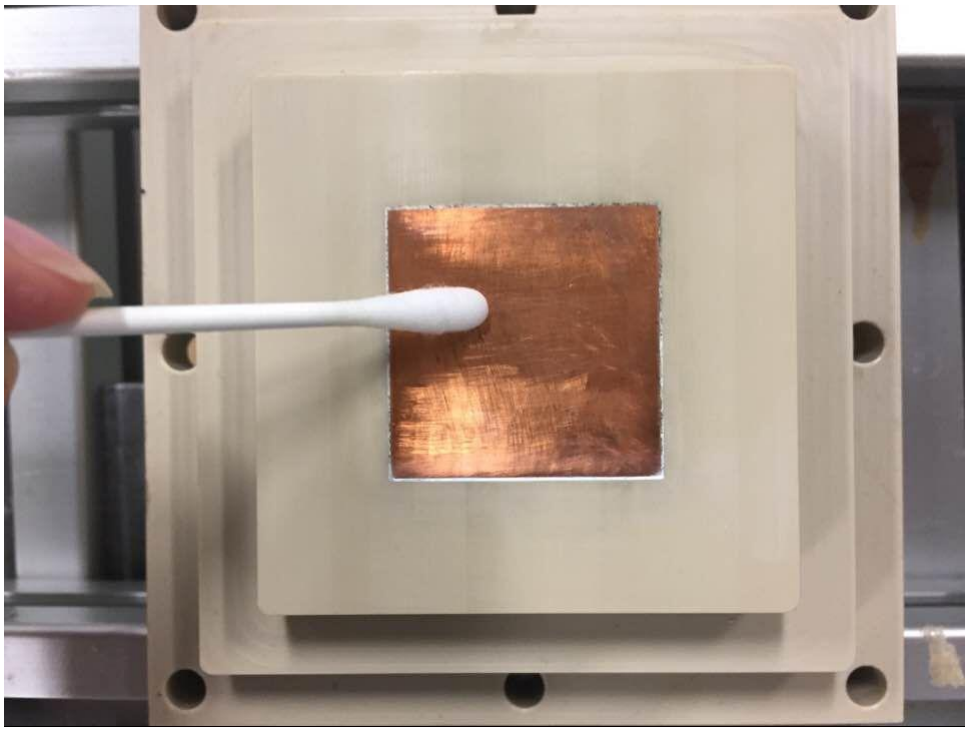

7) Clean surface with distilled water.

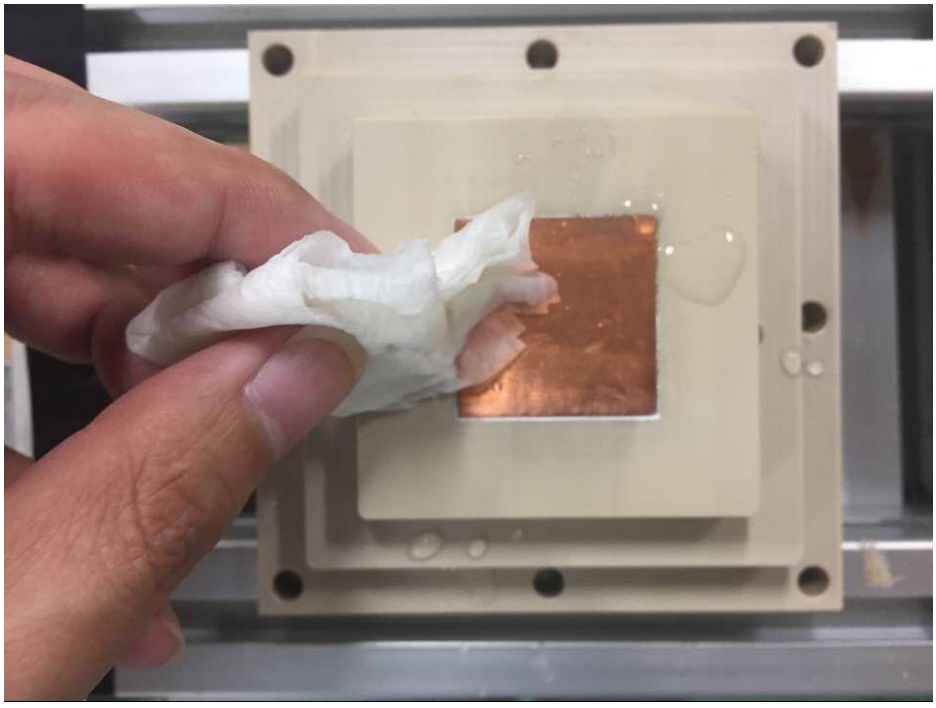

8) Wipe off excess water and put test section back to cover.

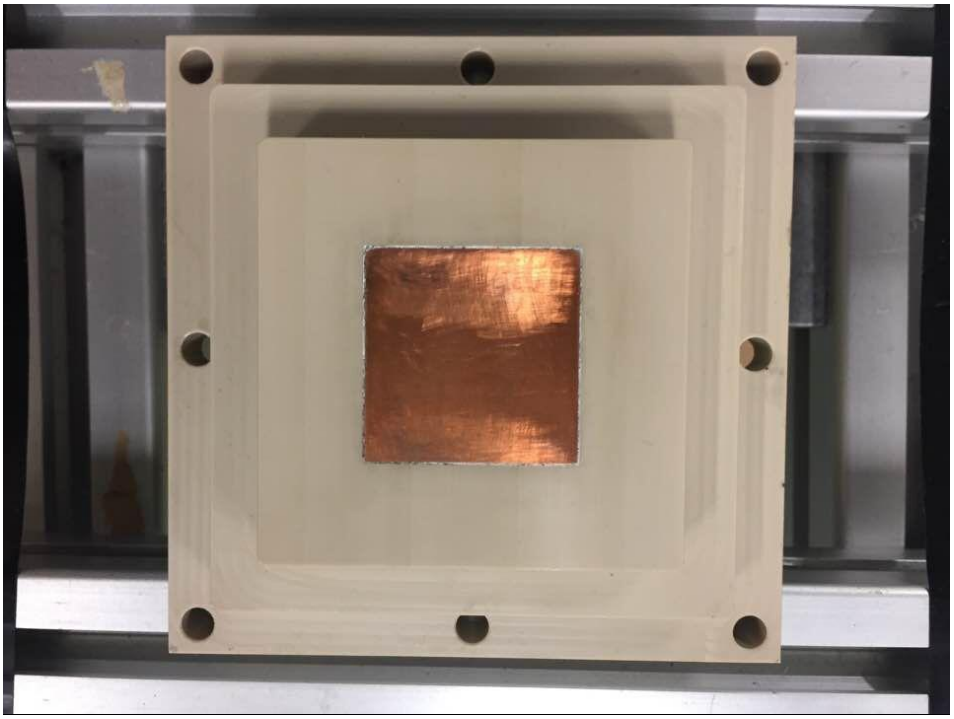

Appendix-C Effective Radius Measurement

The effective radius measurement was carried on in Yokohama National University. There are two methods to measure it [51]. The facility is shown in Figure C-1. First the measured plate is put inside the test section (Figure C-2). Before test, the facility was put inside water. Then lift this facility. At the beginning, the water level is escalated with test section. However, the level will descend after reaching one certain height. Then record the height when water level starts to descend (procedures are shown in Figure C-3). After that the effective radius can be calculated by the following equation.

$$r_{eff} = 2\sigma/\rho_l g h_l \quad \text{(C-1)}$$

Where, r_{eff} is effective radius, σ is surface tension, ρ_l is liquid density, g is gravitational acceleration and h_l means the water level.

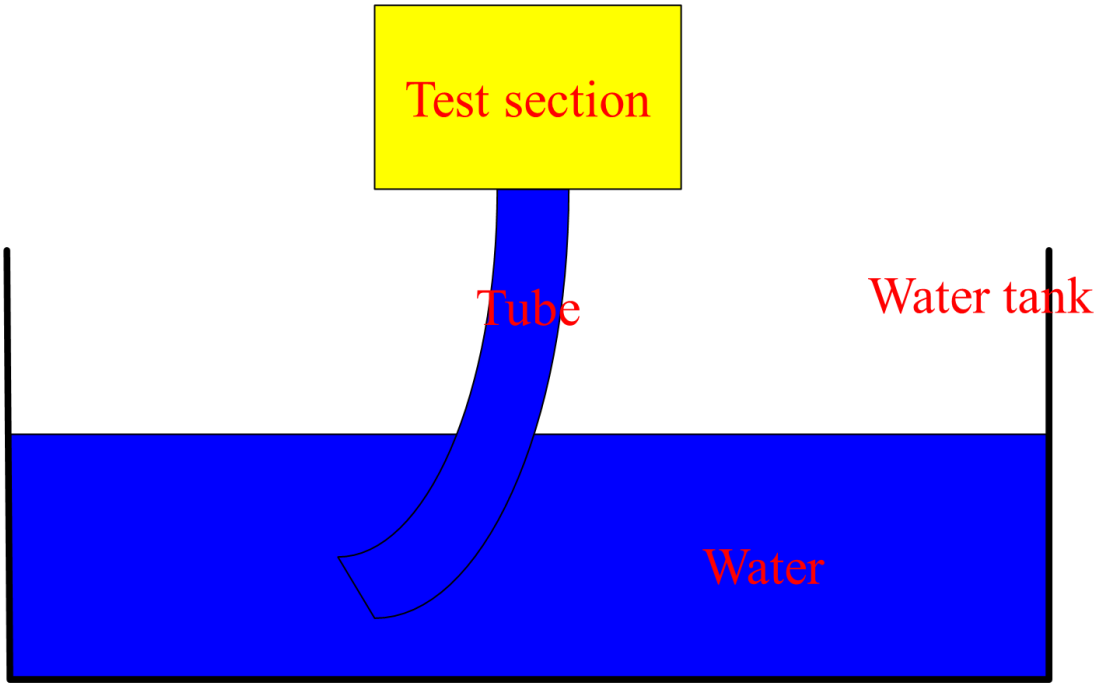

Figure C-1: Schematic facility of the 1st method.

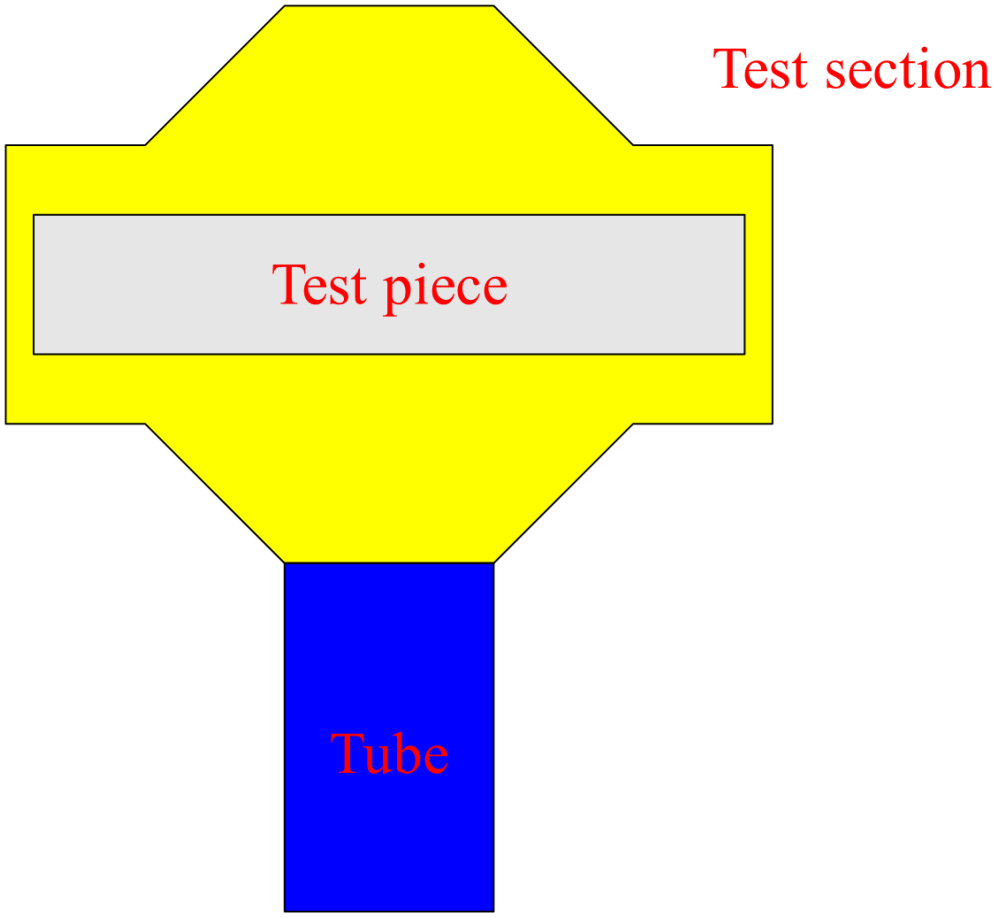

Figure C-2: Test section structure.

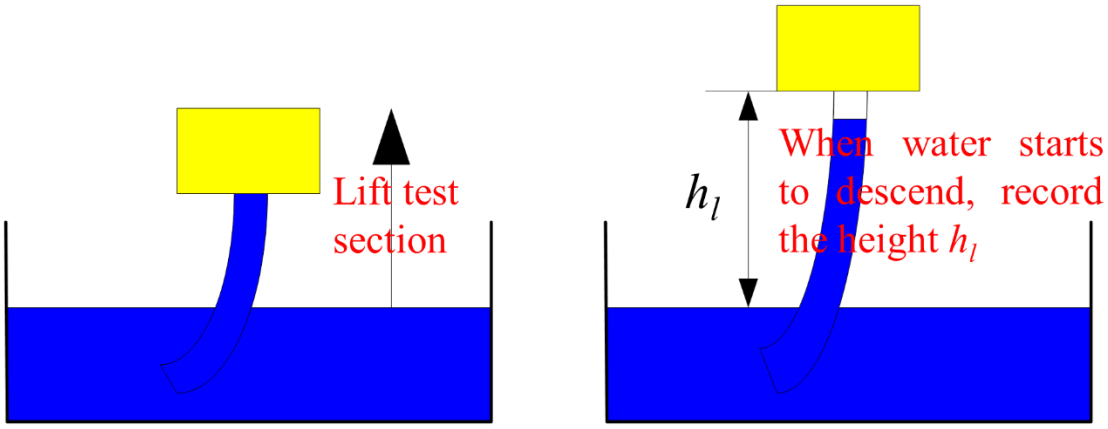

Figure C-3: Work flow in 1st method.

The following is about the 2nd method to measure effective radius. The facility is shown in Figure C-4. One side of test section is connected with high pressure nitrogen. The other side is connected with a little amount of water. Control valve is used to manage the pressure

inside gas tube. When test starts, we turn up valve little by little until some bubble are observed inside water. At this point, record the pressure data of differential pressure meter, defined as Δp. So effective radius can be calculated using the following equation.

$$r_{eff} = 2\sigma/\Delta p \quad \text{(C-1)}$$

Where, r_{eff} is effective radius, σ is surface tension, Δp means pressure drop inside test section.

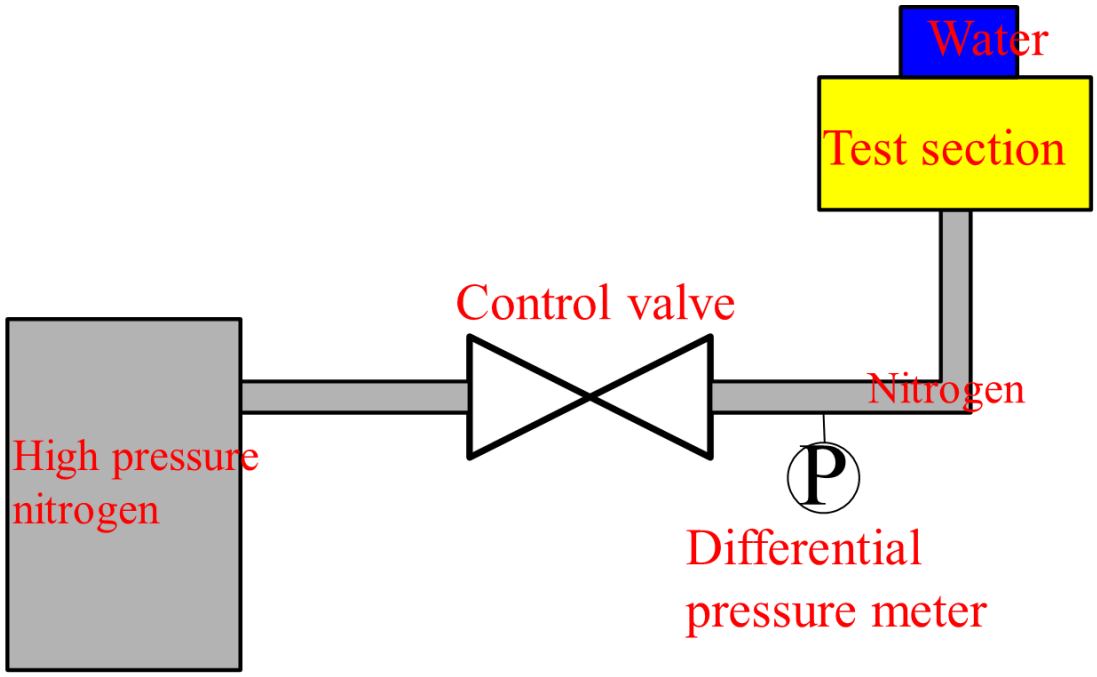

Figure C-4: Schematic map of test facility regarding with the 2nd method.

Through these methods, the effective radius is calculated. Specifically, radius of plate which is made of 5 μm pore size particles is 12.4 μm and radius of plate which is made of 100 μm pore size particles is 105 μm.

Appendix-D Permeability Measurement

The permeability measurement was carried on in Yokohama National University. The facility is shown in Figure D-1. The test procedures are list as follows [52]. Open the

control value to let water penetrate through test section and drop onto the weight meter. Here differential pressure meter is used to record pressure drop inside test section. By using weight meter and stop watch, water flow speed can be decided. After that, the permeability will be determined. The calculating equation is as follows.

$$q_w = K\frac{\Delta p}{\mu_l L} \tag{D-1}$$

Where, q_w is water flow speed, K is permeability, Δp means pressure drop inside test section, μ_l is viscosity of water and L means thickness of test piece.

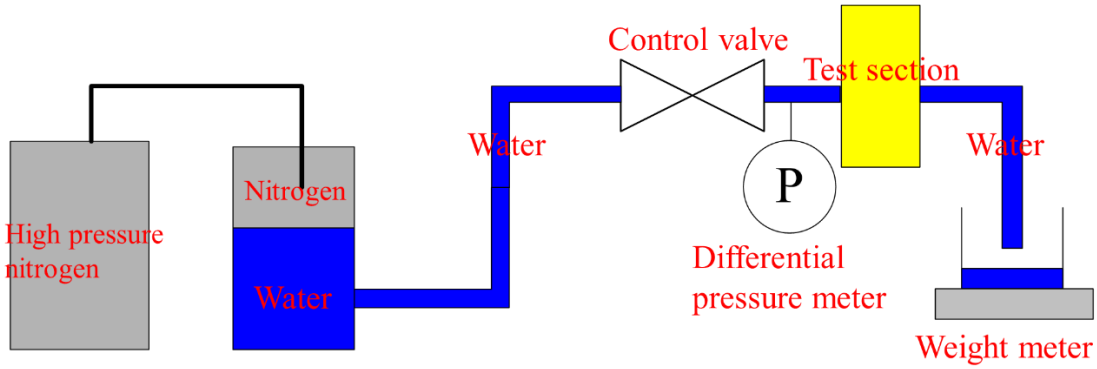

Figure D-1: Schematic map of facility.

Through calculation, the permeability for 100 μm honeycomb plate is 3.04E-11 m^2.

REFERENCES

[1] Collectively, life cycle assessment literature shows that nuclear power is similar to other renewable and much lower than fossil fuel in total life cycle GHG emissions. Nrel. Gov. January 2013.

[2] Severe accident management programmes for nuclear power plants. IAEA safety guide No. NS-G-2.15.

[3] Research and development with regard to severe accidents in pressurized water reactors: summary and outlook. Rapport IRSN-2007/83.

[4] Bal Raj Sehgal, Nuclear safety in light water reactors-severe accident phenomenology, 2012.

[5] T.G. Theofanous, C. Liu, S. Additon, S. Angelini, O. Kymalainen, T. Salmassi, In-vessel coolability and retention of a core melt. Nuclear Engineering and Design. 169 (1997) 1-48.

[6] G. Dewitt, T. Mckrell, J. Buongiorno, L.W. Hu, R.J. Park, Experimental study of critical heat flux with alumina-water nanofluids in downward-facing channels for in-vessel retention applications. Nuclear Engineering and Technology. 45 (2013) 335-346.

[7] Figure. 1-2 from Reactor Physics: http://www.reactor-physics.com/.

[8] China's progress continues, Nuclear Engineering International. August 2015.

[9] Generation III reactor from: https://en.wikipedia.org/wiki/Generation_III_reactor.

[10] Advanced Nuclear Power Reactors from: http://world-nuclear.org/information-library/nuclear-fuel-cycle/nuclear-power-reactors/advanced-nuclear-power-reactors.aspx.

[11] Shoji Mori, Yoshio Utaka, Critical heat flux enhancement by surface modification in a saturated pool boiling: A review. International Journal of Heat and Mass Transfer. 108 (2017) 2534-2557.

[12] J.J. Wei, L. H. Honda, Experiment study of boiling phenomena of heat transfer performances of FC-72 over micro-pin-finned silicon chips, Heat Mass Transfer. 41 (2005) 744-755.

[13] D. Zhong, J. Meng, et al, Critical heat flux for forward-facing saturated pool boiling on pin fin surfaces, International Journal of Heat and Mass Transfer. 87 (2015) 201-211.

[14] J.J. Wei, H. Honda, Effect of fin geometry on boiling heat transfer from silicon chips with micro-pin-fins immersed in FC-72, International Journal of Heat and Mass Transfer. 46 (2003) 4059-4070.

[15] H. Kim, J. Kim, M. Kim, Effects of nanoparticles on CHF enhancement in pool boiling of nano-fluids, International Journal of Heat and Mass Transfer. 49 (2006) 5070-5074.

[16] H. Ahn, M, Kim, The boiling phenomenon of alumina nanofluid near critical heat flux, International Journal of Heat and Mass Transfer. 62 (2013) 718-728.

[17] A.F. Ali, M.S. El-Genk, Effect of inclination on saturating boiling of PF-5060 dielectric liquid on 80- and 137-μm thick copper micro-porous surfaces, International Journal of Thermal Sciences. 53 (2012) 42-48.

[18] Z.-H. Liu, R.-H. Yang, Critical heat flux during natural convective boiling in inclined tubes submerged in saturated liquids, Nuclear Engineering and Design. 235 (24) (2005) 2563-2569.

[19] M. Misale, G. Guglielmini, A. Priarone, Nucleate boiling and critical heat flux of HFE-7100 in horizontal narrow spaces, Experimental Thermal and Fluid Science. 35 (5) (2011) 772-779.

[20] M. Juarsa, N. Putra, W.N. Septiadi, A.R. Antariksawan, Experimental study on the effect of gap size to CCFL and CHF in a vertical of narrow rectangular channel during quenching process, Annals of Nuclear Energy. 72 (2014) 391-400.

[21] S. Liter, M. Kaviany, Pool-boiling CHF enhancement by modulated porous-layer coating: theory and experiment, International Journal of Heat and Mass Transfer 44 (2001) 4287-4311.

[22] G. Hwang, M. Kaviany, Critical heat flux in thin, uniform particle coatings, International Journal of Heat and Mass Transfer 49 (2006) 844-849.

[23] S. Mori, K. Okuyama, Enhancement of the critical heat flux in saturated pool boiling using honeycomb porous media, International Journal of Heat and Mass Transfer 35 (2009) 946-951.

[24] S. Mori, L. Shen, K. Okuyama, Effect of cell size of a honeycomb porous plate attached to a heated surface on CHF in saturated pool boiling, Proceedings of IHTC14, Washington, DC, August 8-13, 2010.

[25] Y. Imai, T. Koga, T. Takamasa, K. Okamoto, K. Mishima, Radiation induced surface activity phenomenon, in: Proceedings of ICONE10, Volume 4, ASME Nuclear Engineering Division, Arlington, VA, 2002, pp. 975-979.

[26] T. Takasama, T. Hazuku, K. Okamoto, K. Mishima, M. Furuya, Radiation induced surface activation on Leidenfrost and quenching phenomena, Experimental Thermal and Fluid Science 29 (3) (2005) 267-274.

[27] K. Okamoto, H. Akiyama, H. Madarame, T. Takamasa, Experiment study on radiation induced boiling enhancement for stainless steel plate, in: Proceedings of ICONE10, Volume 3, ASME Nuclear Engineering Division, Arlington, VA, 2002, pp. 929-932.

[28] 放射線誘起表面活性効果（RISA）。平成２１年度日本原子力学会　熱流動部会.

[29] T. Takamasa, K. Okamoto, K.Mishima, M. Furuya, Journal of the atomic Energy Society of Japan, Vol. 45, No. 2, 42 (2003).

[30] Shoji Mori, Suazlan Mt Aznam, Ryuta Yanagisawa and Kunito Okuyama, CHF enhancement by honeycomb porous plate in saturated pool boiling of nanofluid. Journal of Nuclear Science and Technology, 53 (2016) 1028-1035.

[31] Haiguang Gong, Abdul R. Khan, Nejdet Erkan, Laishun Wang, Koji Okamoto, Critical Heat Flux Enhancement in Downward-facing Pool Boiling with Radiation Induced Surface Activation Effect, Int. J. Heat Mass Transf. 109 (2017) 93-102.

[32] Thermal conductivity of copper from: https://en.wikipedia.org/wiki/Copper.

[33] Chih Kuang Yu, Ding Chong Lu, Pool boiling heat transfer on horizontal rectangular fin array in saturated FC-72, International Journal of Heat and Mass Transfer 50 (2007) 3624-3637.

[34] Chien-Yuh Yang, Chien-Fu Liu, Effect of coating layer thickness for boiling heat transfer on micro porous coated surface in confined and unconfined spaces, Experimental Thermal and Fluid Science 47 (2013) 40-47.

[35] Abdul R. Khan, Nejdet Erkan and Koji Okamoto, Heat transfer effect of an extended surface in downward-facing subcooled flow boiling, Nuclear Engineering and Design, 295 (2015) 148-154.

[36] Taylor BN, Kuyatt CE, Guidelines for evaluation and expressing the uncertainty of NIST measurement results. NIST Tech. Note 1297 (1993) 1–20.

[37] Mohamed S. El-Genk and Zhangxiong Guo, Transient boiling from inclined and downward-facing surfaces in a saturated pool, International Journal of Refrigeration 16 (1993) 414-424.

[38] Zhanxiong Guo and Mohamed S. El-Genk, An experimental study of saturated pool boiling from downward facing and inclined surfaces, International Journal of Heat and Mass Transfer 35 (1992) 2109-2117.

[39] Kutaladze, S. S, Heat Transfer in Condensation and Boiling USAEC Report AEC-tr-3770 (1952).

[40] Kutateladze, S. S, Boiling heat transfer, International Journal of Heat and Mass Transfer 4 (1961) 31-45.

[41] Shoji Mori, Yoshio Utaka, Critical heat flux enhancement by surface modification in a saturated pool boiling: A review, International Journal of Heat and Mass Transfer 108 (2017) 2534-2557.

[42] A.F. Stalder, G. Kulik, D. Sage, L. Barbieri, P. Hoffmann, A snake-based approach to accurate determination of both contact points and contact angles, Colloids And Surfaces A: Physicochemical And Engineering Aspects, 286(1-3) (2006) 92-103.

[43] A.F. Stalder, T. Melchior, M. Müller, D. Sage, T. Blu, M. Unser, Low-bond axisymmetric drop shape analysis for surface tension and contact angle measurements of sessile drops, Colloids and Surfaces A: Physicochemical and Engineering Aspects, 364(1-3) (2010) 72-81.

[44] Yun-Je Cho, Soo-Been Yum, Jeong-Hun Lee, Goon-Cherl Park, Development of bubble departure and lift-off deamter models in low heat flux and low flow velocity conditions, Int. J. Heat Mass Transfer 54 (2011) 3234-3244.

[45] J.F. Klausner, D.M. Bernhard, L.Z. Zeng, Vapor bubble departure n forced convection boiling, Int. J. Heat mass Transfer 36 (1993) 651-662.

[46] L.Z. Zeng, J.F. Klausner, D.M. Bernhard, R. Mei, A unified model for the prediction of bubble detachment diameters in boiling system-Ⅱ Flow boiling, Int. J.Heat Mass Transfer 36 (1993) 2271-2279.

[47] Acceleration pressure drop from: http://www.egi.kth.se/courses/4a1625/files/Two-phase_flow_pressure_drop.pdf.

[48] Capillary action from: https://en.wikipedia.org/wiki/Capillary_action.

[49] Darcy’s law from: https://en.wikipedia.org/wiki/Darcy%27s_law.

[50] Darcy-Weisbach equation from:https://en.wikipedia.org/wiki/Darcy%E2%80%93W-eisbach_equation.

[51] 精密ろ過膜エレメント及びモジュールのバブルポイント試験方法。JIS K 3832-1990.

[52] ファインセラミックス多孔体の水透過率及び水力等価直径試験方法。JIS R 1671-2006.